SEASONAL TO DECADAL VARIABILITY IN THE PHYSICAL AND BIOLOGICAL PROPERTIES OF THE BLACK SEA AND LEVANTINE BASIN AS INFERRED FROM SATELLITE REMOTE SENSING

DOCTOR OF PHILOSOPHY

IN

OCEANOGRAPHY
MIDDLE EAST TECHNICAL UNIVERSITY
INSTITUTE OF MARINE SCIENCES

BY

ANIL AKPINAR

MERSİN-TURKEY
SEPTEMBER 2016

SEASONAL TO DECADAL VARIABILITY IN THE PHYSICAL AND BIOLOGICAL PROPERTIES OF THE BLACK SEA AND LEVANTINE BASIN AS INFERRED FROM SATELLITE REMOTE SENSING

A THESIS SUBMITTED TO
INSTITUTE OF MARINE SCIENCES
OF
MIDDLE EAST TECHNICAL UNIVERSITY

BY

ANIL AKPINAR

IN PARTIAL FULFILMENT OF THE REQUIREMENTS
FOR
THE DEGREE OF DOCTOR OF PHILOSOPHY
IN
THE DEPARTMENT OF OCEANOGRAPHY

SEPTEMBER 2016

Approval of
the thesis:

SEASONAL TO DECADAL VARIABILITY IN THE PHYSICAL AND BIOLOGICAL PROPERTIES OF THE BLACK SEA AND LEVANTINE BASIN AS INFERRED FROM SATELLITE REMOTE SENSING

submitted by **ANIL AKPINAR** in partial fulfilment of the requirements for the degree of **Doctor of Philosophy in the Department of Oceanography, Middle East Technical University** by,

Prof. Dr. Ahmet Erkan Kıdeyş _____
Director, Institute of Marine Sciences

Prof. Dr. Süleyman Tuğrul _____
Head of Department, Oceanography

Assoc. Prof. Dr. Bettina A. Fach Salihoğlu
Supervisor, Institute of Marine Sciences _____

Examining Committee Members:

Assist. Prof. Dr. Sinan Şadi Arkın _____
Oceanography Dept., METU

Prof. Dr. Elif Eker-Develi _____
Faculty of Education, Mersin University

Dr. Francesco d'Ovidio _____
L'OCEAN

Prof. Dr. Zahit Uysal _____
Marine Biology and Fisheries Dept., METU

Assoc. Prof. Dr. Bettina Andrea Fach Salihoğlu _____
Oceanography Dept., METU

Date: *September 1, 2016*

I hereby declare that all information in this document has been obtained and presented in accordance with academic rules and ethical conduct. I also declare that, as required by these rules and conduct, I have fully cited and referenced all material and results that are not original to this work.

Name, Last name: Anıl Akpınar

Signature:

ABSTRACT

SEASONAL TO DECADAL VARIABILITY IN THE PHYSICAL AND BIOLOGICAL PROPERTIES OF THE BLACK SEA AND LEVANTINE BASIN AS INFERRED FROM SATELLITE REMOTE SENSING

Akpınar, Anıl

Ph.D., Department of Oceanography

Supervisor: Assoc. Prof. Dr. Bettina Andrea Fach Salihoğlu

September 2016, 142 pages

Black Sea and Eastern Mediterranean (Levantine basin) have gone through a number of documented changes in the recent decades. Recently acquired satellite data document rapid warming, increased sea level and decreased chlorophyll-a (phytoplankton) in the Black Sea and Levantine basin. Aim of this study is to address warming in the Black Sea and Levantine basin, as well as to investigate the phytoplankton response to changing environmental conditions at seasonal to interannual timescales.

In the first part of the study, sea surface temperature (SST) in the Black Sea and Levantine were investigated over the study period 1982-2012. Warming trends, thermal anomalies and results of an empirical orthogonal functions analysis (EOF) was used to interpret the spatiotemporal variability of SST in the Black Sea and Levantine basins.

In the second part of the study, changes in Chlorophyll-a were investigated for the Black Sea and Levantine basin as well as its responses to changes in physical environment. EOF analysis were conducted on weekly datasets of chlorophyll-a (CHL-A), sea surface temperature (SST) and absolute dynamic topography (ADT) for 1998-2012. EOF analysis was utilized to investigate the variability at seasonal and interannual time scales. Response of CHL-A to SST and ADT as well as to riverine and heat fluxes were investigated.

The first part of the study documented intense warming in the Black Sea and less intense warming in the Levantine basin, both displaying spatio-temporal variability. The second

part of the study documented that the Black Sea chlorophyll-a decline as a result of changing wind pattern, eventually changing the intensity of the circulation, whereas in the Levantine basin, chlorophyll-a decline was linked to decreased winter convective mixing.

This thesis documents the impacts of global change on physics and biology of the Black Sea and Levantine basin, providing an insight into possible consequences of global warming in the regional seas.

Keywords: Black Sea, Levantine basin, physical-biological interactions, global warming, remote sensing

ÖZ

KARADENİZ VE LEVANT BASENİ'NİN FİZİKSEL VE BİYOLOJİK ÖZELLİKLERİNİN SEZONLUK VE ON-YILLIK DEĞİŞKENLİKLERİNİN UZAKTAN ALGILAMA İLE BELİRLENMESİ

Akpınar, Anıl

Doktora, Oşinografi Bölümü
Tez Yöneticisi: Assoc. Prof. Dr. Bettina Andrea Fach Salihoğlu
Eylül 2016, 142 sayfa

Karadeniz ve Doğu Akdeniz (Levant baseni) son on-yıllarda belgelenmiş birçok değişiklikten geçmiştir. Güncel uydu verileri Karadeniz ve Levant baseninde ısınma, artan deniz su seviyesi yüksekliği ve azalan klorofil (fitoplankton) göstermektedir. Bu çalışmanın amacı Karadeniz ve Levant basenindeki ısınmayı belirlemenin yanı sıra, fitoplanktonların değişen çevre koşullarına olan sezonluk ve yıllar arası tepkilerinin araştırılmasıdır. Çalışmanın birinci kısmında, Karadeniz ve Levant basenindeki deniz suyu sıcaklığı (DYS) 1982-2012 için incelenmiştir. Isınma trendleri, sıcaklık anomalileri ve ampirik ortogonal fonksiyon (AOF) analizi sonuçları kullanılarak Karadeniz ve Levant baseni DYS'lerinin zamansal ve mekansal değişkenliği araştırılmıştır.

Çalışmanın ikinci kısmında, Karadeniz ve Levant baseni klorofil-a değişimlerinin yanı sıra, fiziksel çevredeki değişimlere olan tepkisi de incelenmiştir. AOF analizi 1982-2012 arasında haftalık klorofil (CHL-A), deniz suyu sıcaklığı (DYS) ve deniz suyu yüksekliği (ADT) verilerine uygulanmıştır. AOF analizi, sezonluk ve yıllar arası değişimlerin incelenmesinde kullanılmıştır. CHL-A'nın DYS ve ADT'nin yanı sıra, nehir debisi ve ısı akımı değişimlerine olan tepkisi de incelenmiştir.

Çalışmanın birinci kısmı Karadeniz'de aşırı ısınma olduğunu ortaya koyarken, Levant baseni görece daha az ısınma göstermiş olup, her iki bölgede de zamansal ve mekansal değişkenlik görülmüştür. Çalışmanın ikinci kısmı, Karadeniz'deki CHL-A azalmasının değişen rüzgar paterninin sonucu olarak değişen akıntı sisteminin sonucu olduğu, Levant baseninde ise, CHL-A azalmasının azalan kış karışımıyla bağlantılı olduğu ortaya konmuştur.

Bu tez, küresel değişimlerin, Karadeniz ve Levant baseninin fiziksel ve biyolojik yapısı üzerindeki etkilerini belgelemekte ve küresel ısınmanın bölgesel denizlerdeki etkilerinin anlaşılmasında bir örnek teşkil etmektedir.

Anahtar Kelimeler: Karadeniz, Levant baseni, fiziksel-biyolojik etkileşimler, küresel ısınma, uzaktan algılama

To Akgün, Geylan, Duygu, Neriman and Gölge

ACKNOWLEDGEMENTS

I would like to thank my advisor Dr.Bettina Fach for her guidance, patience and support at every stage of my PhD. Wihout her guidance, I believe I would have floundered under stress and loads of data. Her guidance helped me to develop as a scientist.

I gratefully thank Dr. Sinan Arkın for providing me help at the most critical times of my PhD.

I sincerely thank Prof. Dr. Temel Oğuz for helping me at various stages of this work. His scientific expertise and guidance has evolved this work to a better stage.

I would like to thank Dr. Barış Salihoğlu for his support and guidance throughout my study.

My sincere thanks to Elif Yılmaz for her support and patience.

Many thanks to Ceren Güraslan for her support, friendship and neighborhood on the path to PhD.

I thank Fatih Aslan for his friendship, support and encouragement at every stage of my academic life.

I thank Burak Kayael and Ehsan Sadighrad for their friendship and support.

I would like to thank my thesis committee members, Dr. Francesco d'Ovidio, Prof. Dr. Elif Eker Develi and Prof. Dr. Zahit Uysal for valuable contributions.

Chapter 4 was co-authored by Assist. Prof. Dr. Sinan Şadi Arkın and Assoc. Prof. Dr. Bettina Andrea Fach Salihoğlu, and prepared for submission as a research article.

This Ph.D. work has been supported by THE SCIENTIFIC AND TECHNOLOGICAL RESEARCH COUNCIL OF TURKEY (TÜBİTAK) 2211-C scholarship programme.

This study was supported by DEKOSIM Project (Deniz Ekosistem ve İklim Araştırmaları Merkez, Project Code BAP-08-11-DPT.2012K120880) financed by the Ministry of Development of Turkey.

TABLE OF CONTENTS

LIST OF TABLES

LIST OF FIGURES

CHAPTER 1: Thesis Introduction

World oceans are warming (Levitus et al., 2005; IPCC, 2007; Belkin, 2009). Global warming has various direct and secondary impacts on the oceans. Increasing sea surface temperature (SST) modifies the atmosphere (causing instabilities in the lower troposphere) leading to changes in wind (Chelton et al., 2007) and precipitation (Meredith et al., 2015) patterns. As a secondary impact, modified winds and precipitation directly influence circulation in the ocean. Another impact of warming on the oceans is directly on circulation. Warming leads to decreased winter convective mixing (resulting in decreased cold intermediate water formation), increased stratification and finally it contributes to sea level change (steric contribution), all of which in the end modify the circulation in the ocean. Another impact of global warming is on the living part of the oceans, its ecosystem. Chlorophyll-a is a proxy for primary production, which constitutes the base of the marine ecosystems. Various studies have documented decreasing phytoplankton and primary production (Behrenfeld et al., 2006; Boyce et al., 2010; Gregg and Rousseaux, 2014) as a result of increased temperatures. The inverse relationship of temperature and phytoplankton is described as: increased temperatures lead to stratification and prevent nutrient supply leading to decreased primary production (Doney, 2006). Therefore, understanding the links between global warming and phytoplankton is crucial considering that the ocean ecosystem depends on primary production. It is of great importance to investigate the response of phytoplankton to changing environmental conditions (temperature, circulation etc.).

The global oceans are warming and the Black Sea and Mediterranean are no exception. In addition, the Turkish seas Black Sea and Levantine basin both experienced environmental challenges in the past decades. The Black Sea ecosystem, changed significantly since the 1970's due to natural and anthropogenic factors. Human induced pressures including: eutrophication, overfishing, pollution, damming of rivers and the introduction of more than 234 recorded alien species (Mee 1992, Zaitsev 1992, Daskalov 2002, Cociasu and Popa 2005, Yunev et al. 2007). Similar to the case of the Black Sea, the Eastern Mediterranean has also gone through major alterations including

the so-called Eastern Mediterranean Transect, introduction of exotic species (Raitsos et al., 2010; Schmidt et al., 2015) and pollution.

The purpose of this thesis study is to explain in detail: the extent of warming and the response of phytoplankton to changes in the physical environment in the Black Sea and Levantine basin. This works utilizes space-time decompositions of satellite data products from 1982 to 2012 (31 years) to detect the seasonal and interannual variability in the physical and biological properties of the Black Sea and Levantine basin. In order to do so, the thesis focuses on two main objectives. **The first objective is to define the extent of warming, its trends and spatio-temporal variability in the Black Sea and Levantine. The second objective is centered on elucidating the response of phytoplankton (chlorophyll-a) to the physical environment (sea surface temperature, circulation, winds) in both basins.**

The second chapter of this thesis focuses on quantifying warming and the spatio-temporal variability of SST in the Black Sea. The Black Sea is divided into different basins following space-time decomposition patterns (EOF analysis). Sea surface temperature trends, a detailed distribution of monthly and yearly SST anomalies, are evaluated followed by results of EOF analysis on both SST (seasonal variability) and SST anomalies (interannual variability). Connections with large-scale atmospheric patterns are presented.

The third chapter of this thesis investigates the spatio-temporal variability of SST in the Levantine Basin. Seasonal variability is elucidated through EOF analysis. Significant warming trends are presented in regional maps, exposing areas of highest warming. Interannual variability of SST is elaborated through EOF analysis on low-pass filtered SST anomalies. Connections with large-scale atmospheric patterns are presented as basin-wide maps illustrating the regional distribution of their impact on SST. Further, a comparison of SST in the Black Sea and Levantine basin, their similarities and differences are presented within this chapter.

The fourth chapter aims to identify the changes in chlorophyll-a, and its response to physical parameters in the Black Sea. Space-time variability of temperature, circulation and winds are investigated along with chlorophyll-a, both at seasonal and interannual time scales. Changes in chlorophyll-a, previously called a regime shift, are attributed to changes in the physical environment. Wind driven circulation in the Black

Sea is shown to intensify following a very warm period, which led to abated cross-shelf transport of nutrients, leading to the observed decrease in chlorophyll.

The fifth chapter follows a similar structure as the fourth chapter, however it focuses on the Levantine basin. Chlorophyll dynamics with a special focus on offshore waters, particularly the Rhodes Gyre, are investigated utilizing space-time decompositions. Contribution of decreased winter convective mixing (as a result of increased temperatures) and cyclonic circulation intensity to phytoplankton blooms are examined. Comparison of Black Sea and Levantine phytoplankton responses to physical parameters are presented.

The sixth and final chapter gives a summary on the extensive analysis conducted on sea surface temperatures and the response of phytoplankton to physical environment in the Black Seas and Levantine, emphasizing the importance of each chapter.

CHAPTER 2: Recent trends in the sea surface temperature of the Black Sea

2.1 Introduction

The Black Sea is a semi-enclosed inland basin that has limited water exchange with the Mediterranean Sea and the Azov Sea. The signature of this limited exchange is observed as high salinity in deep waters, whereas the low salinity at the surface is an imprint of high river discharge. Together these processes are sustaining a permanent stratification in the Black Sea (Ozsoy and Unluata 1997) which leads to its deep waters being permanently anoxic. Due to the stratified nature of the Black Sea with a shallow mixed layer, sea surface temperatures (SST) respond expeditiously to atmospheric forcing (Schrum et al., 2001; Ginzburg et al., 2004; Nardelli et al., 2010). Feedback in between the ocean and atmosphere is observed since SST regulates the ocean-atmosphere heat exchange. Recently, precipitation extremes in the Black Sea region have been related to enhanced lower tropospheric instability as a result of high SST's (Meredith et al., 2015).

An important feature of the Black Sea, the Cold Intermediate Layer (CIL), is fueled by the extent of this response to atmosphere. CIL formation and renewal is limited to winter convective mixing. Various studies (Ivanov et al., 2001; Gregg and Yakushev, 2005; Belokopytov, 2010) point to the importance of atmospheric conditions on the formation and renewal of the CIL. Continuous warming of the upper ocean may result in reduced ventilation of the Black Sea, further increasing its oxygen-deficiency in the long term. Depletion of CIL has already been documented through various studies (Staneva and Stanev 2002; Krivosheya et al., 2002; Oguz et al., 2003; Capet et al., 2016). Thus observations of SST are crucial for monitoring warming trends in the Black Sea and its impact on CIL formation and replenishment.

Except for a few exceptions (i.e. Patagonian Shelf, Eastern North Pacific, Southern Australia), increased SST's have resulted in decreased production in most of the mid-latitude oceans as a result of increased stratification (Gregg et al., 2005; Behrenfeld et al., 2006). Recently, McQuatters-Gollop et al. (2008) have shown similar trends for the Black Sea with the exception of 2001.

The Black Sea ecosystem has been exposed to severe ecosystem changes since the 1970's (Oguz et al., 2004). These changes are rather complex and it may not possible to explain all ecosystem changes with physical forcing alone. It is also not the scope of this study to explain all ecosystem changes, however it is of importance to note that SST is an important proxy for observing the response of the ecosystem to changing environmental conditions. Thus SST is a vital parameter both for observing ecosystem response to warming and climatic patterns (Oguz et al., 2003; Oguz, 2005b) and resulting transitions and regime shifts (McQuatters-Gollop et al., 2008; Oguz and Velikova, 2010).

Considering the vulnerability of Black Sea's hydrography and ecosystem to climate forcing, monitoring SSTs and their temporal and spatial variability is of critical interest. SST data obtained from satellite sensors are the best possible candidate for this purpose considering their spatio/temporal coverage. Satellite SST data have previously been used in studies examining seasonal and interannual variability of the Black Sea for 1981 to 2000 using AVHRR data at 18km resolution (Ginzburg et al., 2004). They have found a positive SST trend 0.09 ^{o}C/year. Their work showed a relationship between ENSO events and their effect on the Black Sea SST. The relationship of Black Sea SSTs to large-scale atmospheric forcing was investigated by Kazmin and Zatsepin (2007), using satellite, in-situ and reanalysis data for 1950 to 2005. Their work has shown that wind patterns change in response to changes in NAO. They've found that strengthening/weakening Southern wind causes surface air temperatures and sea surface temperatures increase/decrease. Ginzburg et al. (2008), extending their previous study (Ginzburg et al., 2004), investigated temporal, regional and synoptic variability, its correlations with Cold Intermediate Layer (CIL) temperatures, and SST response to large-scale atmospheric forcing (NAO, ENSO and EA-WR) for 1982-2002 using 18km (1982-1984) and 9km (1985-2002) data and have found a warming trend of about 0.06 ^{o}C. Kazmin et al. (2010) have used SST data for 1982-2004 at 18km to determine the long-term variability of Black Sea and Aegean Sea winter SST's, and their connection with atmospheric forcing (NAO and EA-WR) and have shown that despite some differences, general SST variability in the Black Sea and Aegean is similar. Shapiro et al. (2010) have investigated long term trends in Black Sea SST using World Ocean Database (2001) for 1900 to 2000 and has shown a warming trend of about 0.063 ^{o}C for 1985-2000. Another satellite SST investigation over the Black Sea was conducted by Nardelli et al. (2010). Their work focuses on construction of an optimally interpolated

SST dataset (~7km resolution) for the Black Sea for 1985-2005 and investigating spatio-temporal variability of Black Sea SST using Empirical Orthogonal Functions (EOF) analysis over this dataset and its relation with NAO index. Their work demonstrated a significant correlation (-0.65) between low-pass filtered SST's and NAO index.

Although the variability of Black Sea SST has been subject to the various studies above, an investigation including the recent changes in SST is missing. Previous work on SST has been limited to data covering until 2005 and coarse resolution satellite products. In this study the focus is therefore on investigating long-term changes in SST over 31 years (1982-2012) looking at not only the entire Black Sea but also focusing on regional differences in SST trends and variability. This study presents an up to date investigation of seasonal and interannual variability of sea surface temperature on a regional scale using ~4 km resolution data (Group for High Resoultion Sea Surface Temperature (GHRSST)) over 31 years (1982-2012). Though previous studies discuss an east/west gradient of SST in the Black Sea (Ginzburg et al.2000, Ginzburg et al., 2008, Nardelli et al. 2010), the details in this spatial variability is not clearly defined. Changes in SST's are generally expected to be similar over the entire Black Sea and its specific regions, however some regional variability exists due to different regional circulation characteristics. Therefore, this study does not only describe trends for the entire basin, but provides a detailed analysis of SST variability in nine different regions of the Black Sea defined by EOF analysis.

2.2 Material and Methods

2.2.1 Satellite sea surface temperature data

Sea surface temperature data used in this study is the AVHRR (Advanced Very High Resolution Radiometer) Pathfinder Version 5.2 (PFV5.2) data and was obtained from the US National Oceanographic Data Center and GHRSST (http://pathfinder.nodc.noaa.gov). The PFV5.2 data are an updated version of the Pathfinder Version 5.0 and 5.1 collections described in Casey et al. (2010). The dataset used in this study comprises of daily 4km daily SST fields for the period 1982-2012. Comparison of global Pathfinder data with in situ buoy data revealed an accuracy of $0.02\ ^{o}$ C$\pm$ $0.5\ ^{o}$ C and comparisons with radiometric skin temperature measurements using Marine Atmospheric Emitted Radiance Interferometer (MAERI) showed $0.14\ ^{o} \pm 0.31\ ^{o}$ C (Kilpatrick et al., 2001). An instrument noise of $0.6\ ^{o}$ C has been suggested in

the Black Sea (Nardelli et al., 2010). Daily images of night-time overpass sea surface temperature data from 1998 to 2012 were obtained, to avoid any impact of diurnal heating. Pixels with low quality flags and pixels affected by clouds were removed from the analysis, and subsequently daily SST fields were composited into monthly fields resulting in 372 monthly images. Considering the aim of this work is to describe the recent trends for the period 1982-2012 and to address regional variability, it was both sufficient and necessary to use monthly data to describe temporal variability and provide increased spatial coverage respectively.

2.2.2 Supplementary Datasets

In order to compare the interannual trends of SST, two other SST products were utilized. Optimum Interpolation Sea Surface Temperature (OISST) data (Reynolds et al., 2007; Reynolds et al., 2009) from NOAA (https://www.ncdc.noaa.gov/oisst). OISST dataset covers 0.25^{o} daily sea surface temperature obtained using a combination of AVHRR and AMSR-E. AVHRR+AMSR-E data is available from 2002 to 2011, whereas the remaining time period is AVHRR data only. The second additional dataset utilized is the Hadley SST (Rayner et al. , 2003) obtained from Met Office (www.metoffice.gov.uk/hadobs/hadisst/)

Considering the coupling of sea surface temperature to the atmosphere, heatflux and wind were utilized as additional datasets to elucidate interannual variations of SST. Cross-Calibrated Multi-Platform Ocean Surface Wind Vector L3.0 First-Look Analyses (CCMP) (ftp://podaacftp.jpl.nasa.gov/allData/ccmp/L3.0/flk/) was used for wind data, providing using 0.25 degree resolution, 6 hourly wind fields from 1987 to 2011. The wind stress was computed following Trenberth et al. (1990). Heat flux data was obtained from ERA-interim dataset
(http://data-portal.ecmwf.int). Heat flux data in this dataset was calculated using reanalysis fields of surface net solar radiation, surface net thermal radiation, surface latent heat flux and surface sensible heat flux at 0.125^{o} resolution.

OISST, Hadley SST and CCMP datasets were interpolated to the same grid as GHRSST dataset. Daily fields of each dataset were then used to construct the monthly datasets. These monthly datasets were used throughout the analysis. Anomaly datasets were constructed by subtracting weekly (12 months) climatology (1982-2012) from the

original data (i.e.SST_month1_anomaly=SST_month1-SST_month1_climatology) for comparison with GHRSST anomaly data set.

2.2.3 Empirical Orthogonal Functions (EOF) Analysis

The satellite dataset contains gaps due to instrumentation errors or cloud coverage. It is not possible to decompose the SST into components using standard EOF analysis on dataset with gaps. Therefore a gap filling technique is required. Data Interpolating Empirical Orthogonal Functions (DINEOF) (Beckers and Rixen 2003) were used to fill the gaps in the data. Data are stored in a matrix; missing data are initially set to zero. Then Singular Value Decomposition (SVD) is conducted to calculate first EOF mode. This first spatial mode is then multiplied by the corresponding temporal amplitude and used to replace the missing data (step A). Then the SVD is performed again (step B). This is an iterative process, where step A and step B are repeated until convergence is reached. Optimum number of EOFs are found by cross validaton. A random set of data is set aside to be compared with the interpolated data.The optimum number to be retained is the one with the minimum error between the dataset put aside and the interpolated dataset This procedure intends to fill data gaps; the EOF analysis is a side product of this technique.

2.2.4 Definition of regions

In order to investigate spatial variability, the Black Sea has been divided into different regions defined by investigating at the spatial signals of the SST distribution via Empirical Orthogonal Functions (EOF) analysis, as well as bathymetry and the well-known surface circulation system. The EOF analysis to assess the spatial SST variability was done using the using the Data INterpolating Empirical Orthogonal Functions (DINEOF) technique on the monthly data set, which has been successfully applied to various SST data in other studies (Alvera-Azcarate et al., 2005; Mauri et al., 2008; Ding et al., 2009; Li et al., 2014).

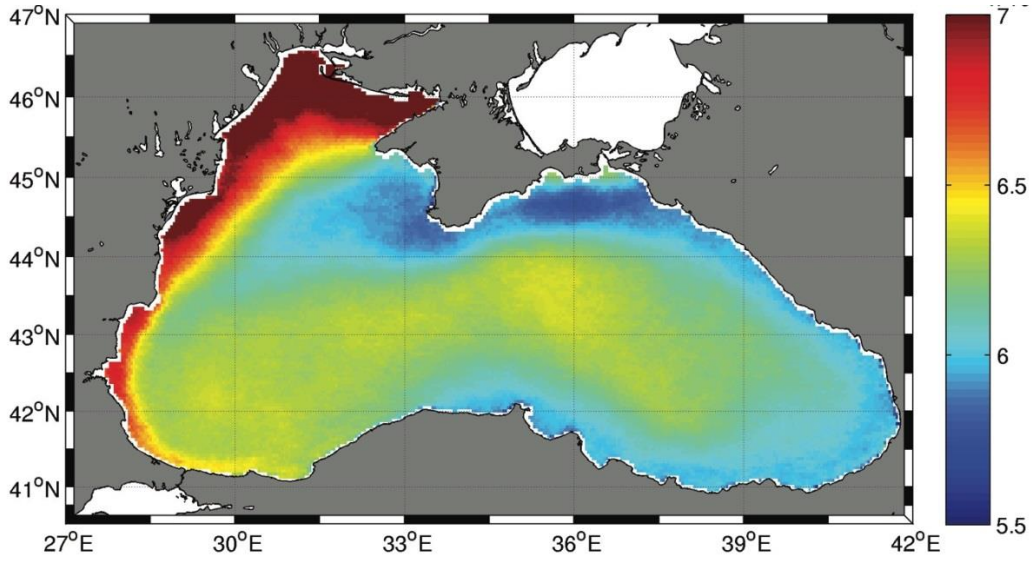

Figure 1 First spatial EOF mode of sea surface temperature ($x10^{-3}$).

Since the first spatial mode of EOF explains ~97% of the total variance (Figure 1) this mode was used as a proxy to define the main regions. The general surface circulation of the Black Sea (Korotaev et al., 2003) was used as the secondary tool to define the regions. Although DINEOF results suggest a smooth definition for regional variability, regions were defined with strict borders considering the surface circulation and the anticyclonic eddies associated with them. This lead to dividing the Black Sea into 9 regions (Figure 1): Batumi (R1), Western Cyclonic Gyre (R2), Eastern Cyclonic Gyre (R3), Western Anatolian Coast (R4), Eastern Anatolian Coast (R5), Caucasian&Crimean Coast (R6), Sevastopol (R7), North-Western Shelf (R8) and Shelf/Deep Transition (R9).

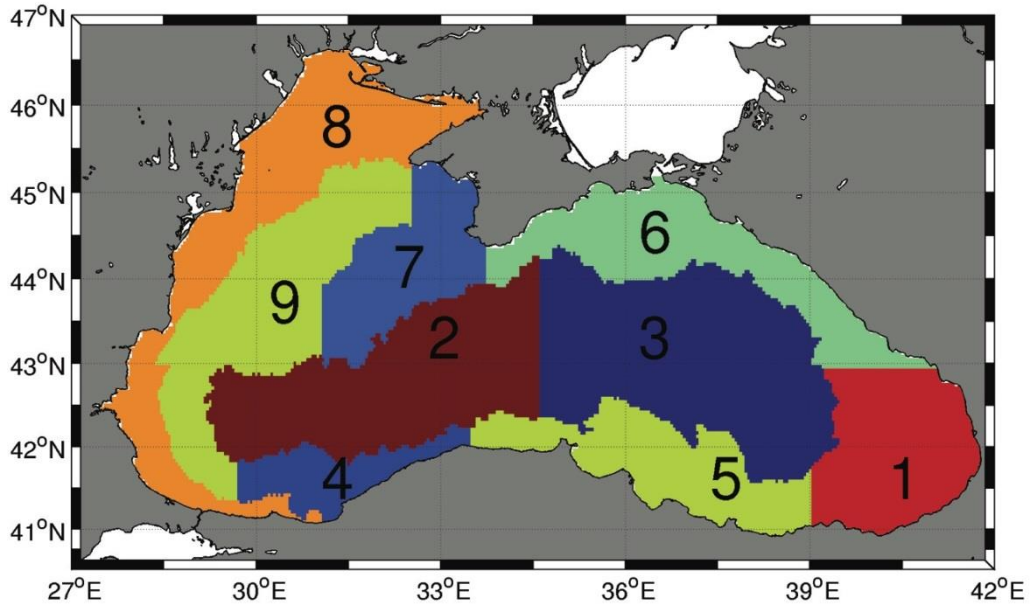

Figure 2 Black Sea sub-regions defined for analysis of regional variability in SST warming trends.

In the 1st spatial EOF mode (Figure 1) the Batumi eddy, located on the eastern coast near the Georgian coast is not clearly seen. However this anticyclonic eddy is known to be quasi-persistent (Oguz et al., 1993; Korotaev et al., 2003; Zatsepin et al., 2003) and is clearly visible in monthly SST climatology (1982-2012) maps with higher SST's in this region (not shown here). Therefore, it was selected as a separate region in the eastern Black Sea (Figure 2, region 1). The western and eastern cyclonic gyres are clearly seen in the SST 1st spatial mode and are clearly defined in previous studies with colder SST's due to their cyclonic nature (Oguz, 1993; Korotaev, 2003; Zatsepin et al., 2003) (Figure 2 regions 2 and3). Western Anatolian and Eastern Anatolian Coast have been defined as two separate regions, considering their mesoscale activity and riverine inputs. EOF results showed a clear distinction between the east and west Anatolian coasts (Figure 2, Figure 1 regions 4 and 5). The eastern Anatolian coast exhibits extensive anticyclonic mesoscale activity with quasi-persistent features such as Sinop and Kizilirmak eddies. Upwelling events have previously been documented for Western Anatolian Coast (Sur et al. 1994).

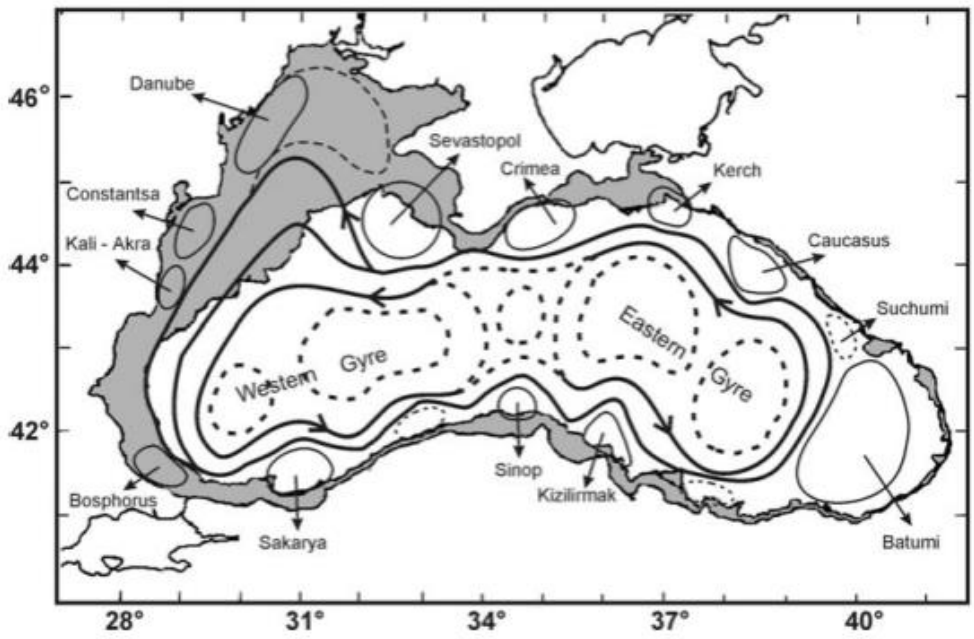

Figure 3 Black Sea general surface circulation adapted from Korotaev et al. (2003)

The Caucasian and Crimean Coasts have been combined to another region (Figure 2, region 6), considering the signal in the EOF results and its rich eddy-activity including Suchumi, Caucasian, Kerch and Crimean eddies (Korotaev et al. 2003; Zatsepin et al., 2003). The region around Sevastopol regions has been separated from this region, considering the intensity and impact of the Sevastopol eddy varies on its western edge. Therefore, even though the Sevastopol and Caucasian and Crimean regions seem as a single SST band at a glance, they were separated on the tip of the Crimean peninsula (Figure 2, region 7). The northwestern Shelf has been selected as another region considering it is reported to be an area of extensive atmospheric cooling (Tolmazin 1985) and a site for cold water formation (Ovchinnikov 1987, Ozsoy and Unluata 2003). Considering the impact of major rivers (such as Danube river) may extend all the way down to the Bosphorus Strait, this region was extended towards southeast of the straight (Figure 2, region 8). Shelf/deep transition was selected as the final region (Figure 2, region 9). This region was defined as a transition zone from shelf to deep and is partially influenced by baroclinic instability due to altering riverine fluxes from the Northwestern Shelf, the branching of the Rim Current, the intensity of Sevastopol eddy, as well as the Western Gyre.

2.3 Results

The statistical analysis of the sea surface temperature data in the entire Black Sea as well as in the nine different sub-regions defined above are presented here focusing on the seasonal and spatial variability of the warming trends, interannual variability, as well as sea surface temperature anomalies.

2.3.1 Seasonal and spatial variability

Maximum SST value for the whole Black Sea is recorded in August (24.3± 1.25 oC) and minimum value in February (6.45 ± 0.71 oC). The maximum mean SST (25.21 oC) was registered in the Batumi region and the minimum mean SST (4.97 oC) to northwestern shelf region. Standard deviations indicate the inter-annual variability is highest in autumn (σ=1.32 in October) and lowest in winter (σ=0.71 in February) over the Black Sea. As an indicator of spatial variability of SST in the Black Sea, SST amplitude between the regions has been calculated (difference between maximum and minimum average SST obtained in each region). This value (ΔT) varied from 0.98 oC in summer when the SST was homogeneous throughout the whole basin and up to 3.43 oC in winter, when intensive cooling is observed in the northwest. Largest SST amplitude is most commonly observed to be the difference between the northwestern and eastern Black Sea. Seasonal SST difference within each basin is also estimated and varies between 16.91 ^{o}C to 17.77 ^{o}C for all basins, except for northwestern shelf region, where this value is the highest with 19.05 ^{o}C.

Seasonal evolution of SST for each basin shows that Batumi region has the warmest and northwestern shelf has the coldest waters throughout the year (Figure 4). Western Anatolia has the second coldest temperatures during winter months whereas it becomes one of the warmest regions starting in autumn. Observations of local SST maxima in autumn and in May for this region have previously been reported by Ginzburg et al. (2000). There is an evident east- northwest SST gradient, with the Caucasian and Eastern Anatolia regions being much warmer and Sevastopol, Shelf and Shelf/deep transition regions being colder. Lower SST values in these three northwestern regions can be explained both via latitude, colder air temperatures and the prevailing winds. Although North-Western Shelf region is the coldest during most of the year, the Sevastopol region becomes the coldest region in May-July.

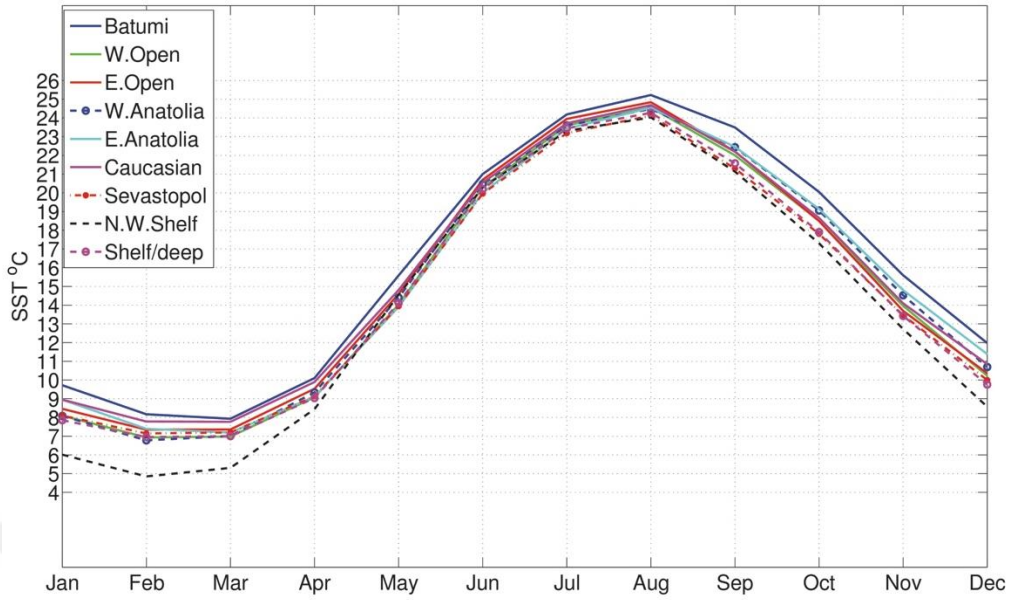

Figure 4 Mean seasonal evolution of SST averaged over 1982-2012 average in each region.

2.3.2 Inter-annual trends

Temporal evolution of sea surface temperatures in the entire Black Sea shows a positive SST trend of 0.078±0.038 ^{o}C/year the whole period under investigation (1982-2012) (Figure 5). OISST and Hadley SST datasets are also used to calculate SST trends. OISST and Hadley SST data have positive trends of 0.06 ^{o}C/year and 0.05 ^{o}C/year respectively. OISST and Hadley SST datasets extend until 2015. Their warming trends for 1982-2015 were the same as for 1982-2012 periods. Considering 1982-1998 period was dominated by negative SST anomalies (see **2.3.4 SST** Anomalies) and 1999-2012 periods was dominated by positive anomalies, these were considered as two different periods. Black Sea SST trend for 1982-1998 was 0.066±0.092 ^{o}C/year and trend for 1999-2012 was 0.120±0.127 ^{o}C/year. Both periods have positive SST trends, however, the trend of the second period is almost twice of the first one.

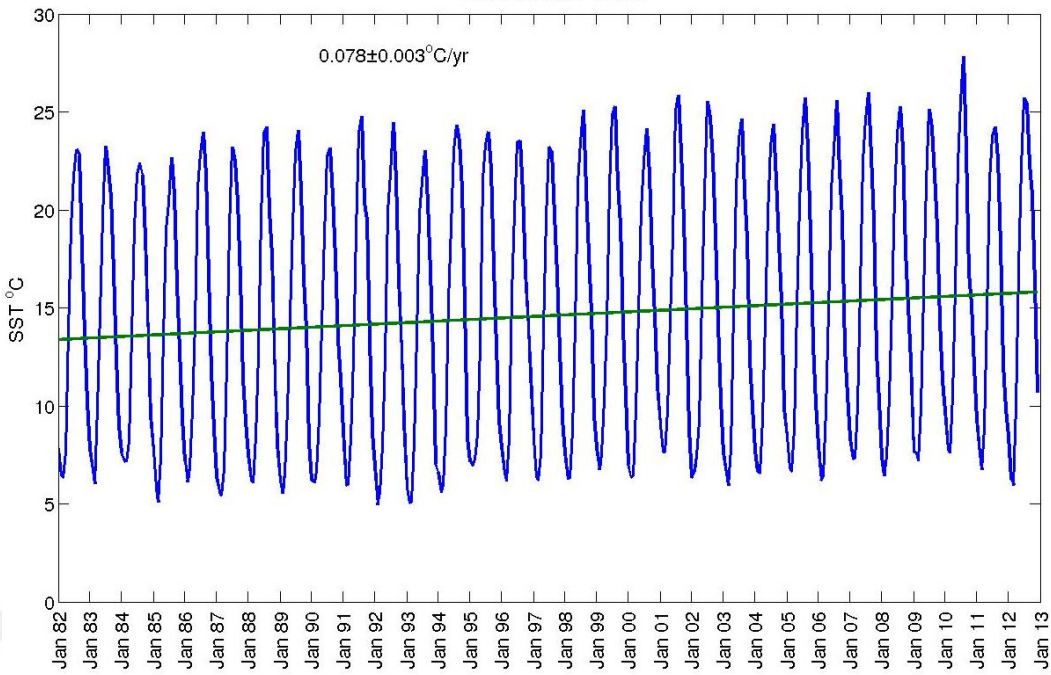

Figure 5 Interannual variability of monthly mean SST from January 1982 to December 2012 averaged over the entire Black Sea.

Calculating regional trends it can be shown that the Eastern Cyclonic Gyre and Caucasian&Crimean coast have the highest warming trends and Western Anatolian Coast has the lowest warming trend (Table 1). Seasonal trends calculated for the whole Black Sea (Figure 5) reveal high warming rates from 0.064 ^{o}C/year in Fall to 0.084 in summer but with relatively low warming rates in winter (0.038 ^{o}C/year) (Table 2). After separating the 31-year data set into two separate periods as detailed above, a negative trend (-0.0133 ^{o}C/year) was found for winter in 1982-1998. These results suggest that the warming of the Black Sea occurs mainly in summer and spring.

Table 1 SST trends of each sub-region in the Black Sea from January 1982 to December 2012.

Basin	Annual rate (^{o}C/year)
Black Sea	0.0780±0.003
1	0.0756±0.003
2	0.0744±0.003
3	0.0828±0.003
4	0.0708±0.003
5	0.0780±0.003
6	0.0864±0.003
7	0.0780±0.003
8	0.0780±0.003
9	0.0756±0.003

Table 2 Seasonal SST trends for Black Sea from 1982 to 2012.

Season	Annual rate (^{o}C/year) (1982-2012)	1982-1998	1999-2012
Winter	0.0381	-0.0133	0.0340
Spring	0.0740	0.0621	0.1149
Summer	0.0839	0.0486	0.0617
Fall	0.0642	0.0888	0.0232

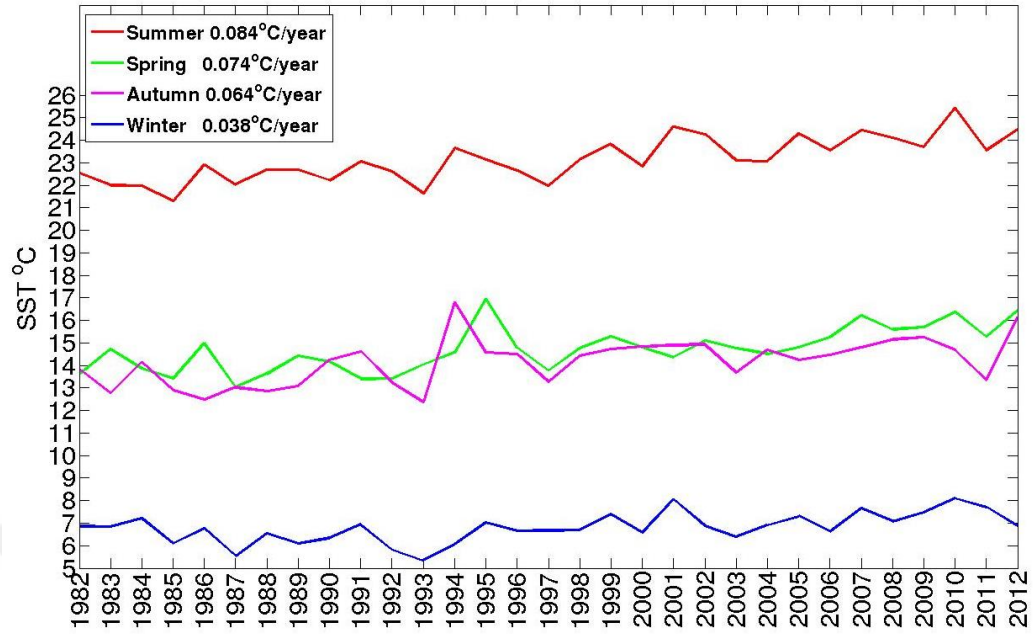

Figure 6 Inter-annual SST variability of seasons for Black Sea from 1982 to 2012.

To explore the regional and temporal variability in detail, trends were calculated separately for each month and in each region (Figure 6, Table 3). These trends exhibit a wide monthly variability for different regions. The north-western shelf and Shelf/deep transition regions show the highest warming trend in January. In other words the coldest part of the Black Sea, namely the Northwestern part, has the highest warming rate for January during 1982-2012.

Table 3 SST trends for each region and month. Trends significant at the 0.05 significance level are marked in bold.

Region/Month	1	2	3	4	5	6	7	8	9	10	11	12
1	0,04	**0,04**	0,02	0,04	**0,08**	**0,08**	**0,09**	**0,09**	**0,06**	**0,07**	**0,07**	**0,07**
2	0,03	**0,03**	**0,04**	**0,06**	**0,09**	**0,09**	**0,1**	**0,10**	**0,06**	0,04	0,03	**0,05**
3	**0,05**	**0,05**	**0,04**	**0,06**	**0,09**	**0,09**	**0,08**	**0,10**	**0,06**	**0,07**	**0,06**	**0,07**
4	0,03	**0,04**	**0,05**	**0,06**	**0,07**	**0,09**	**0,09**	**0,10**	**0,05**	0,04	0,03	0,03
5	0,03	**0,04**	**0,04**	**0,06**	**0,09**	**0,08**	**0,09**	**0,10**	**0,06**	**0,06**	**0,06**	**0,05**
6	**0,05**	**0,05**	**0,03**	**0,06**	**0,08**	**0,08**	**0,09**	**0,10**	**0,06**	**0,1**	**0,08**	**0,09**
7	**0,04**	**0,04**	**0,04**	**0,05**	**0,09**	**0,09**	**0,09**	**0,09**	**0,05**	**0,07**	0,05	**0,07**
8	**0,05**	**0,03**	0,03	**0,05**	**0,08**	**0,09**	**0,1**	**0,10**	**0,04**	**0,06**	**0,06**	**0,07**
9	**0,05**	**0,04**	**0,05**	**0,05**	**0,09**	**0,09**	**0,1**	**0,09**	**0,04**	0,05	0,04	**0,06**

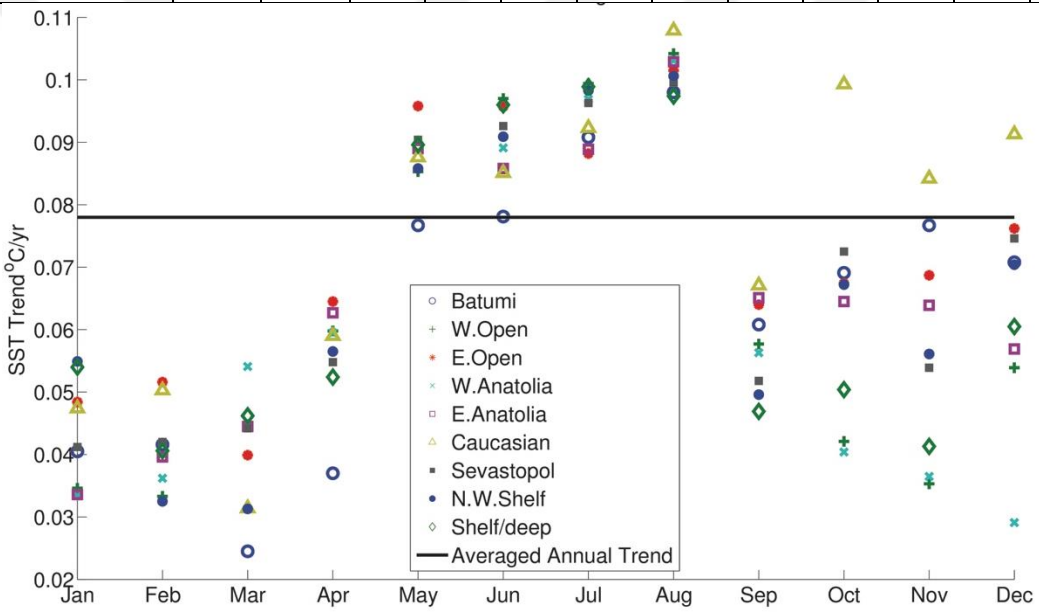

Figure 7 Linear trends for each month in the regions. Solid line represents the average annual SST trend.

2.3.3 EOF Results

The EOF technique was applied to investigate the spatio-temporal variability of sea surface temperature in the Black Sea. The variance explained in the first three modes represents 97% of the total variance. The first mode corresponds to most of the SST variability (95.7%). Its spatial structure (Figure 2) shows all positive values with higher magnitudes in the northwestern shelf, medium magnitudes around the eastern and western cyclonic gyres and Rim current, and lower magnitudes around the eastern

Turkish coast, Batumi, Caucasian and Crimean coasts and Sevastopol. Its temporal mode (Figure 8) represents a seasonal cycle with interannual variability. Positive (negative) values in summer (winter) produce higher (lower) temperatures over the Black Sea.

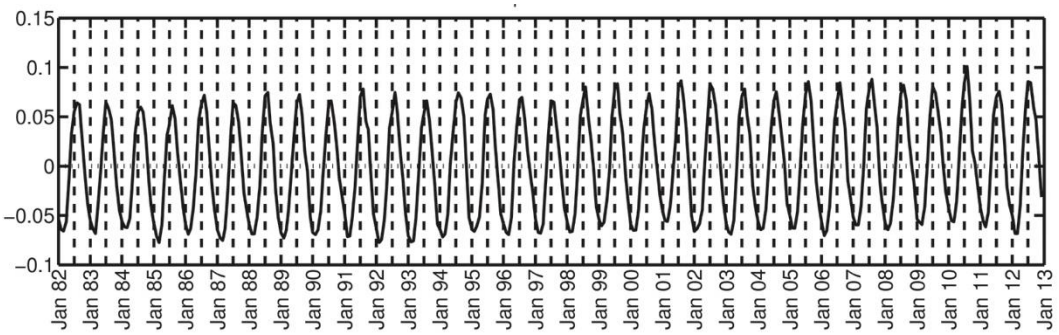

Figure 8 First temporal EOF mode of SST

The second mode represents a low percentage of the total variance (1.3% or 30% of the total variance excluding the first mode). Its spatial mode (Figure 9) represents a separation of the eastern Black Sea. Positive magnitudes are observed in the northwestern shelf and the deeper basin whereas slightly negative values are observed on the coasts west of 37^{o}E and negative values on the eastern Black Sea. Corresponding temporal evolution (Figure 10) mostly exhibits negative magnitudes. Positive magnitudes of the temporal evolution represent relatively colder conditions for the eastern Black Sea and warmer conditions for the northwestern shelf. Intense negative magnitudes are observed in summer and fall, resulting in decreased SST's in the northwestern shelf and increased SST's in the eastern basin. This mode represents the opposition of phase between the northwestern shelf and eastern basin as a result of atmospheric conditions and particularly sporadic events. For example, being one of the coldest years in the last decade, 2003 is represented by positive magnitudes in June-July, meaning the eastern basin exhibited reduced SST.

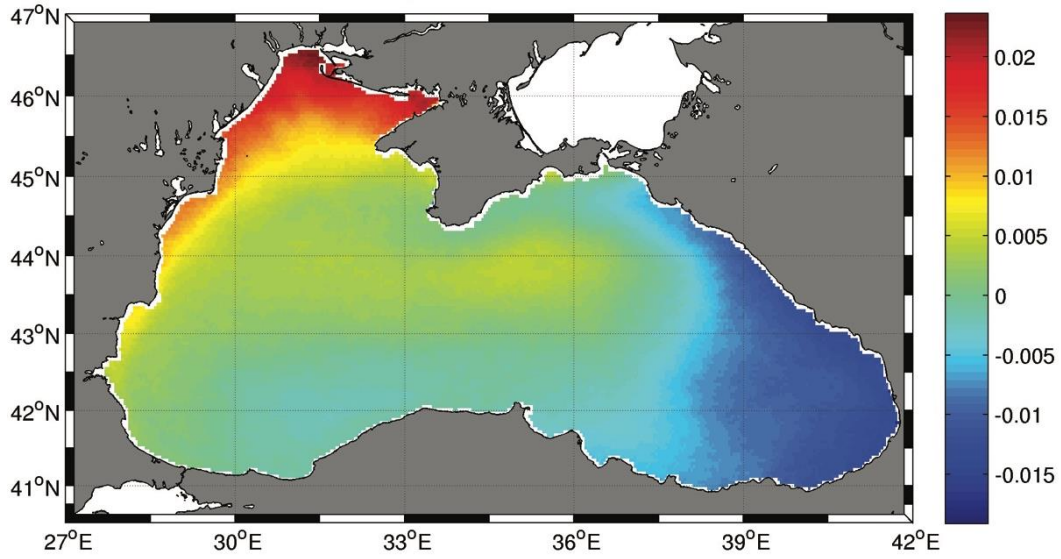

Figure 9 Second spatial EOF mode of SST

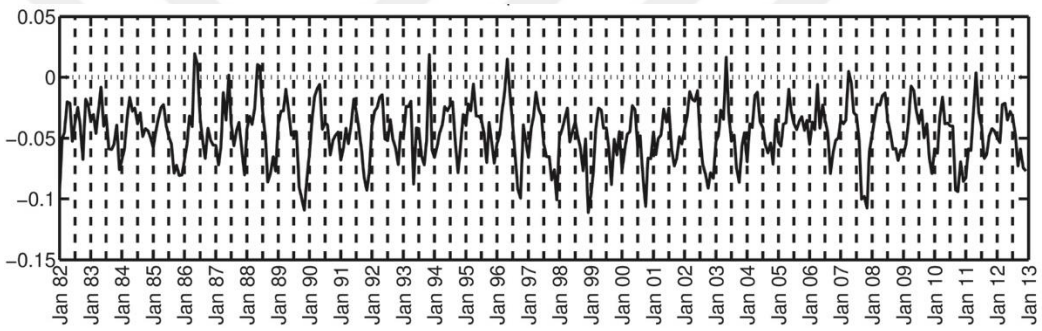

Figure 10 Second temporal EOF mode of SST

The third mode explains 0.2% of the total variance (or 5% excluding the first mode). Its spatial mode (Figure 11) displays a general south-west to north-east phase separation with positive magnitudes on the northeastern part and negative magnitudes on the southeastern part of the Black Sea. Positive EOF magnitudes are also observed around the river mouths in the northwestern shelf. The corresponding temporal mode (Figure 12) is highly variable in amplitude. This mode might be assumed to reflect a combined impact of river discharges on the northwestern shelf and prevailing wind regimes (southwestern and northeastern) on the Black Sea. However, correlations between satellite derived wind components (zonal and meridional wind speed, wind stress and wind stress curl) and SST temporal mode 3 were fairly low (ranging from 0.2 to 0.3).

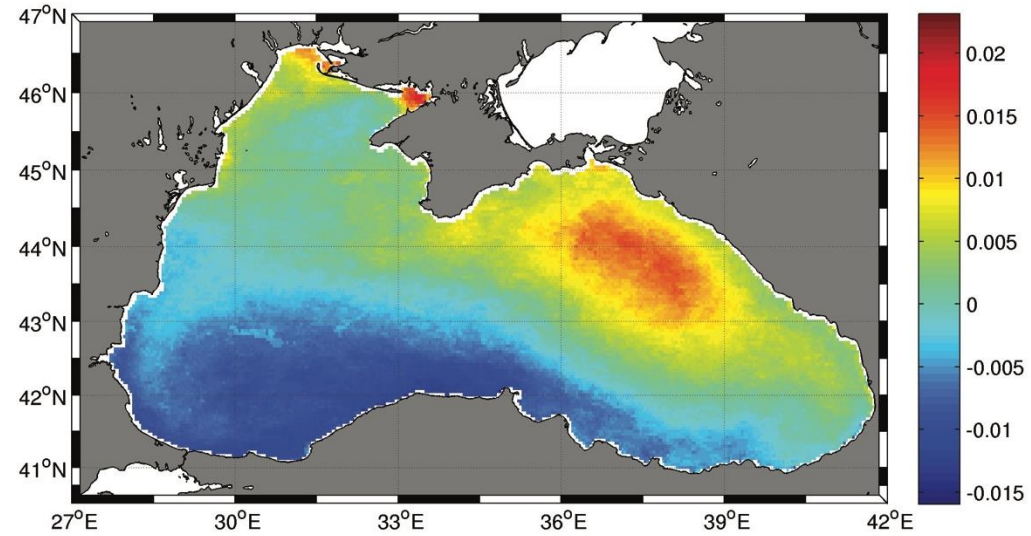

Figure 11 Third spatial EOF mode of SST

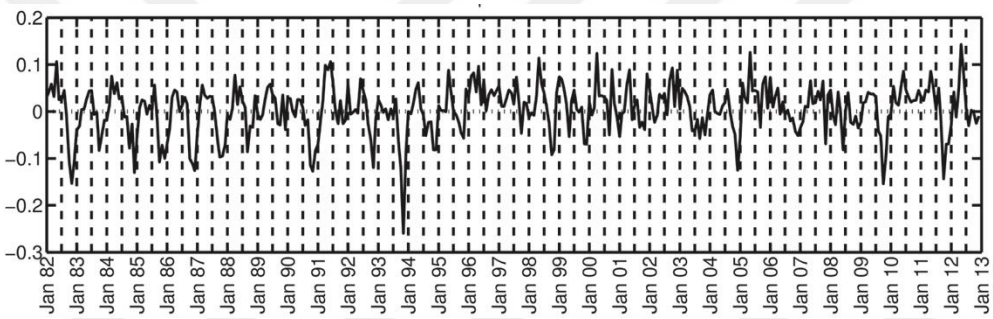

Figure 12 Third temporal EOF mode of SST

2.3.4 SST Anomalies

Monthly SST anomalies have been calculated for entire Black sea and each of its sub-basins as the difference between the monthly temperature and the climatic mean for that month. For the whole period 1982-2012, there is a clear shift from negative anomalies to positive anomalies. 1982-1998 is dominated by negative anomalous years whereas 1999-2012 is dominated by positive anomalous years (Figure 7). Negative (positive) anomalies constitute 75 %(25%) of total number of anomalies for 1982-1998 whereas for 1999-2012, negative (positive) anomalies constitute 22 %(78%) of total anomalies. This clear shift from negative to positive anomalies is observed in each region as well. Percentages for different regions have pretty close values to entire Black Sea's values: negative (positive) anomaly percentages vary 25 to 29 %(71-75%) for 1982-1998 and for 1999-2012 they vary from 70 to 79 %(21-30%). Figure 13 shows time-series distribution of anomalies for the whole Black Sea. Maximum positive anomalies are

seen on August 2010 (+3.5 ^{o}C), October 1994 (+3^{o}C), and October 2012 (+2.7 ^{o}C) whereas maximum negative anomalies are seen on July 1985 (-3^{o}C), December 1993 (-2.7 ^{o}C) and May 1987 (-2.4 ^{o}C). Regional anomalies possess larger values than the maxima and minima for the whole basin. The largest positive anomaly was detected in Sevastopol region on August 2010 (+3.78 ^{o}C) and the largest negative anomaly was obtained in Caucasian&Crimean region on July 1985. July 1985 has the largest negative anomaly values for all regions except Batumi and Western Anatolia regions which had their negative maxima on October 1993 and October 1988 respectively. Similarly, August 2010 had the largest positive anomaly values for regions 5-9, whereas for regions 2-4 it was October 1994 and for Batumi it was May 2012.

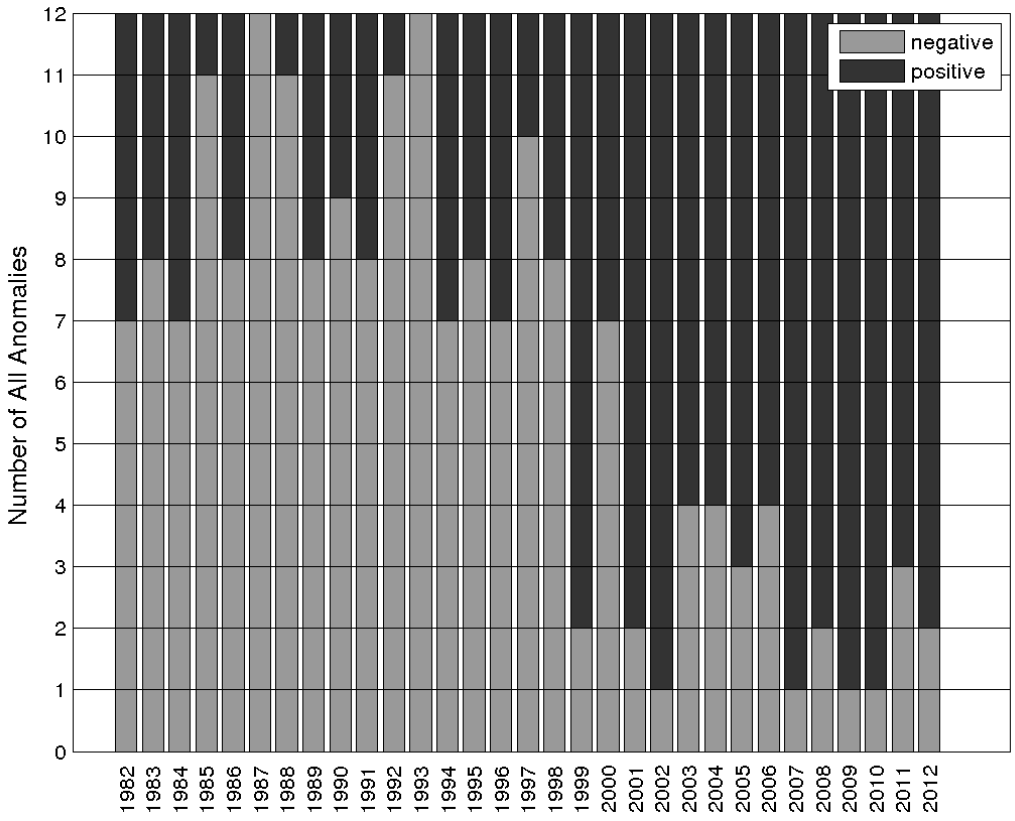

Figure 13 Monthly SST Anomalies for Black Sea.

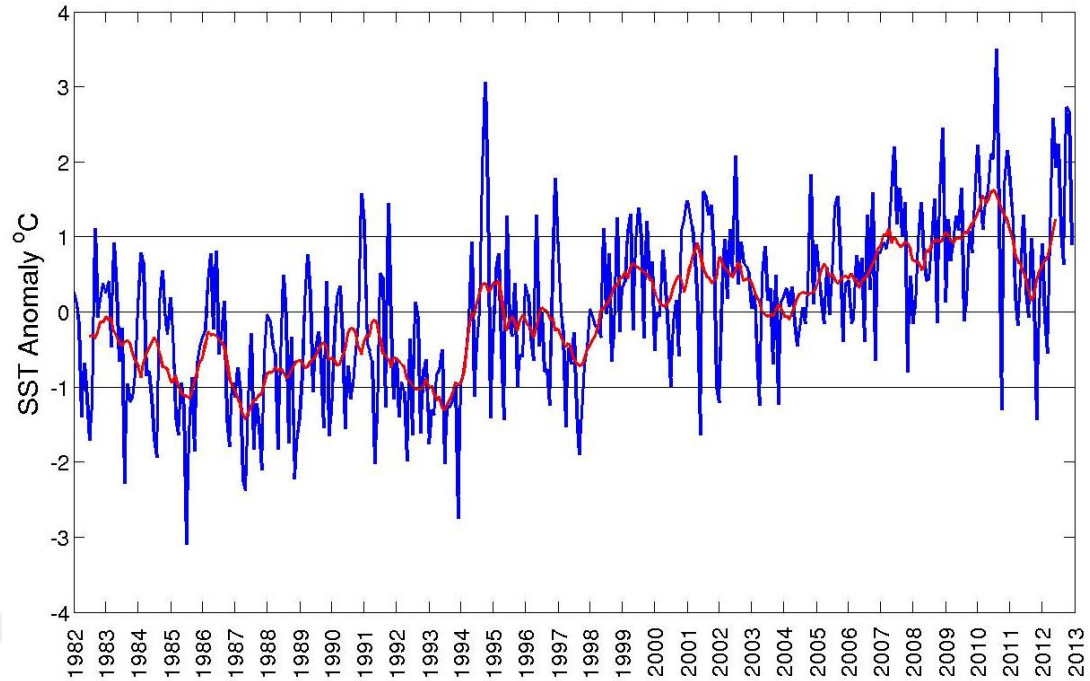

Figure 14 Inter-annual variability of monthly SST anomalies over the Black Sea. Red line represents low-pass filtered (moving average with a window of 12 months) SST anomalies. Solid black lines marked at -1°C and 1 °C represent threshold for intense anomalies.

In order to identify intense anomalous years, a threshold for the anomalies was set. Standard deviations of monthly SST's for the period range from 0.7 in winter to ~1.7 °C in autumn and most of the standard deviation is around 1.0 °C . Therefore 1.0 °C was used as a threshold to identify extreme anomalies. Extreme anomalies with monthly average differences of more than 1 °C from the 31 year mean gave 69 positive and 69 negative months. Inter-annual and monthly variability of intense anomalies over the Black Sea are given in Figure 15 and Figure 16 respectively.

Largest numbers of positive intense anomalies were observed in 2001, 2010 and 2012 and largest numbers of negative intense anomalies were observed in 1985, 1987 and 1993. Negative intense anomalies constitute majority before 1998 and positive intense anomalies after 1998, with the exception of 2003 with no positive intense anomalies. Although 2003 has positive anomalies (Figure 13), it does not have any intense positive anomalies and instead 2 months (April and November) of intense negative anomalies making it an exceptional year for 1999-2012.

Largest numbers of intense anomalies (Figure 16) were observed in October (18 years) and June (16 years). Winter (January, February, and March) has the lowest number of intense anomalies. This distribution of intense anomalies results in a pretty similar with the annual distribution of SST standard deviations (Figure 17).

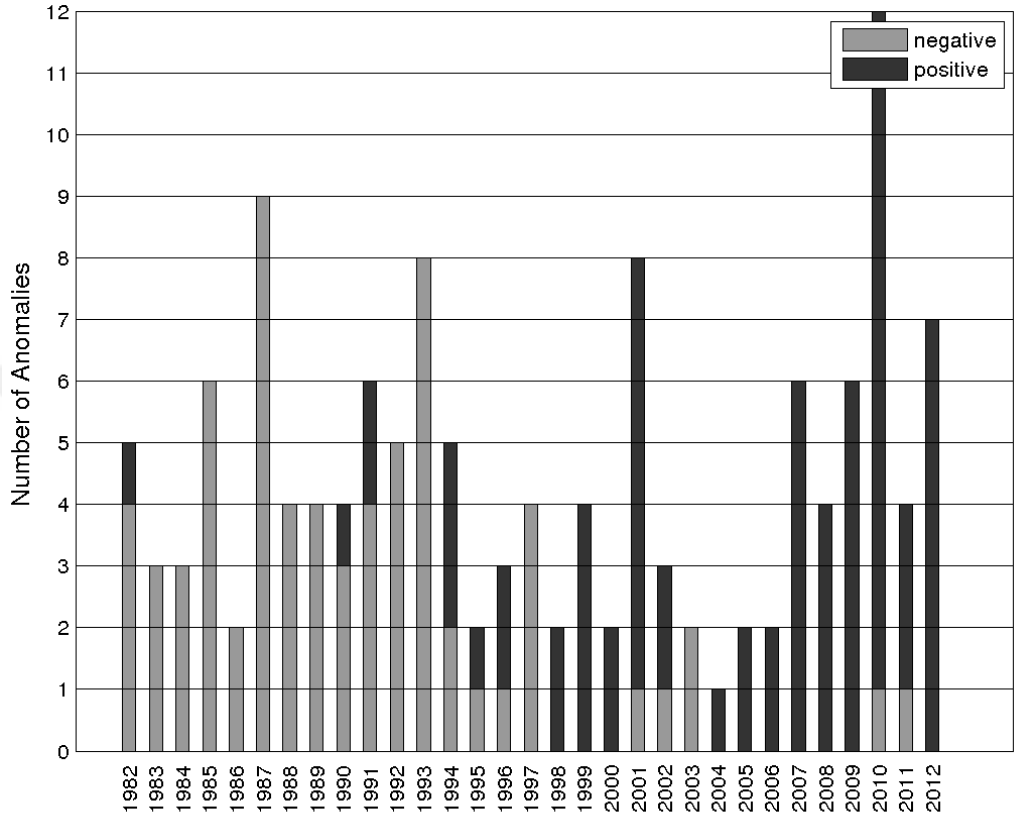

Figure 15 Inter-annual variability of intense SST anomalies (exceeding -1 ^{o}C and 1 ^{o}C).

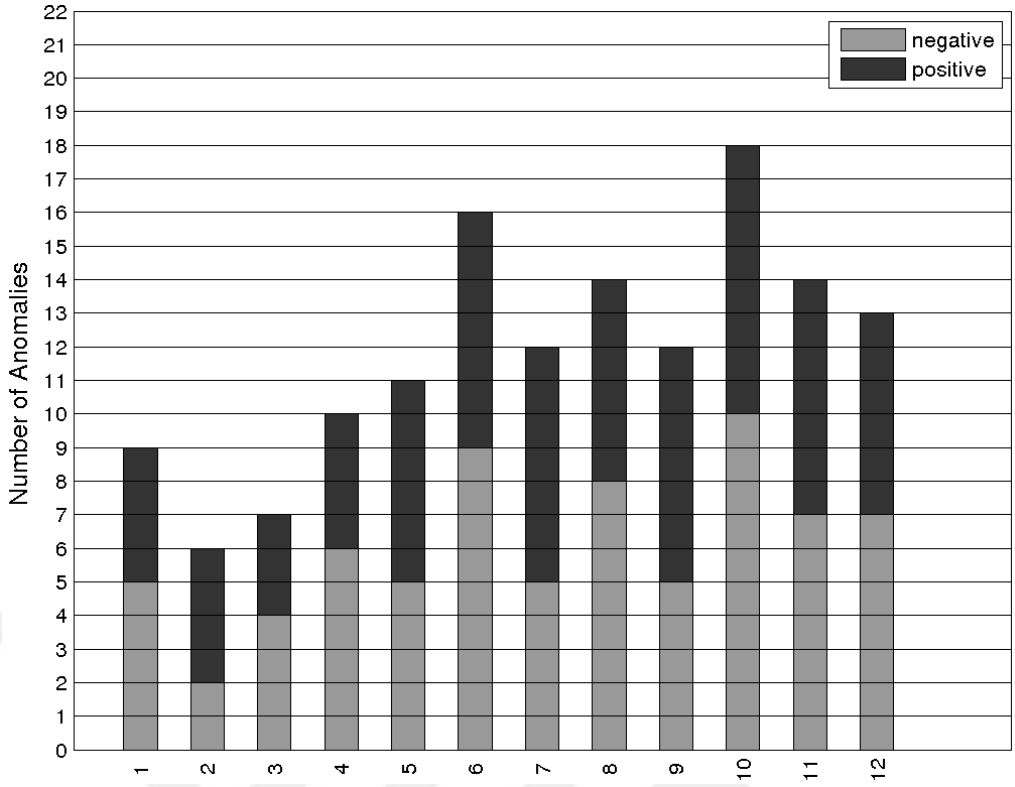

Figure 16 Monthly variability of intense SST anomalies (exceeding -1 ^{o}C and 1 ^{o}C).

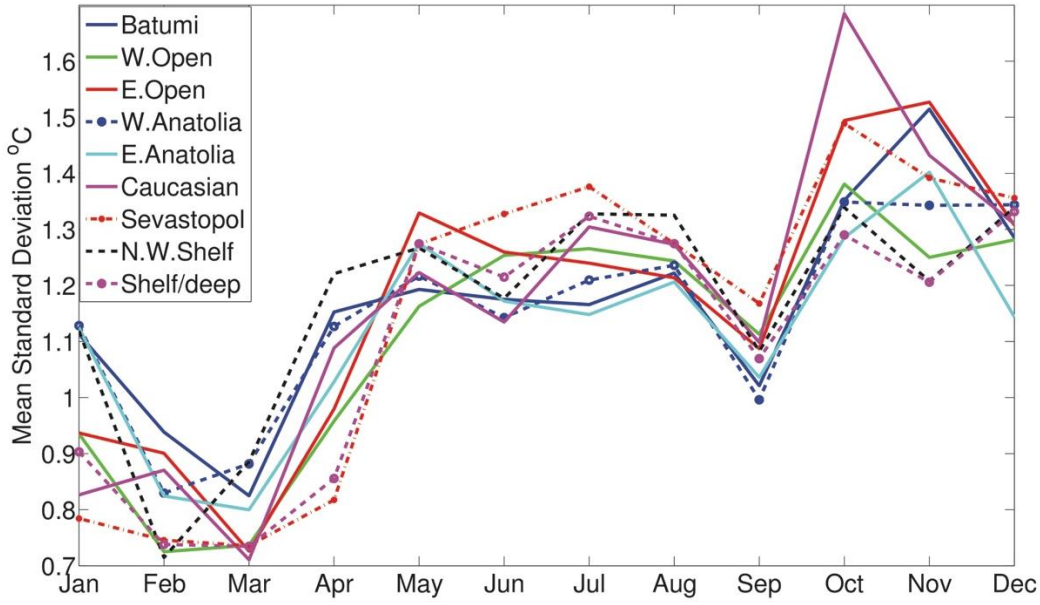

Figure 17 Annual distribution of SST standard deviation for each region

Inter-annual distributions of intense anomalies for each region are given in Figure 18-Figure 26. 2001, 2010 and 2012 have the largest number of positive intense anomalies in each region. Although regional anomalies are generally parallel with whole basin anomalies, regional anomalies show differences from Black Sea anomalies. In 1982,

Eastern Gyre and Eastern Anatolia do not have any positive intense anomalies, whereas all the other regions and the Black Sea show positive intense anomalies. Although there are no intense positive anomalies for the whole basin in 1983, Batumi, W.Anatolia and Shelf regions have positive intense anomalies. Similarly, for 1984 there are no positive intense anomalies in the whole Black Sea and all regions show only negative intense anomalies except Western Anatolian region, which has positive intense anomalies. In 1985 there are no positive intense anomalies neither in Black Sea nor in any of the regions. In 1986, Shelf and Shelf/deep transition regions have positive intense anomalies and Western Anatolian only reveals positive intense anomalies and no intense negative anomalies. 1987 and 1988 are completely dominated by intense negative anomalies in each region. In 1989, eastern part of the Black Sea (Batumi, Eastern Gyre, Eastern Anatolia, and Caucasian) and Shelf regions show positive intense anomalies. Contrary to 1989, in 1990 eastern regions (Batumi, Eastern Gyre and Caucasian) reveal only negative intense anomalies. 1991 has positive intense anomalies in every region except the Northwestern Shelf. In 1992, only region displaying any positive intense anomaly is the Western Anatolia. In 1993, only Batumi and Western Anatolia have positive intense anomalies. 1994 reveals many positive intense anomalies in the whole basin as well as in each region. Although negative anomalies still dominate in 1995; there are also positive intense anomalies in each region. In 1996, Batumi, Eastern Gyre and Caucasian regions show only positive intense anomalies. 1997 is dominated by negative intense anomalies. Only Batumi region has positive intense anomaly in 1997. In 1998, when we look at whole basin (Figure 13), there are no negative anomalies; however there are a few negative intense anomalies in regions. In 1999, only negative intense anomaly observed is in the Caucasian region. In 2000, eastern regions (Batumi, E.Gyre, E.Anatolia, and Caucasian) do not show any negative intense anomalies. 2001 is a year dominated by positive intense anomalies but also possesses a few negative intense anomalies in each region. Although 2002 is not as intense as 2001, it is also dominated by positive intense anomalies. In 2002, Caucasian, Sevastopol and Shelf/deep transition regions possess only positive intense anomalies. 2003 is the coldest year in this sub-period (1999-2012) with only negative intense anomalies over the Black Sea. Even though 2003 is the coldest in this period, there are still a few positive intense anomalies in each region except Batumi. In 2004, only Batumi, Caucasian and Sevastopol regions show negative intense anomalies. In 2005, Western Gyre, Western Anatolia and Eastern Anatolia have negative intense anomalies. In 2006, only the deeper parts of the Black

Sea (Western and Eastern Gyre regions) show negative intense anomalies. 2007 has much more positive intense anomalies than 2005&2006 over the entire Black Sea. Northwestern regions (Western Gyre, Sevastopol, Northwestern Shelf and shelf/deep transition regions) show negative intense anomalies. 2008 and 2009 are dominated with positive intense anomalies in every region as well as the entire Black Sea. 2010 has the maximum number of positive intense anomalies in the entire study period. It also reveals a few negative anomalies in different regions. Only Batumi and Caucasian regions don't show any negative intense anomalies in 2010. Despite being weak compared to 2010, 2011 is also dominated by positive intense anomalies; however it also contains negative intense anomalies in each region. Similarly 2012 is dominated by positive intense anomalies and Batumi is the only region displaying any negative intense anomaly.

In terms of negative intense anomalies, 1985-1987 and 1992-1993 are the predominant periods which are followed by 1997. Negative intense anomaly period is weakened starting from 1994. 1994-1996 is relatively a weaker cold period followed by 1997 an intense cold year. Although 1998 contains only positive intense anomalies, it is not the start of the warmer period, instead it is 1999. Despite 1998 contains no negative intense anomalies (exceeding $-1^{o}C$), it contains negative anomalies (Figure 13). 1999 is dominated by positive anomalies but 2000 contains more negative anomalies. 2001 is dominated by intense anomalies. Positive intense anomalies start with 2001, followed by 2002 which is also warm, but not as intense as 2001. It is then followed by a cold year 2003, followed again by a short transition period 2004-2006 which are dominated by positive anomalies but not so many intense positive anomalies. 2007-2010 is the predominant positive intense anomaly period (with 2010 being the warmest) followed by a milder 2011 and again a stronger positive intense anomaly in 2012.

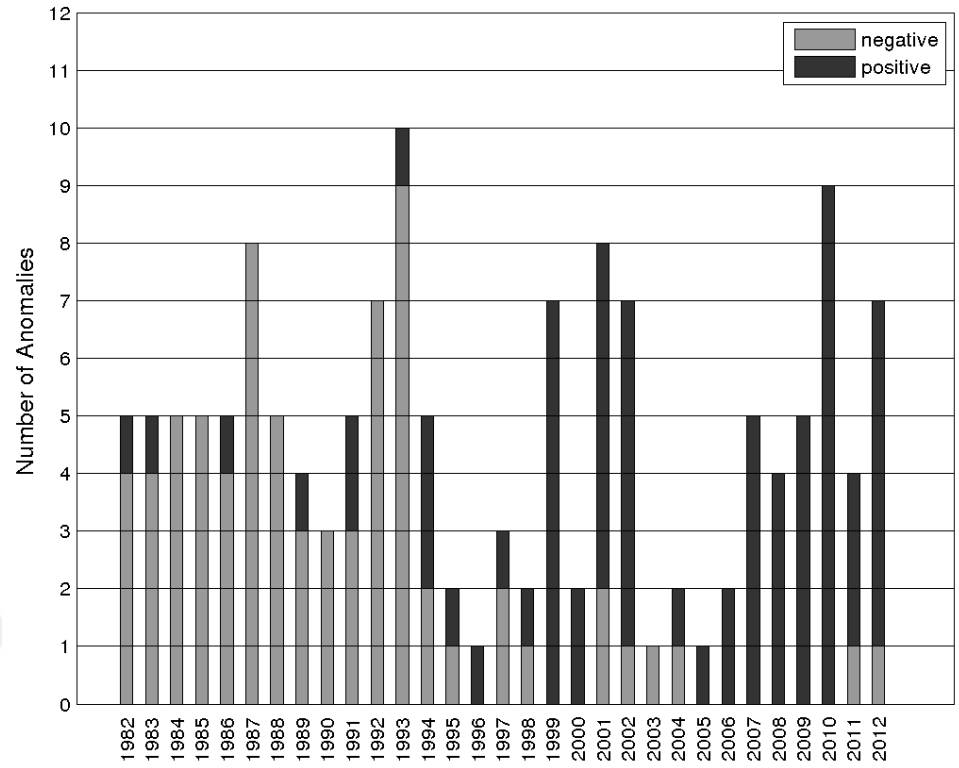

Figure 18 Inter-annual distribution of intense SST anomalies for Batumi

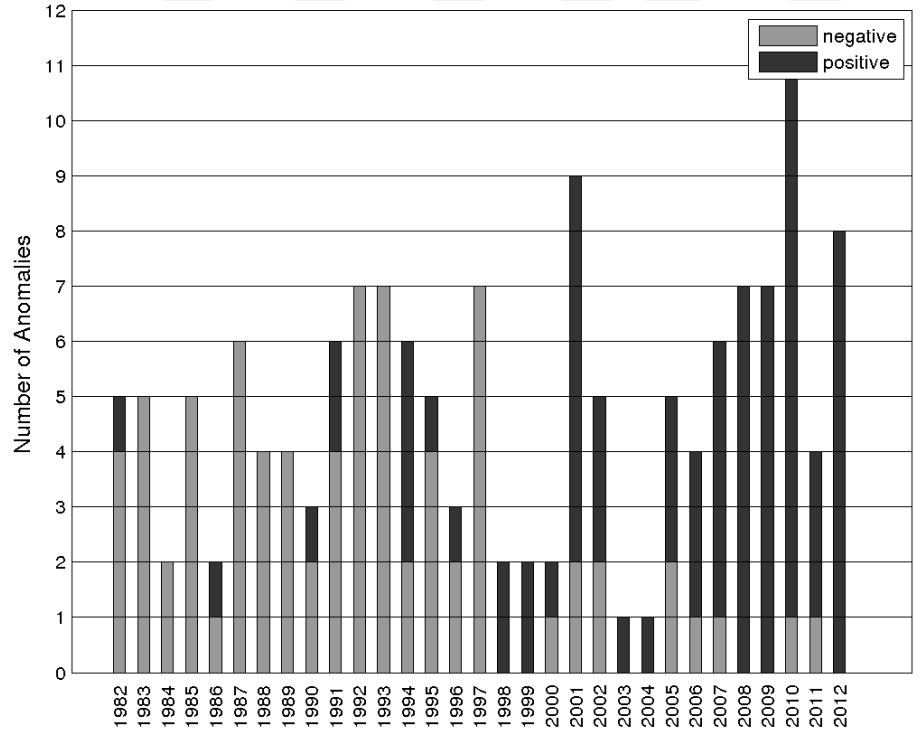

Figure 19 Inter-annual distribution of intense SST anomalies for Western Gyre

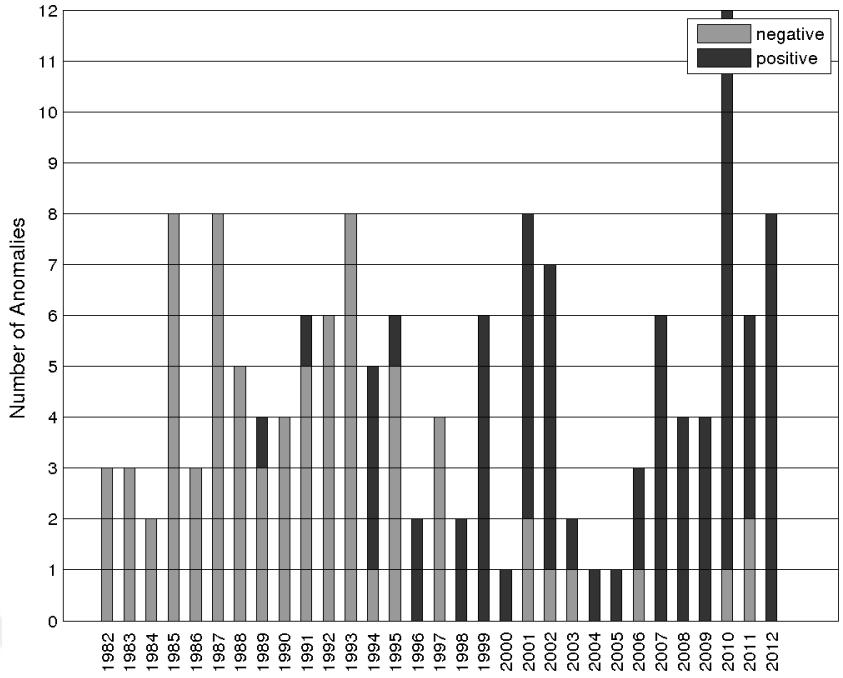

Figure 20 Inter-annual distribution of intense SST anomalies for Eastern Gyre

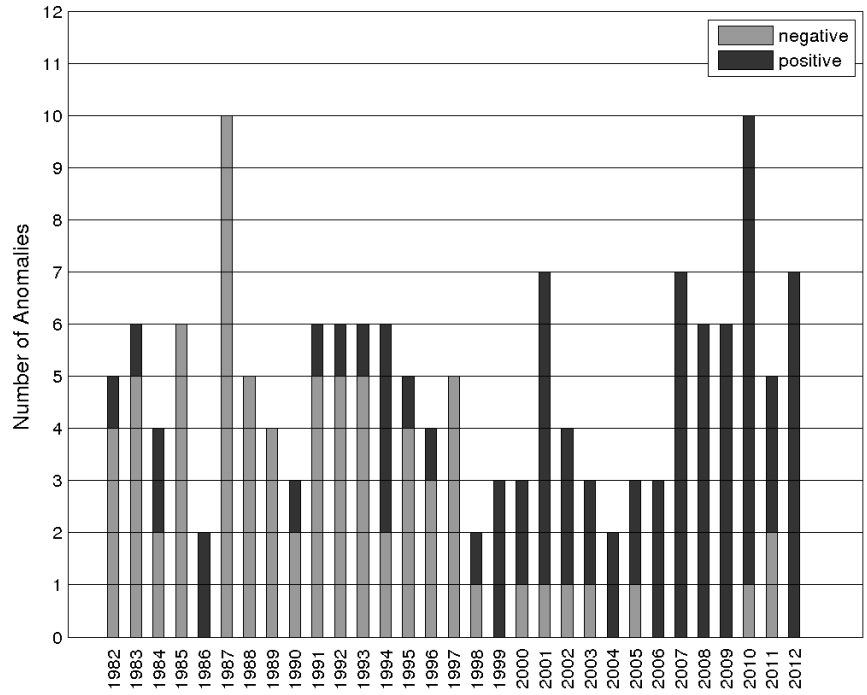

Figure 21 Inter-annual distribution of intense SST anomalies for Western Anatolia

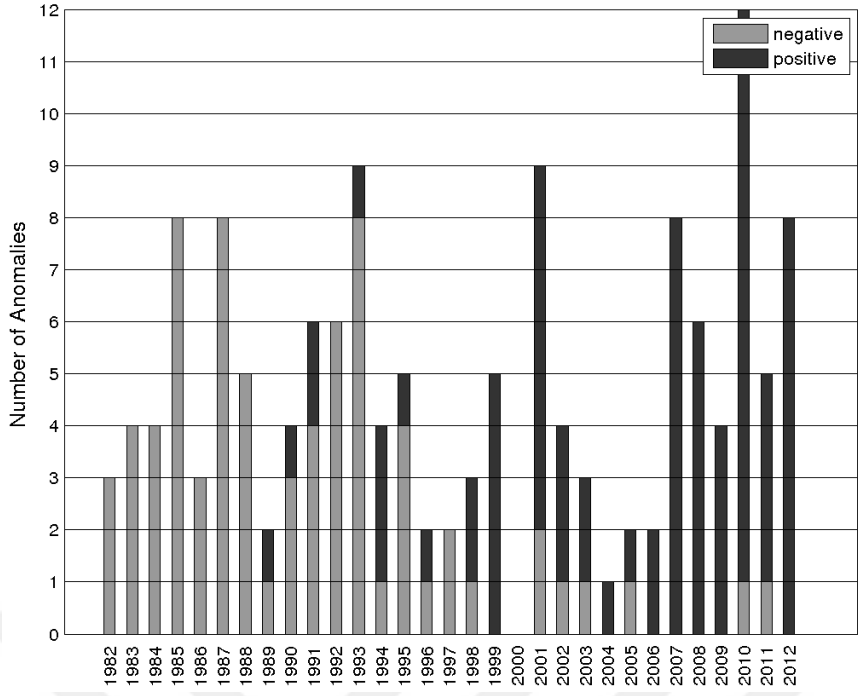

Figure 22 Inter-annual distribution of intense SST anomalies for Eastern Anatolia

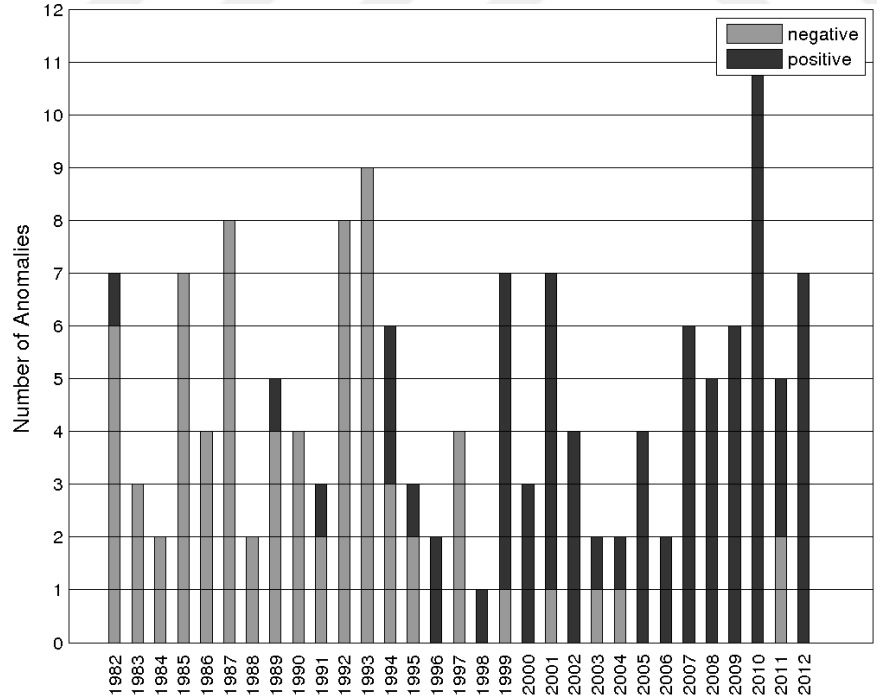

Figure 23 Inter-annual distribution of intense SST anomalies for Caucasian&Crimean coast

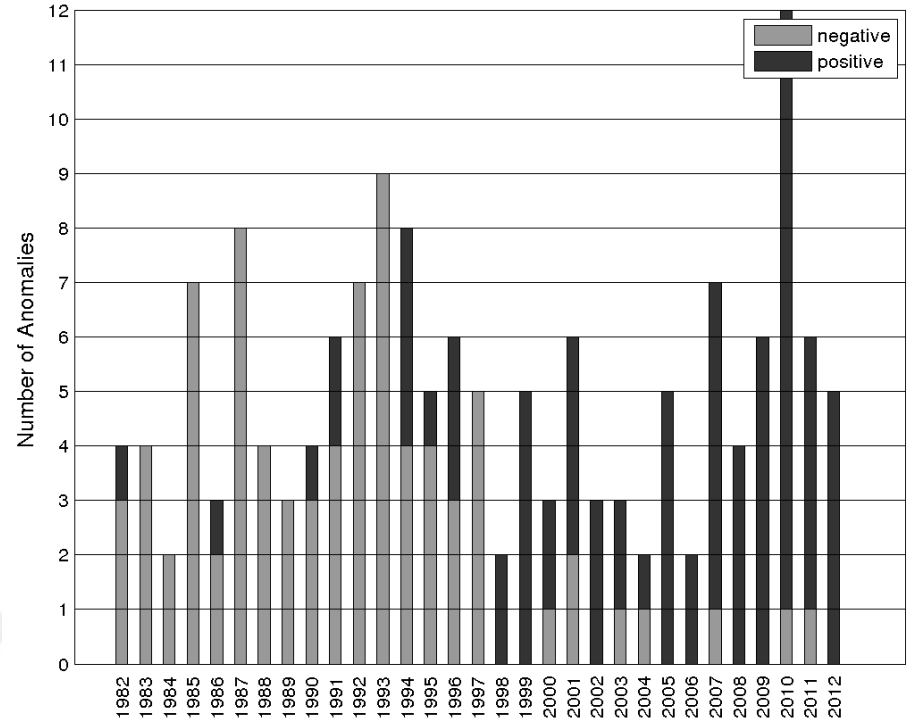

Figure 24 Inter-annual distribution of intense SST anomalies for Sevastopol

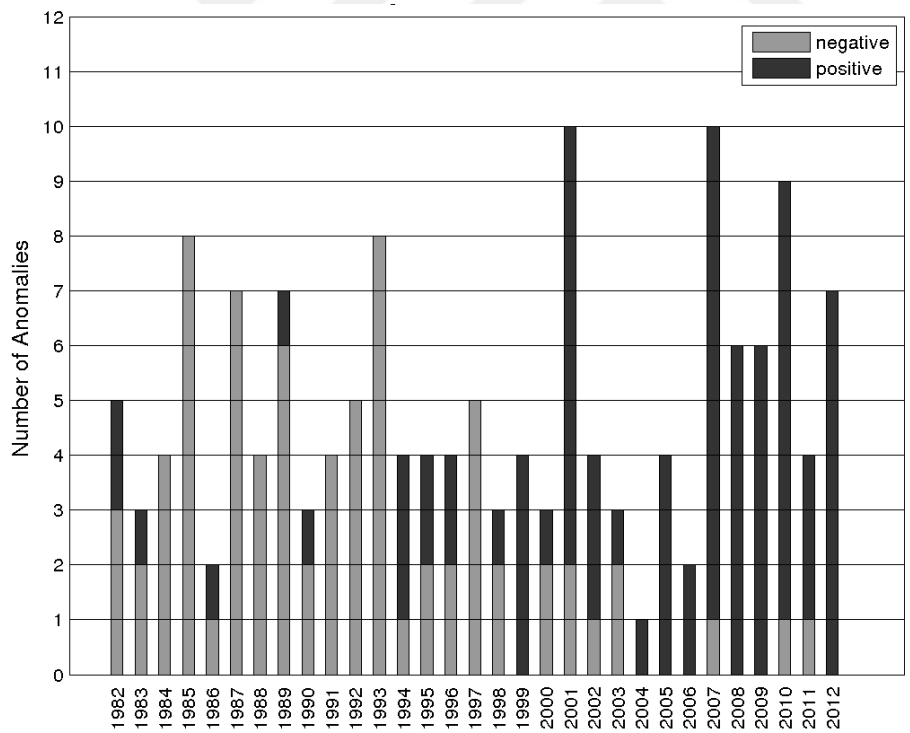

Figure 25 Inter-annual distribution of intense SST anomalies for Shelf

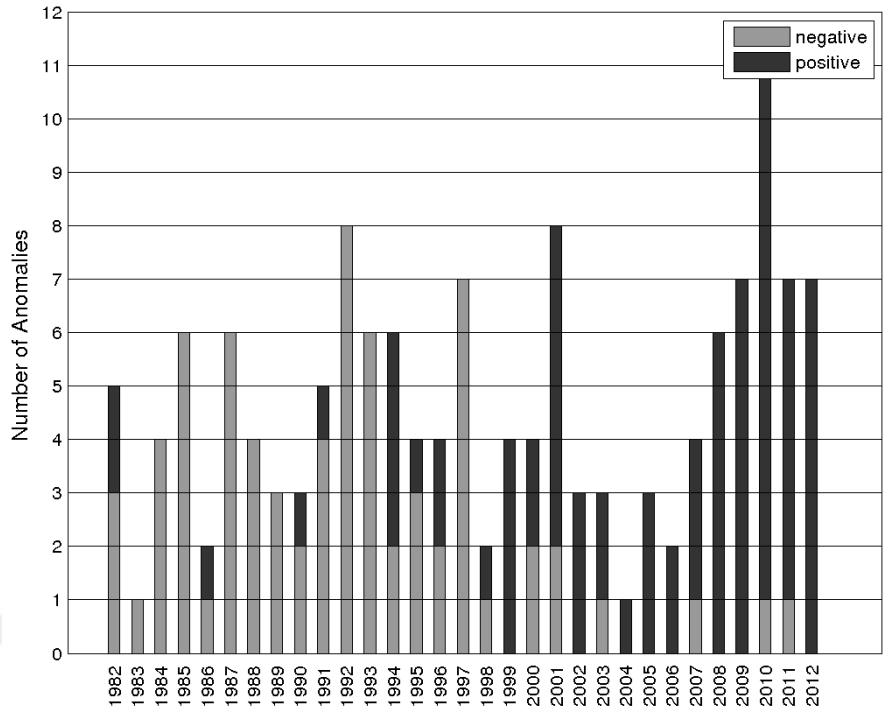

Figure 26 Inter-annual distribution of intense SST anomalies for Shelf/deep transition

2.3.5 EOF on SST Anomalies

The majority of variance is explained by 1st EOF mode of SST, which exhibits the seasonal signal of SST (Figure 8). In order to discriminate processes beyond the seasonal signal, EOF analysis was conducted on SST anomalies. However, the results were dominated by high-frequency signals. Therefore, a low-pass filter (1 year moving average) was applied prior to EOF analysis. The following dataset will be referred to as the filtered sea surface temperature anomalies (F-SSTA) from hereafter.

The first three modes of F-SSTA explain 93% of the total variance. First F-SSTA mode represents 89% of total variance. Its spatial structure (Figure 27) exhibits positive magnitude all over the Black Sea with higher magnitudes on the northeastern and northwestern parts. The corresponding temporal signal (Figure 28) represents a decadal warming trend with oscillations of minima and maxima every three to six years. This mode represents the overall warming of the Black Sea, and marks more pronounced warming particularly on the northeastern coast. This is an expected result considering this region has the highest warming trends.

Second F-SSTA mode explains 2.5% of total variance (20% excluding the first mode). Its spatial structure (Figure 29) is slightly similar to the 2nd EOF mode of SST (Figure 9). However the F-SSTA mode represents a more pronounced northeastern-

southwestern phase differentiation, whereas the unfiltered data shows phase differentiation between the eastern and northwestern Black Sea. The corresponding temporal mode (Figure 30) displays biyearly maximum minimum oscillations. Positive (negative) magnitudes of the temporal mode results in enhanced positive (negative) SST on the northeastern Black Sea and negative (positive) SST on the southwestern Black Sea.

Third F-SSTA mode represents only 1.5% of total variance (or 14% of total variance excluding the first mode). Its spatial structure (Figure 31) exhibits positive magnitudes on the northern Black Sea and negative magnitudes on western and eastern gyre positions. This mode suggests intensification and weakening of the cyclonic gyres. Its temporal mode (Figure 32) displays 4 to 6 year oscillations. Highest intensification of gyres is observed in 1995-1996 and 2006, whereas the weakening is observed in 1993-1994 and 1999.

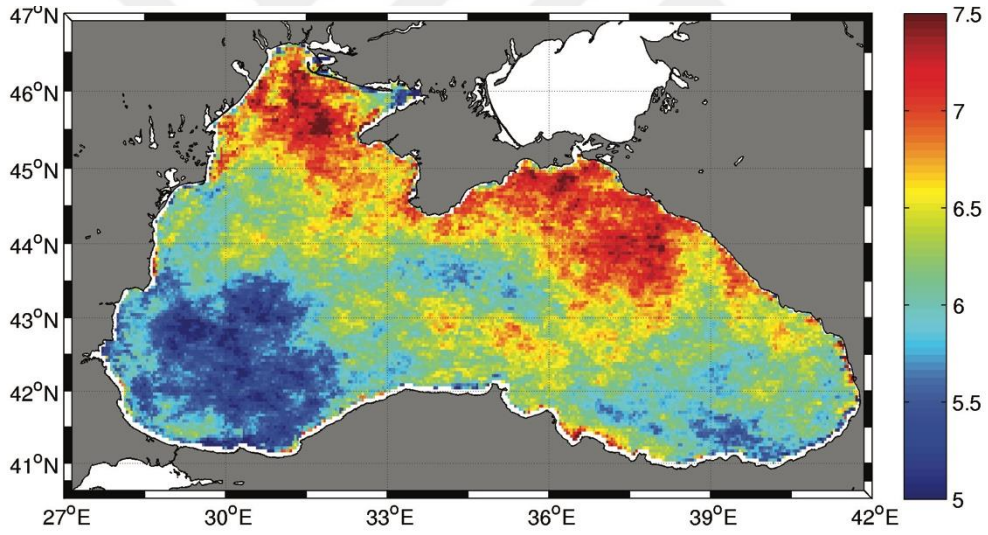

Figure 27 First spatial EOF mode of F-SSTA (x10^{-3}).

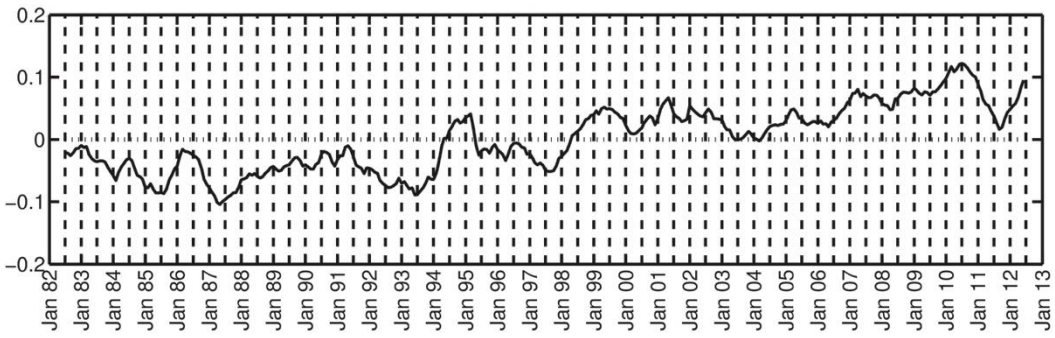

Figure 28 First temporal EOF mode of F-SSTA

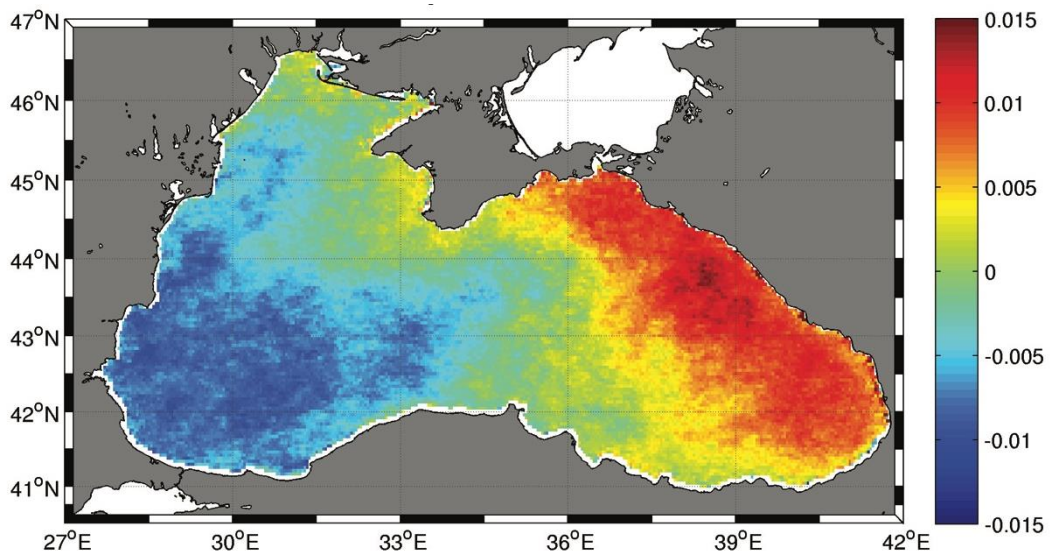

Figure 29 Second spatial EOF mode of F-SSTA

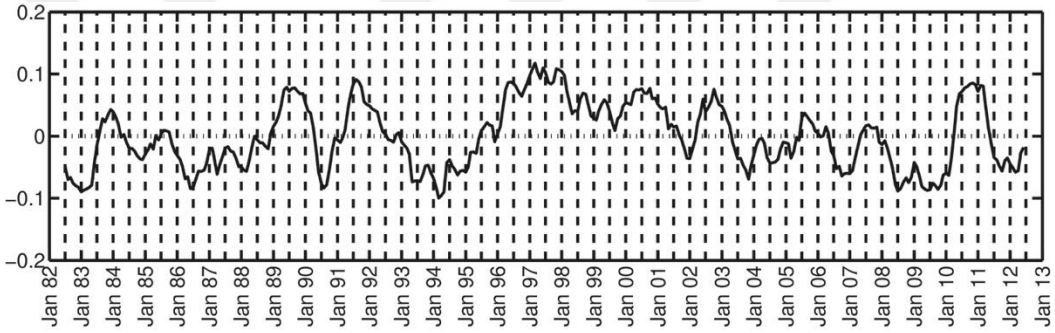

Figure 30 Second temporal EOF mode of F-SSTA

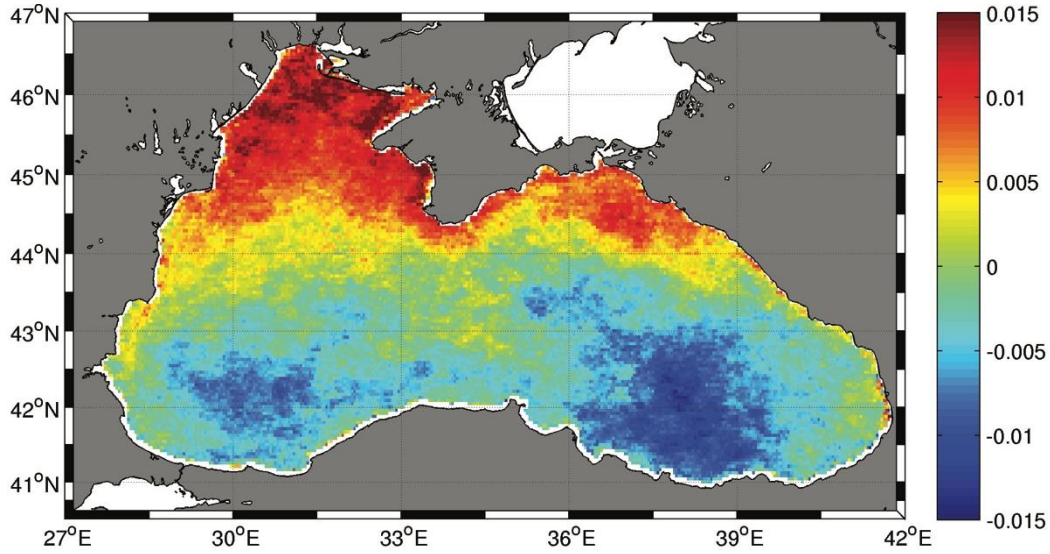

Figure 31 Third spatial EOF mode of F-SSTA

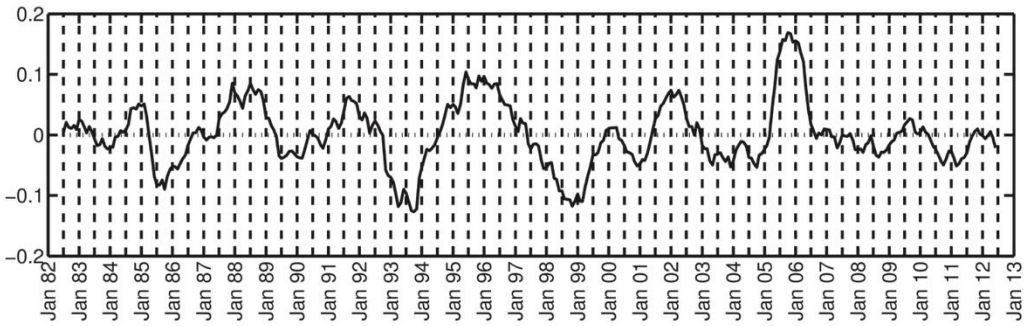

Figure 32 Third temporal EOF mode of F-SSTA

2.3.6 Connections with large-scale atmospheric patterns

In order to assess the response of the Black Sea to teleconnection patterns of North Atlantic Oscillation (NAO) and East-Atlantic West-Russia (EA-WR) indices, F-SSTA time series was compared with low-pass filtered (12 month moving average) indices.

In positive phase of NAO enhances cold and dry air masses are carried to southern Europe and Black Sea region by northwesterly winds generated by pressure gradient between the Azores high pressure and Icelandic low pressure systems (Hurrell et al., 2003; Oguz et al., 2006). Positive phase of the EA-WR arises by the combined effect of the increased anticyclonic anomaly center over the North Sea and the increased cyclonic anomaly center over the Caspian Sea (Oguz et al., 2006). Positive phase of the EA-WR index introduces cold and dry air masses from the northeast-northwest (Oguz et al., 2006). When NAO and EA-WR are both positive, Black Sea is exposed to cold air masses from the northwest and northeast, whereas when both are negative, Black Sea is exposed to warm air masses from the southwest and southeast resulting in mild winters (Krichak et al., 2002; Oguz et al., 2006).Positive NAO and negative EA-WR results in either cold air intrusions from the northwest or warm air from southeast depending on strength and coverage of pressure systems, whereas in the opposite case, cold air masses are introduced from the north leading to colder winters (Oguz et al., 2006).

F-SSTA is negatively correlated with NAO (-0.49) without time lag and even more negatively correlated to EA-WR (-0.53), however with one month time lag. Evolution of SST versus NAO and EA-WR indices are given in Figure 33.

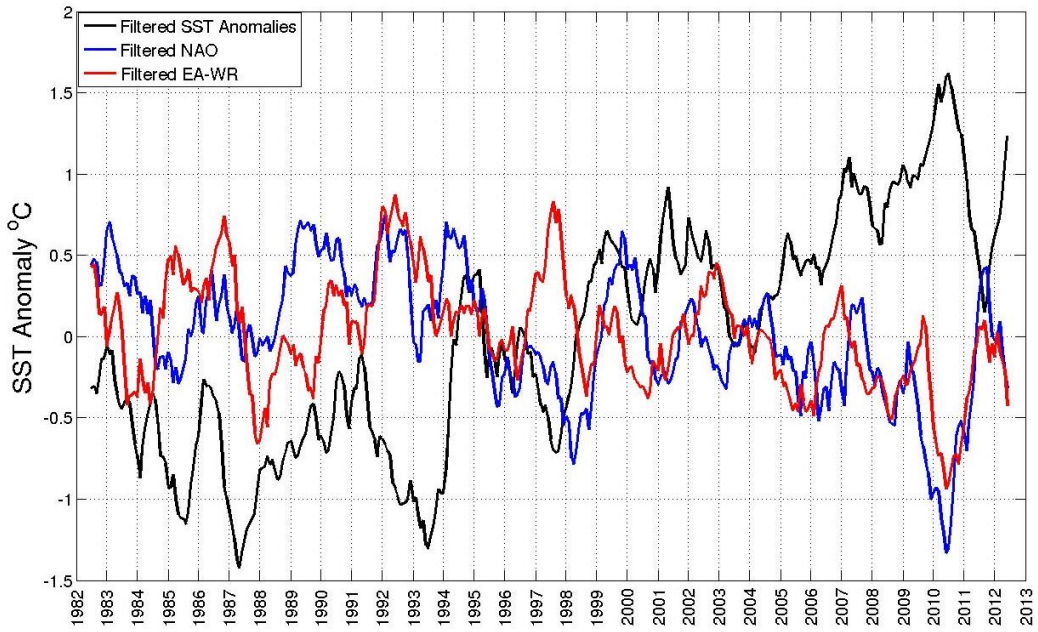

Figure 33 Inter-annual distribution of low-pass filtered SST anomalies, NAO and EA-WR indices.

2.4 Discussion and conclusions

The analysis of spatio-temporal variability and SST trends of the entire Black Sea as well as nine different regions separately, showed that the highest and lowest warming trends were found at Caucasian Coast and Western Anatolian Coast respectively. The basin-wide warming trend was found as 0.078°C/year. Trends obtained from OISST and Hadley SST datasets were relatively lower, 0.06 °C/year and 0.05 °C/year respectively. This is expected considering the resolution and construction of these datasets are different. The warming trend found in this study is similar to those of previous studies, where 0.09 °C/year was calculated using 18 km resolution data for 1981-2000 (Ginzburg et al., 2000) and 0.06°C/year was calculated for 1982-2002 (Ginzburg et al., 2008). Other studies showed a warming trend of 0.063 °C/year for 1985-2000 using World Ocean Database (Shapiro et al., 2010) and the warming trend calculated over the first temporal mode of anomalies of optimally interpolated SST field revealed 0.075 °C/year (Nardelli et al., 2010).

In this study winter temperatures show the lowest warming trend among seasons and the only season showing a cooling trend during 1982-1998. A detailed trend analysis for each month and region (Table 3) exhibited extensive variability, with warming trends

reaching up to 0.1 ^{o}C/year in summer throughout the Black Sea, displaying the highest monthly trends in region 6, whereas the warming trends in winter were similar in all the regions (in 0.03-0.05 ^{o}C/year range).

The DINEOF analysis conducted on the GHRSST dataset revealed that most of the variability was explained by the first mode (97%), which represented a clear seasonal cycle. Temporal evolution of this mode is highly correlated (0.9) with heat flux. Therefore, this mode explains only the seasonal evolution of Black Sea. The second EOF mode represents a phase separation between the northwestern shelf and eastern Black Sea. The third mode suggests the impact of the wind regimes previously discussed by Kazmin and Zatsepin (2007). They have shown that strength/weakness of the southern-western and northern-eastern winds cause SST increase/decrease. , However the correlations with wind parameters (u,v, wind stress components and wind stress curl) were low in our study. This is of particular interest because the coldest part of the Black Sea is the Northwestern Shelf which is warming with a similar rate of the whole basin. Especially, winter temperatures are of critical interest as this is the site subject to cold air outbreaks from the Balkans. Results show that winter warming trends (Table 3) of the Northwestern Shelf are similar with other regions, suggesting milder winters in the area meaning less exposure to cold air outbreaks/winds which is crucial for cold intermediate layer formation. Even though visual examination of the results (trends and EOF spatial modes) strongly suggest a north-east, south-west partitioning of SST, and these coincide with the two major wind regimes over the Black Sea (Kazmin and Zatsepin 2007), neither SST nor its EOF modes showed considerable correlations. One possible reason for this may be the differences in resolution of the datasets. Unfortunately wind data used in this study was available at 0.25 ^{o} only, whereas SST data was available at 4km resolution. Another reason may be the localized coupling of SST and wind. It has been previously shown that SST and wind are coupled along fronts (Chelton et al., 2007; Castelao 2012) and wind stress curl and divergence are linearly related to local crosswind and downwind components of the SST respectively. This may very well be the case for the Black Sea, considering the thermal fronts along the axis of the Rim Current. However, this requires regional analysis of the wind fields, and is not the main focus of this study.

Detailed analyses of Black Sea SST anomalies has shown that 1982-1998 was dominated by negative anomalies whereas 1999-2012 was dominated by positive

anomalies. A threshold based on standard deviations (±1 ^{o}C) was set to identify intense anomalies for each region. Different regions exhibited great variability in terms of intense anomalies. One of the reasons for this large variability is the number of data gaps over space and time. Another reason is the contribution of mesoscale circulation features within each region. Even though 2003, 2006 and 2012 were the coldest years of 1998-2012 period, they were still dominated by positive anomalies, once again emphasizing the difference of 1982-1998 and 1999-2012 periods.

In order to investigate SST variability beyond the seasonal cycle, an EOF analysis was conducted on the low-pass filtered anomaly dataset. The spatial structure of the first mode revealed a patchy pattern. The corresponding temporal mode denoted a positive warming trend. Thus, the 1st spatial mode (see Figure 27, Chapter 3) displays the regions of the Black Sea with the highest and lowest warming. Although the study period and conducted gap-filling methodologies are different, DINEOF results are similar to OISST results (Nardelli et al., 2010).

Further, correlations between low-pass filtered SST anomalies and low-pass filtered indices (NAO and EA-WR) were investigated to identify any links to large-scale atmospheric forcing. F-SSTA was found to be negatively correlated with NAO (-0.49) without time lag and even more negatively correlated to EA-WR (-0.53), however with one month time lag. Nardelli et al., (2010) found a negative correlation of -0.65 with NAO. However, they have investigated correlations with EOF modes. The values given above represent correlations with F-SSTA, not the temporal modes. All low-pass filtered wind (u,v, wind stress and wind stress curl) and heatflux anomalies were investigated for correlation with SST. Despite that the heat flux was highly correlated with SST (0.9), F-SSTA – heat flux anomaly correlation was only -0.35 (with 10 months lag). Wind speed anomalies U' and V' were correlated with F-SSTA with -0.45 (with 3 months lag) and -0.32 (with 10 months lag) respectively. Wind stress anomaly also showed a low correlation (0.33 with 12 week lag). Wind stress curl anomaly was correlated to F-SSTA (0.4 with 8 months lag).

This work investigated the spatio-temporal variability and warming trends of Black Sea SST using high-resolution satellite SST data for 1982-2012. Impacts of wind and heat flux on the SST were investigated as well as atmospheric teleconnections. This is the first time SST was investigated with such high resolution (4km) data for a long time

period of 31 years (1982-2012). Unfortunately, the results obtained do not promise a bright future for the Black Sea. Rapid warming of Black Sea will most likely result in increased stratification, reduced mixing, decline of cold water formation/renewal events and eventually reduced oxygen in deeper layers (Capet et al., 2016). Rapid warming of Black Sea will also influence the phytoplankton dynamics leading the system to abrupt changes and even regime shifts (McQuatters-Gollop et al., 2008). Another important problem may arise considering the spatial distribution of warming. Results of this analysis revealed the areas with the highest warming trends as the eastern and northeastern parts of the Black Sea. This is particularly important in terms of Turkish anchovy fisheries. Anchovy overwintering in Turkish coast (Chashchin, 1996; Schulman, 2002) is crucially important for Turkish fisheries. In case such warming continues, it is likely that migration and overwintering patterns of anchovy will change. This may lead to anchovy to stop migrating, because of warmer temperatures in their area of origin, or lead to a change in migration patterns. In such a case, Caucasian coast may become an alternative for the eastern Turkish coast, resulting in a decrease in the catches of the Turkish fishing fleet.

CHAPTER 3: Recent trends in the sea surface temperature of the Levantine Basin and analysis of similarities and differences with the Black Sea

3.1 Introduction

The Mediterranean is a semi-enclosed sea connected to the Atlantic by Strait of Gibraltar, to the Black Sea by Dardanelles Strait and to the Red Sea by the Suez Canal. It is composed of two basins (Eastern and Western Mediterranean) separated by the Strait of Sicily. The Levantine basin, focus area of this study, is a major sub-basin of the Eastern Mediterranean, that exchanges water with the Ionian Sea, Aegean Sea and Red Sea (through Suez Canal).

The Eastern Mediterranean has gone through major alterations including: variations of fresh water input from Black Sea through the Bosphorus (Zervakis et al., 2000), redistribution of salinity (Klein et al., 1999), changes in the atmospheric forcing in the Aegean together with long-term salinity change (Theocharis et al., 1999), and changes in the circulation scheme leading to blocking the flow of Modified Atlantic Water and Levantine Intermediate Water (Malanotte-Rizzoli et al., 1999). Combination of these events, the so-called Eastern Mediterranean Transient (EMT) was the main climatic event affecting the circulation and water mass properties in the Mediterranean in the last century (Theocharis et al., 2002).

The circulation of the Eastern Mediterranean has been studied by the POEM (Physical Oceanography of the Eastern Mediterranean) group via both in-situ and modelling studies (Özsoy et al., 1989; 1991; 1993). The POEM derived scheme of circulation for the Eastern Mediterranean consists of Mid-Mediterranean Jet, Cilician Current, Asia Minor Current, Ionian-Atlantic Stream, Cretan Cyclone, IeraPetra Anticyclone, Rhodes Gyre, Shikmona Eddy, West Cyprus Gyre and Mersa-Matruh Gyre as the most-pronounced features, as well as smaller features such as the Anaximander and Antalya anticyclonic eddies (Özsoy et al., 1991). Though the general circulation scheme is accepted by scientists today, there is still on-going debate on the main pathway of the Atlantic water through the Mediterranean and the basin-scale surface current (Amital et al., 2010; Ciappa, 2014). Steric effects (mainly of thermal origin) on

sea level trends in the basin will most likely alter the surface circulation (Criado-Aldeanueva et al., 2008) and aggrandize the debate on the issue. Thus, investigation and continuous monitoring of sea surface temperature (SST) and SST trends are crucial, considering the contribution of thermal origin to sea level is found to be ~55% for 1992-2005 (Criado-Aldeanueva et al., 2008).

Like other marine ecosystems the Mediterranean is also subject to warming (Belkin, 2009.). However, another vital issue arises for the Mediterranean from warming. Intrusions of tropical species introduced through either the Suez Canal or, to a lesser extent, the Strait of Gibraltar are increasing as the Eastern Mediterranean is warming (Raitsos et al., 2010; Schmidt et al., 2015). Thus understanding the spatial and temporal variability in SST is of crucial interest, considering the Mediterranean is denominated as a climate change hotspot (IPCC 2007; Shaltout et al., 2014.).

Satellite SST data have previously been used in various studies in the Mediterranean Sea. Marullo et al. (1999a) and Marullo et al. (1999b) investigated the seasonal and interannual variability of the Eastern Mediterranean and found a positive trend 0.15^{o}C/year. Criado-Aldeanueva et al. (2008) investigated the steric contribution to sea level in the Mediterranean and found a positive SST trend of 0.061 ^{o}C/year for 1992-2005. Nykjaer (2009) has found warming trend 0.03^{o}C/year and 0.05 ^{o}C/year for 1985-2006 in the Western and Eastern Mediterranean respectively. Skliris et al. (2012) has calculated warming trends as 0.037 ^{o}C/year for the whole Mediterranean and 0.042 ^{o}C/year for the Eastern Mediterranean for 1985-2008. Shaltout et al. (2014) investigated the trends in the whole Mediterranean Sea and sub-regions and found a similar trend 0.042 ^{o}C/year for the Levantine sub-basin for 1982-2012 period using 0.25 ^{o} resolution data. Zveryaev (2015) documented the intraseasonal and interannual variability of Mediterranean SST. Macias et al. (2015) have found positive trends 0.67 ^{o}C/year for the entire Mediterranean and 0.77 ^{o}C/year for the Eastern Mediterranean.

Although various studies have analyzed SST and its variability, a study using high resolution data focusing on the Levantine is missing. This study presents an up to date investigation of seasonal, regional and temporal variability of the Levantine SST and its connection to atmospheric patterns using ~4km resolution data (Group for High Resoultion Sea Surface Temperature (GHRSST)) over 31 years (1982-2012).

3.2 Material and Methods

3.2.1 Satellite sea surface temperature data

AVHRR Pathfinder Version 5.2 (PFV5.2) were used as the SST dataset in this study and were obtained from the US National Oceanographic Data Center and GHRSST (http://pathfinder.nodc.noaa.gov). The PFV5.2 data are an updated version of the Pathfinder Version 5.0 and 5.1 collections described in Casey et al. (2010). The dataset used in this study comprises of daily 4km daily SST fields for the period 1982-2012. Comparison of PFV5.2 data with in-situ measurements revealed a bias -0.23±0.01 ^{o} C and root mean square 0.51±0.01 ^{o} C in the Mediterranean Sea (Pisano et al., 2016).

In this study, 31 years of daily data was analyzed for the period 1982-2012 for the Levantine Basin. In order to avoid impacts of diurnal heating, only nighttime data were used. Pixels with low quality flags and pixels affected by clouds were removed from the analysis, leaving weekly images with very low spatial coverage. Only pixels with acceptable quality and best quality were used. Pixels at the land/sea boundary were also removed because they contained too much error (as suggested by Kenneth Casey at NOAA, personal communication). Considering the aim of this work is to describe the recent trends for the period 1982-2012 and to address regional variability, it was both sufficient and necessary to use monthly data to describe temporal variability and provide increased spatial coverage respectively. Therefore, monthly data has been constructed for the study period using weighted averaging, neglecting empty/cloud covered pixels, resulting in 372 monthly images. In order to assess variability in space and time, DINEOF algorithm has been applied to the monthly dataset.

3.2.2 SupplementaryDatasets

To further compare the interannual trends of SST, two other SST products were utilized. Optimum Interpolation Sea Surface Temperature (OISST) dataset is obtained (Reynolds et al., 2007; Reynolds et al., 2009) from NOAA (https://www.ncdc.noaa.gov/oisst). OISST dataset contains 0.25^{o} daily sea surface temperature data comprising of AVHRR and AMSR-E. AVHRR+AMSR-E data is available from 2002 to 2011, whereas the remaining time period is AVHRR data only.

Another additional dataset is the Hadley SST obtained from Met Office (www.metoffice.gov.uk/hadobs/hadisst/).

In order to understand the impact of atmosphere on sea surface temperature, heatflux and wind were used as additional datasets. Cross-Calibrated Multi-Platform Ocean Surface Wind Vector L3.0 First-Look Analyses (CCMP) (ftp://podaacftp.jpl.nasa.gov/allData/ccmp/L3.0/flk/) was used for wind data, providing using 0.25 degree resolution, 6 hourly wind fields from 1987 to 2011. The wind stress was computed following Trenberth et al. (1990). Heat flux data was obtained from ERA-interim dataset (http://data-portal.ecmwf.int). Heat flux data was calculated using reanalysis fields of surface net solar radiation, surface net thermal radiation, surface latent heat flux and surface sensible heat flux at 0.125^{o} resolution. OISST, Hadley SST and CCMP datasets were interpolated to the same grid as GHRSST dataset. Then for each dataset, daily fields of each dataset were used to construct monthly datasets which are used throughout the analysis. Anomaly datasets were also constructed for comparison with GHRSST anomaly data set. First monthly climatology datasets were created (12 months data) which was then substracted from the original dataset. For example, anomaly dataset for January 2000 (January2000anomaly) was constructed by subtracting mean of all January data (Januaryclim) from January 2000 data (January2000anomaly=January2000-Januaryclim).

3.2.3 Empirical Orthogonal Functions (EOF) Analysis

Satellite dataset contains gaps due to instrumentation errors or cloud coverage. It is not possible to conduct standard EOF analysis on datasets with gaps. Data Interpolating Empirical Orthogonal Functions (DINEOF) (Beckers and Rixen 2003) were used to fill the gaps in the data. This method stores the data in a matrix where missing data are initially set to zero. Singular Value Decomposition (SVD) calculates first EOF mode which is then multiplied by the corresponding temporal signal and used to replace the missing data (step A). In the next step, SVD is performed again (step B). This is an iterative process, where step A and step B are repeated until convergence is reached. This procedure was developed to fill data gaps and the EOF analysis is a side product of this technique, however in this study, the main aim is to conduct EOF analysis successfully and data filling is a side product.

3.3 Results

The statistical analysis of the sea surface temperature data in the Levantine Basin is presented here focusing on the seasonal and spatial variability of the warming trends, interannual variability, as well as sea surface temperature anomalies. Relationship of SST with heatflux, wind and climatic teleconnection patters are also presented.

3.3.1 Seasonal and spatial variability

Maximum mean SST value for the Levantine is in August ($26.3 \pm 0.8\ ^{o}C$) and minimum mean SST in March ($16.1 \pm 0.56\ ^{o}C$). Monthly evolution of SST and its standard deviations are given in Table 4.

Table 4 Monthly evolution of SST and standard deviations in the Levantine Basin.

Month	*1*	*2*	*3*	*4*	*5*	*6*	*7*	*8*	*9*	*10*	*11*	*12*
Mean	17.1	16.2	16.1	16.9	19.5	22.8	25.1	26.3	25.7	24.2	21.5	18.9
STD.	0.61	0.53	0.56	0.51	0.73	0.70	0.80	0.80	0.67	0.70	0.82	0.72

Maximum SST's are observed at the outflow of Nile River, along the entire eastern coast and in the Cilician Basin, whereas the minimum SST's are observed in the Rhodes Gyre (Figure 34).

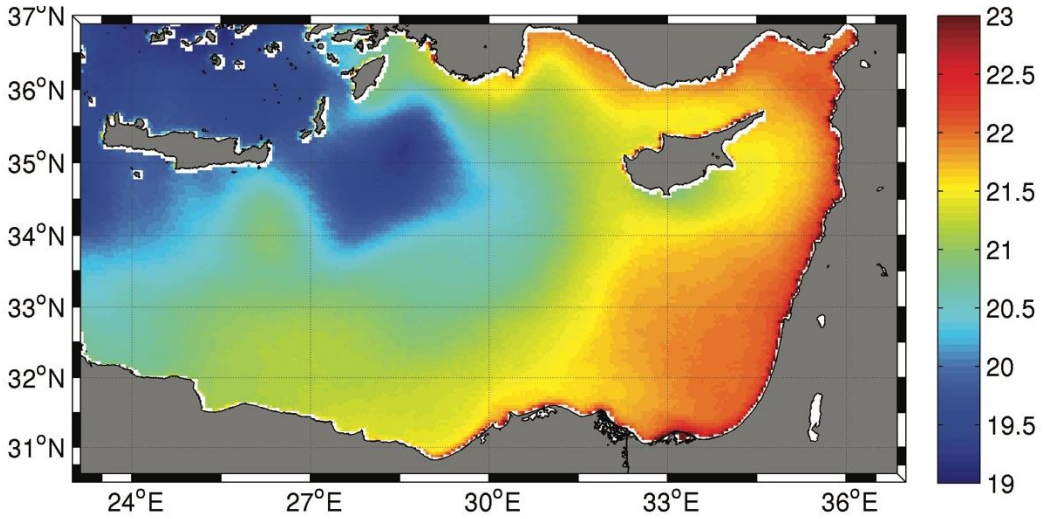

Figure 34 Climatological (1982-2012) SST field of the Levantine Basin.

3.3.2 EOF Results

The variance explained in the first three modes of the EOF analysis represents 97% of the total variance. The first mode explains most of the SST variability (92.5%) in the basin. Its spatial structure (Figure 35) exhibits all negative values, with more negative values on the eastern part. Its temporal mode (Figure 36) represents a seasonal cycle with interannual variability. Positive (negative) magnitudes in winter (summer) result in decreased (increased) SST values over the Levantine.

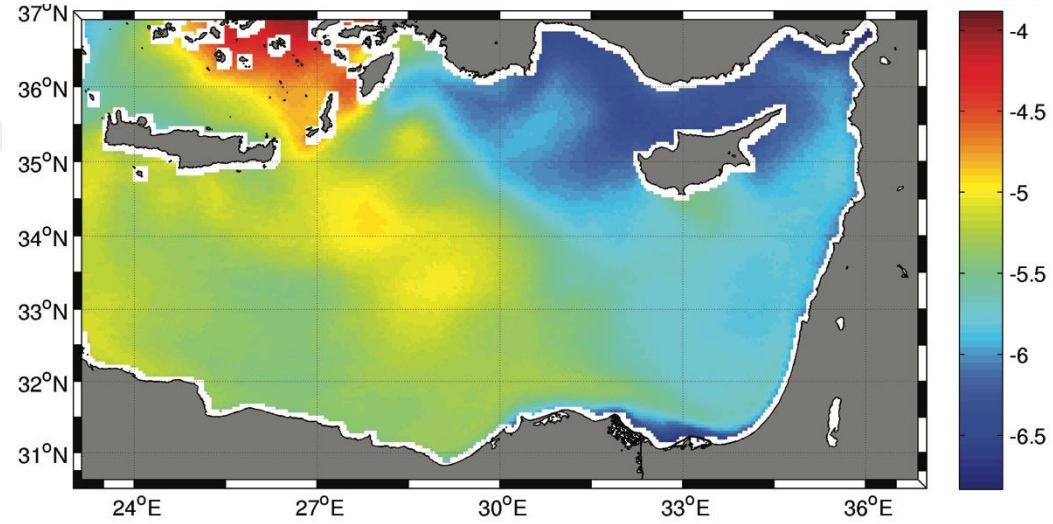

Figure 35 First spatial EOF mode of SST (x10^{-3}).

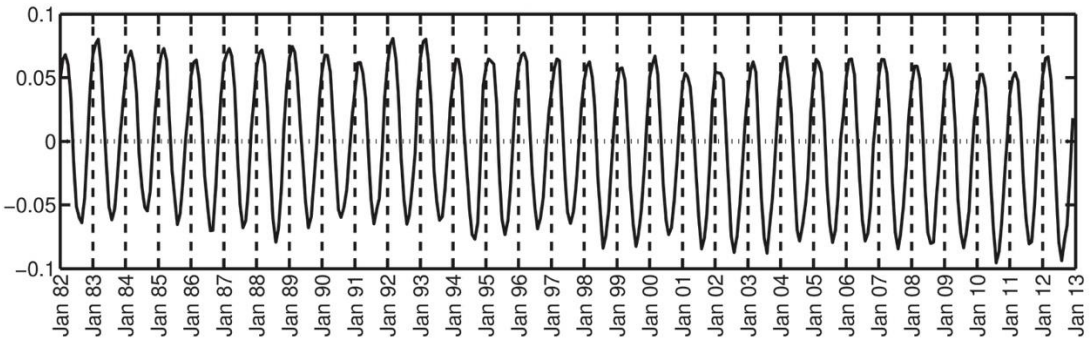

Figure 36 First temporal EOF mode of SST.

Second mode represents a low percentage of the total variance (4% or 50% of the total variance excluding the first mode.) Its spatial structure (Figure 37) is similar to the climatology of SST. It exhibits negative magnitudes in Cretan Sea and around Rhodes Gyre. Imprint of Iera-Petra eddy is clearly exhibited in this map. Positive magnitudes are observed all over the eastern part. It displays a SST gradient starting from 30°E, 31.5°N

and extends along the northeastern axis, encircles Cyprus and continues along the Anatolian coastline, suggesting the imprint of basin-wide circulation around this region (Libyo-Egyptian Current and Asia Minor Current). Corresponding temporal mode (Figure 38) displays positive magnitudes for the whole period. Larger magnitudes are mostly observed in winter leading to a more pronounced SST phase separation, whereas smaller magnitudes are generally observed in late spring and summer which result in a relatively uniform SST field.

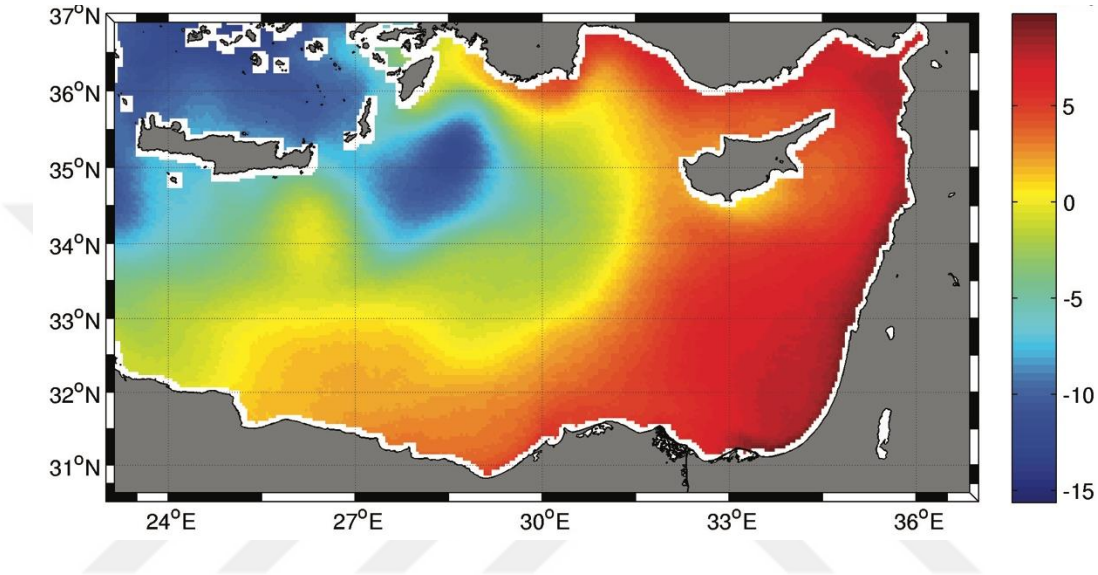

Figure 37 Second spatial EOF mode of SST (x10^{-3}).

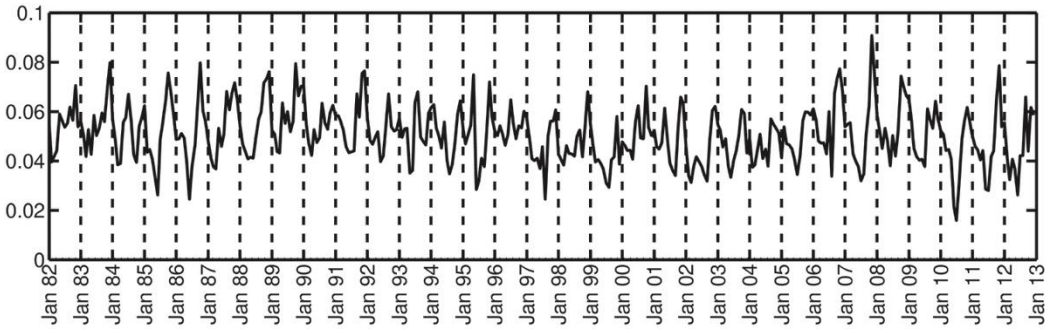

Figure 38 Second temporal EOF mode of SST

The third mode explains 0.5% of the total variance (or 6% excluding the first mode). Its spatial mode (Figure 39) displays a zonal phase separation with positive magnitudes on the southern part and negative magnitudes on the northern part. Only exception is observed on the Nile River discharge area. Its temporal mode (Figure 40) displays an almost seasonal oscillation with positive values generally observed in winter and negative values around late spring and summer. Considering the phase separation between Iera-Petra and Rhodes-Anaximander regions and the gradient at Latakia region,

this mode suggests the imprint of active wind field on SST. This temporal SST mode is correlated (-0.66) with the first mode of wind stress curl (Figure 41). However, considering the structures observed around Nile discharge area and İskenderun Bay, it is important to note the impact of river discharges in this mode. Therefore it is most likely that the third mode of SST reflects a combined effect of the wind regime and river discharges.

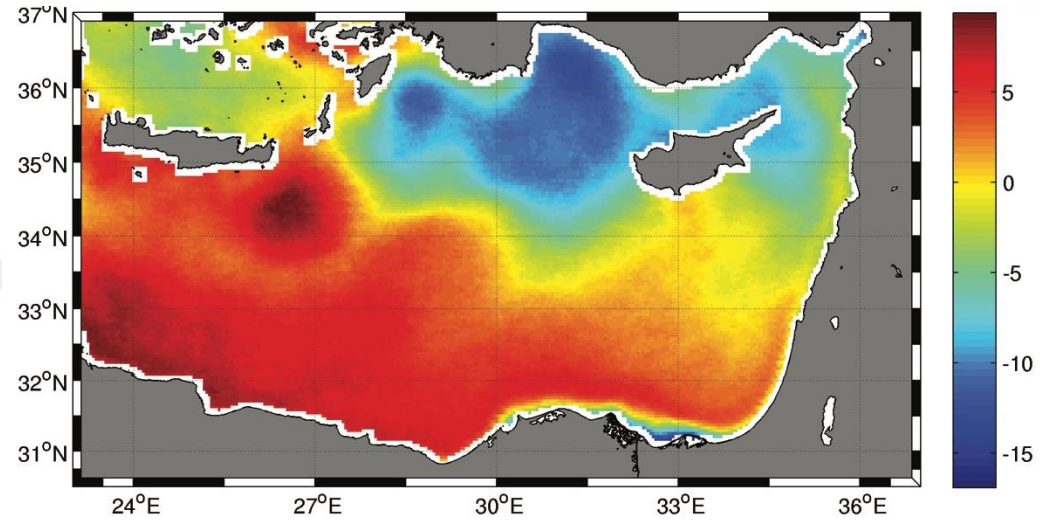

Figure 39 Third spatial EOF mode of SST (x10^{-3}).

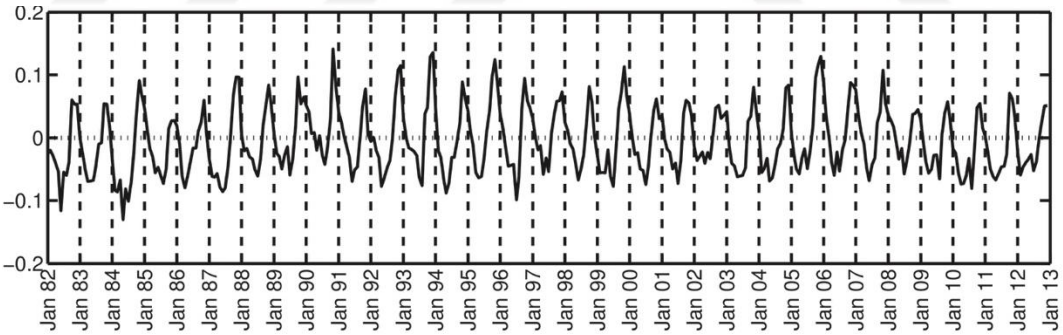

Figure 40 Third temporal EOF mode of SST

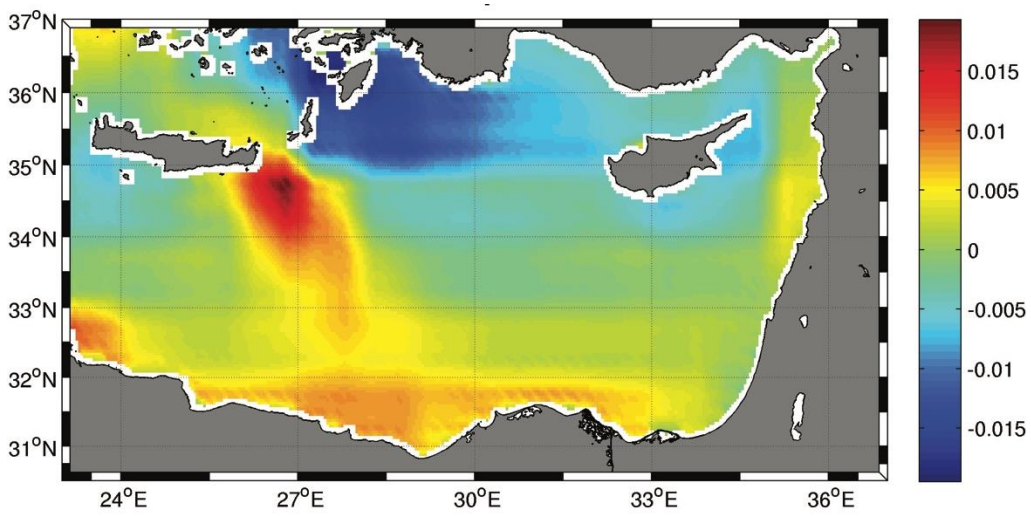

Figure 41 First temporal mode of Wind Stress Curl over the Levantine.

3.3.3 Inter-annual trends

Temporal evolution of basin-averaged sea surface temperatures in the Levantine show a positive trend of 0.06±0.018 °C/year for the period under investigation (1982-2012) (Figure 42). SST trends are also calculated using the OISST and Hadley SST datasets. OISST and Hadley SST data have positive trends of 0.04°C/year and 0.05 °C/year respectively. OISST and Hadley SST datasets extend until 2015. Trends of OISST for the 1982-2015 were the same as for 1982-2012. Trends of Hadley SST for 1982-2015 were 0.04 °C/year. Calculated trends are slightly different, which is expected considering the preparation methodology and resolution of the datasets are different.

Seasonal SST trends calculated for the Levantine reveal low warming rates of 0.036 °C/year in winter to high warming rates of 0.066 °C/year in summer. Considering 1982-1997 period was dominated by negative SST anomalies (see: **3.3.4 SST** Anomalies) and 1998-2012 periods was dominated by positive anomalies. All seasonal trends are given in Table 5. The regional distribution of SST trends is given in Figure 43. Regions of highest warming trends for 1982-2012 are Rhodes and Iera-Petra regions.

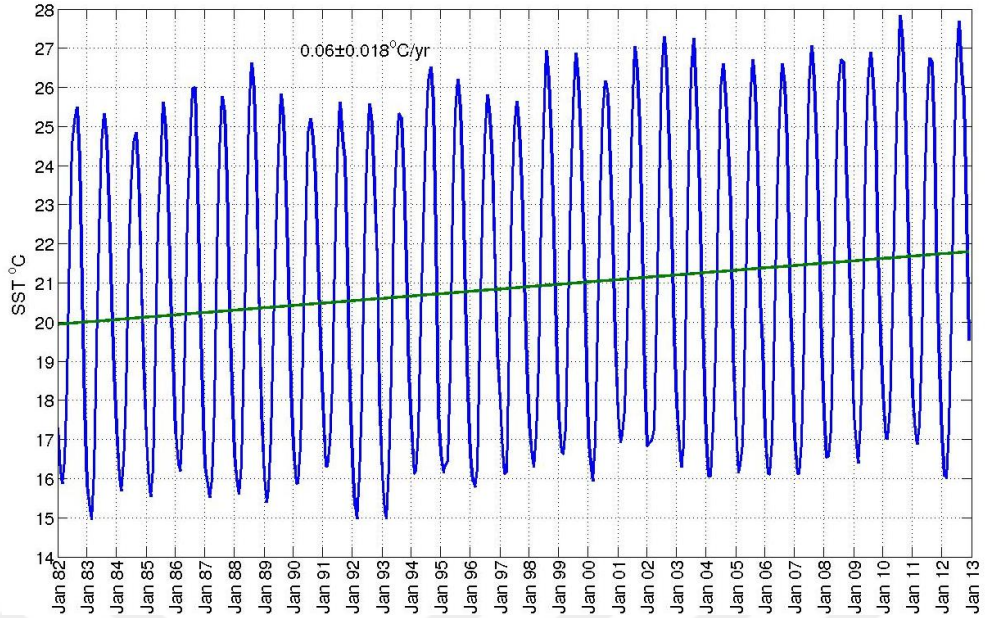

Figure 42 Interannual variability of monthly mean SST from January 1982 to December 2012 averaged over the entire Levantine

Table 5 Seasonal SST trends for Levantine from 1982 to 2012.

Season	Annual rate (^{o}C/year) (1982-2012)	1982-1997	1998-2012
Winter	0.036	0.021	0.010
Spring	0.050	0.035	0.027
Summer	0.066	0.032	0.044
Fall	0.055	0.049	0.012

To explore the regional and temporal variability of SST trends, trends were calculated for each month. Regional distribution of SST trends for each month are given in Figure 44-Figure 55. These trends display a wide monthly variability and regional variability. Winter and spring months display uniform warming trends over the basin. In June (Figure 49), highest warming is observed below Crete and around Rhodes Gyre. In July (Figure 50) and August (Figure 51) intense warming is observed between 26^{o} Eand 31 ^{o} E and particularly on the Cretan Sea (in August). Observing highest warming trends in summer months may be a consequence of alterations in radiation. In September (Figure 52), October (Figure 53) and November(Figure 54) highest and lowest warming trends are distributed in dipole patterns over the basin, with the highest warming trends over regions with mesoscale activity. This is most probably caused by mesoscale features

around these locations, whose intensity alters inter-annually depending on the strength of the boundary current.

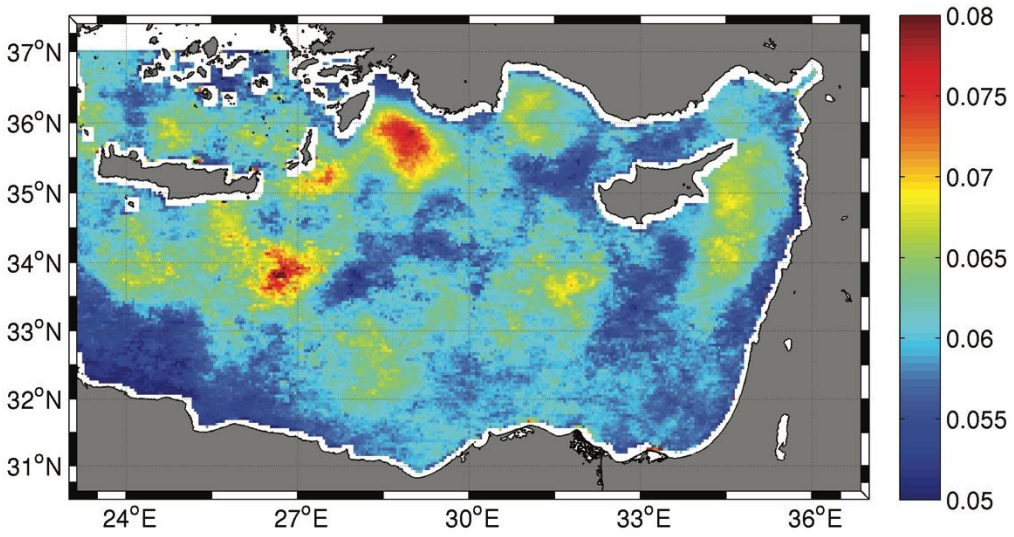

Figure 43 Regional distribution of SST Trends (^{o}C/year) for 1982-2012.

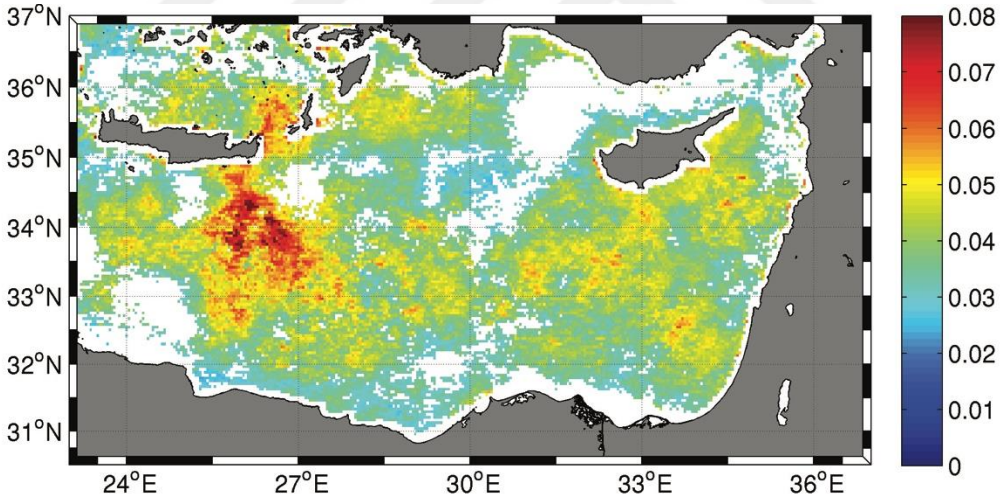

Figure 44 Regional distribution of SST trends for January. Uncolored regions represent statistically insignificant trend.

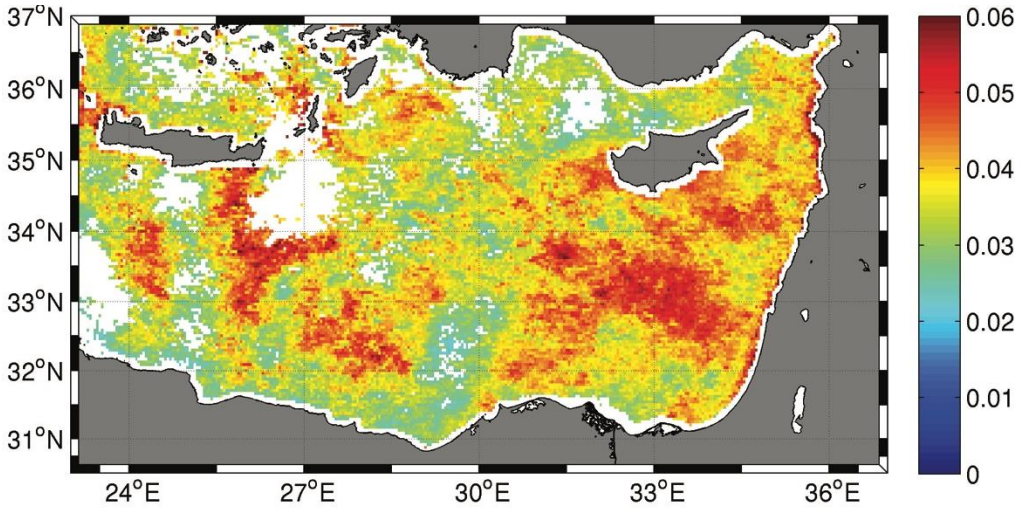

Figure 45 Regional distribution of SST trends for February. Uncolored regions represent statistically insignificant trend.

Figure 46 Regional distribution of SST trends for March. Uncolored regions represent statistically insignificant trend.

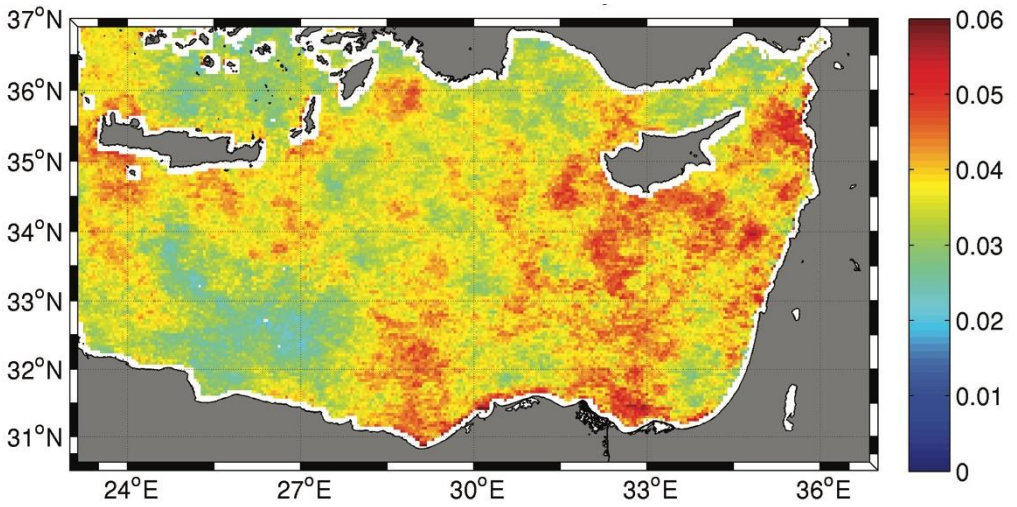

Figure 47 Regional distribution of SST trends for April. Uncolored regions represent statistically insignificant trend.

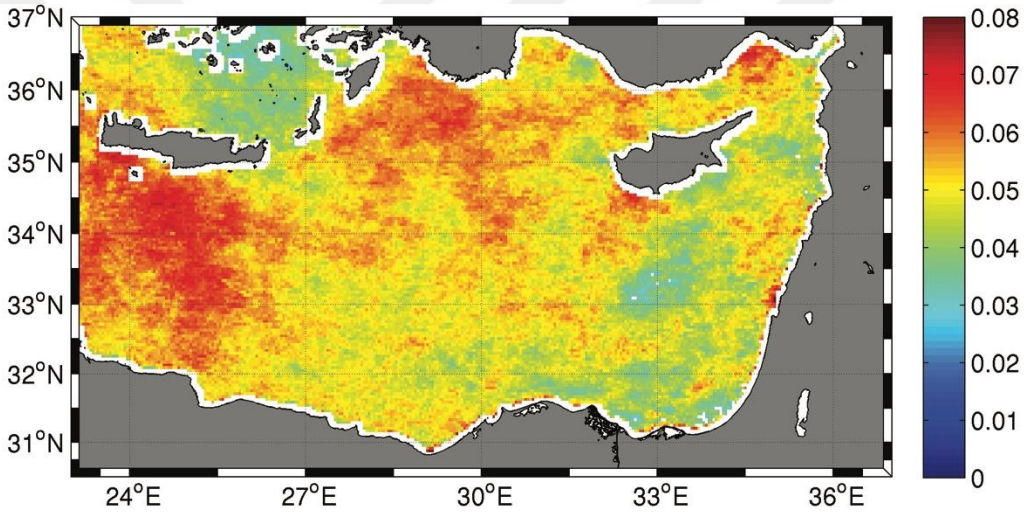

Figure 48 Regional distribution of SST trends for May. Uncolored regions represent statistically insignificant trend.

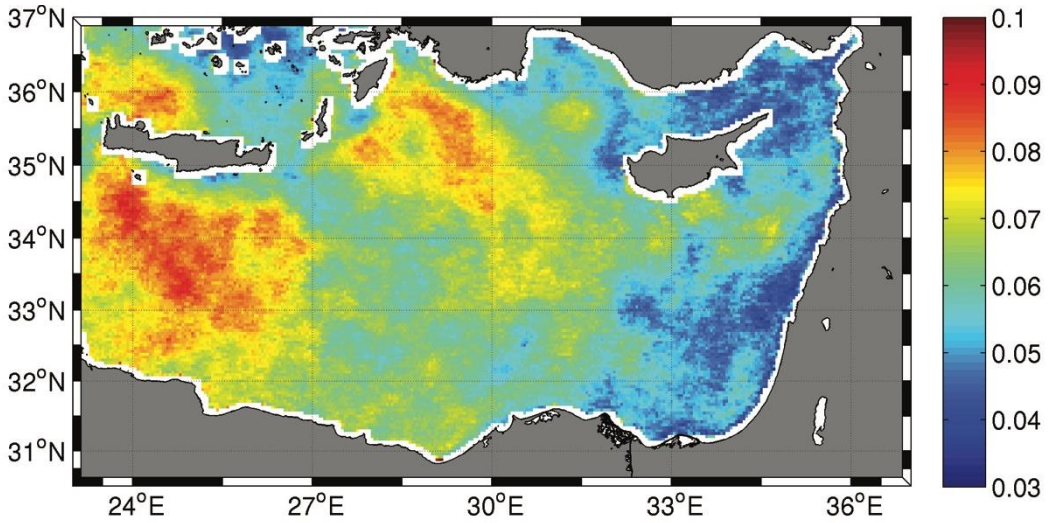

Figure 49 Regional distribution of SST trends for June. Uncolored regions represent statistically insignificant trend.

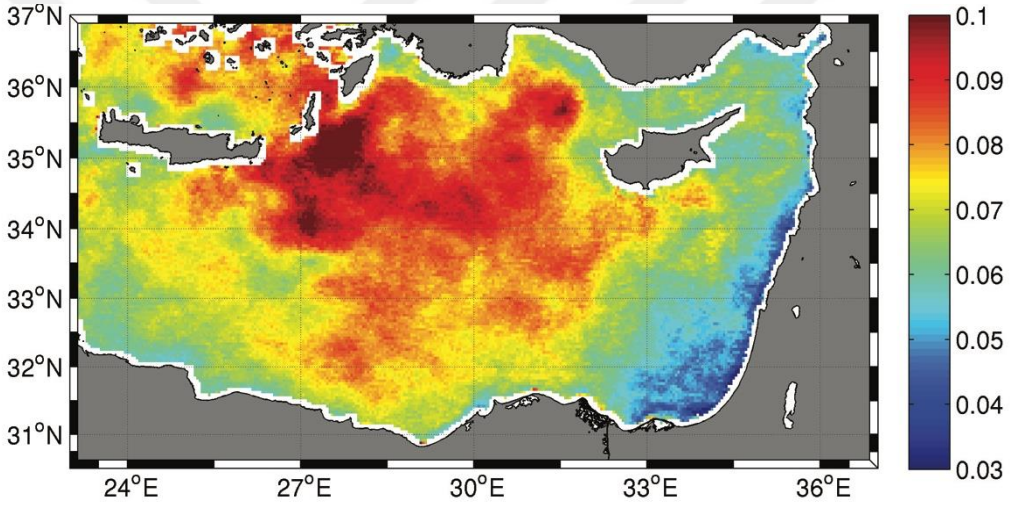

Figure 50 Regional distribution of SST trends for July. Uncolored regions represent statistically insignificant trend.

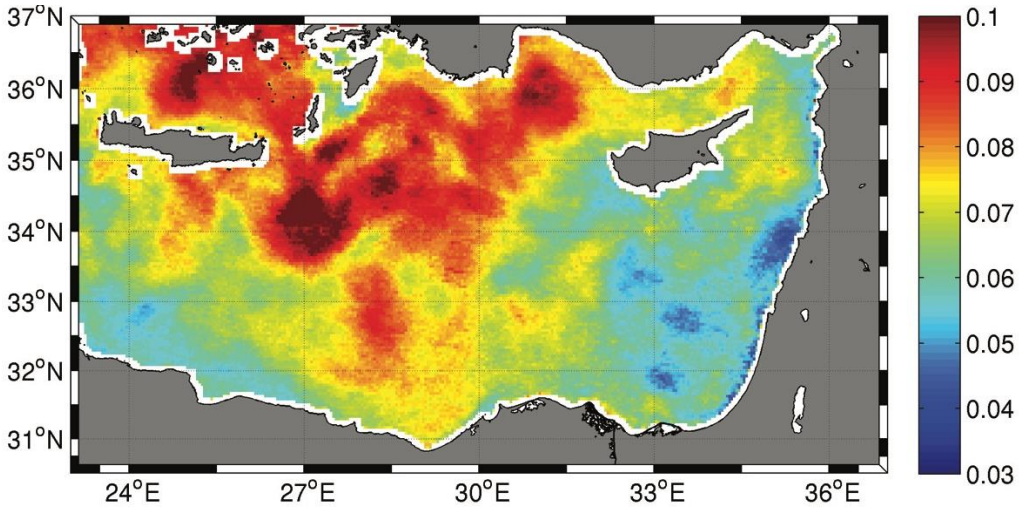

Figure 51 Regional distribution of SST trends for August. Uncolored regions represent statistically insignificant trend.

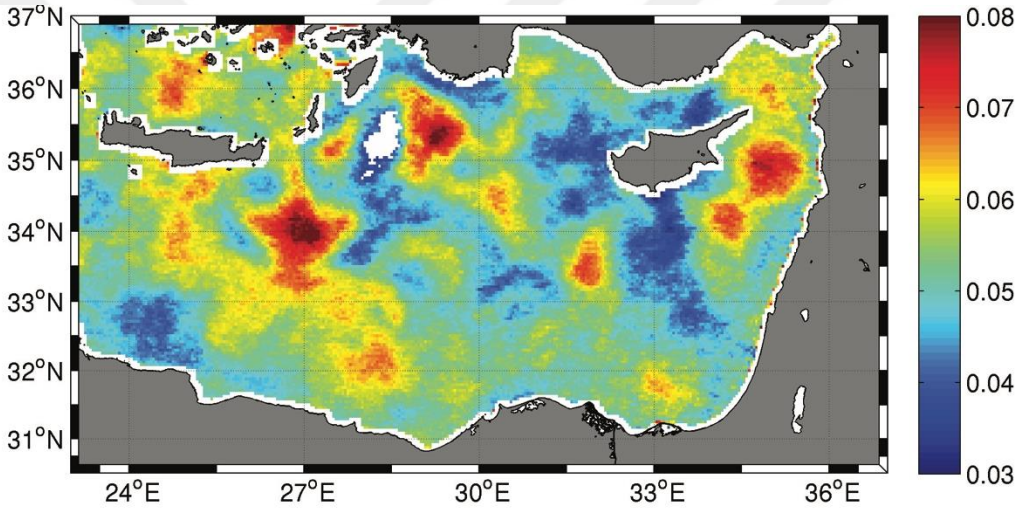

Figure 52 Regional distribution of SST trends for September. Uncolored regions represent statistically insignificant trend.

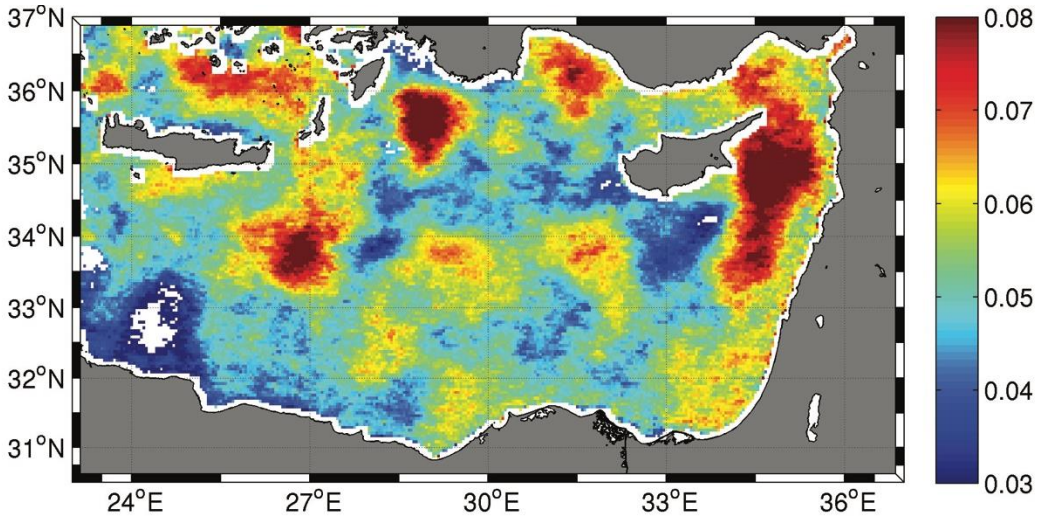

Figure 53 Regional distribution of SST trends for October. Uncolored regions represent statistically insignificant trend.

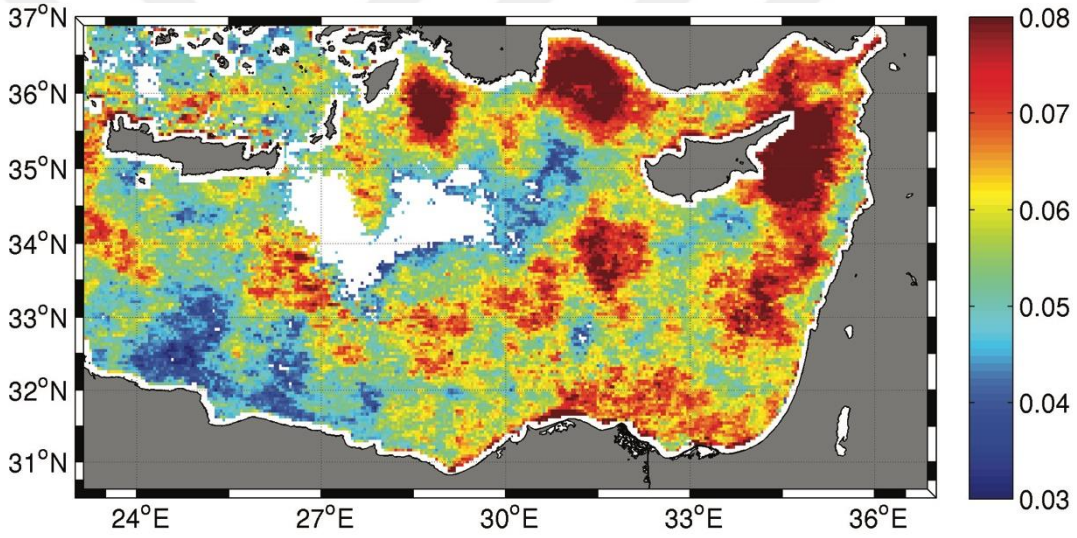

Figure 54 Regional distribution of SST trends for November. Uncolored regions represent statistically insignificant trend.

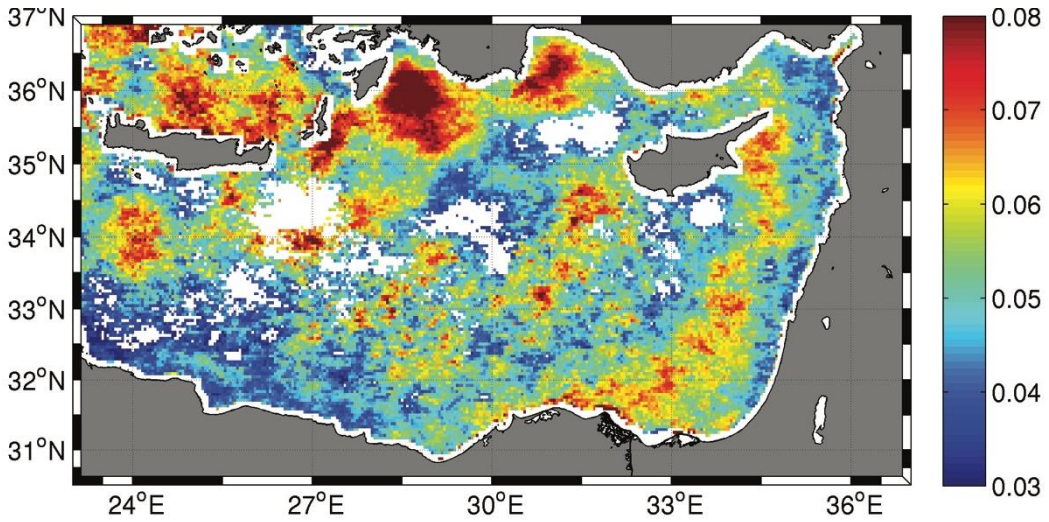

Figure 55 Regional distribution of SST trends for December. Uncolored regions represent statistically insignificant trend.

3.3.4 SST Anomalies

Monthly SST anomalies have been calculated for the Levantine as the difference between the monthly temperature and the climatic mean for that month. For the whole period 1982-2012, there is a clear shift from negative anomalies to positive anomalies. 1982-1997 is dominated by negative anomalous years whereas 1998-2012 is dominated by positive anomalous years (Figure 56). Negative (positive) anomalies constitute 80 %(20%) of total number of anomalies for 1982-1997 whereas for 1998-2012, negative (positive) anomalies constitute 20 %(80%) of total anomalies. %). Figure 57 shows time-series distribution of anomalies for the whole Levantine. Maximum positive anomalies are seen on December 2010 (+1.6^{o}C), October 2012 (+1.5 ^{o}C), November 2004 (+1.5 ^{o}C) and July 2012 (+1.45 ^{o}C) whereas maximum negative anomalies are observed on August 1984 (-1.7 ^{o}C), May 1987(-1.6 ^{o}C), November 1988 (-1.5 ^{o}C) and May 1992 (-1.5 ^{o}C). The maximum positive anomaly for the 1982-1997 period is observed in October 1994 (+1.4 ^{o}C) whereas the maximum negative anomaly for the 1998-2012 period was observed on November 2005 (-0.96 ^{o}C).

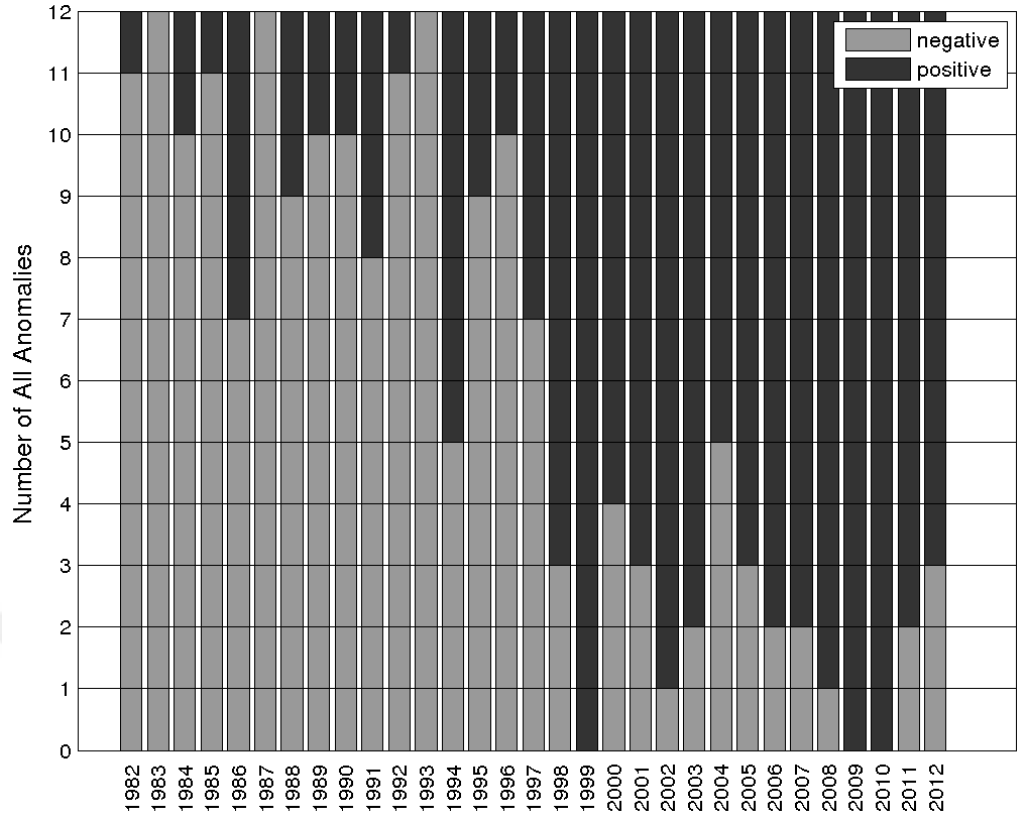

Figure 56 Monthly SST Anomalies for Levantine Basin.

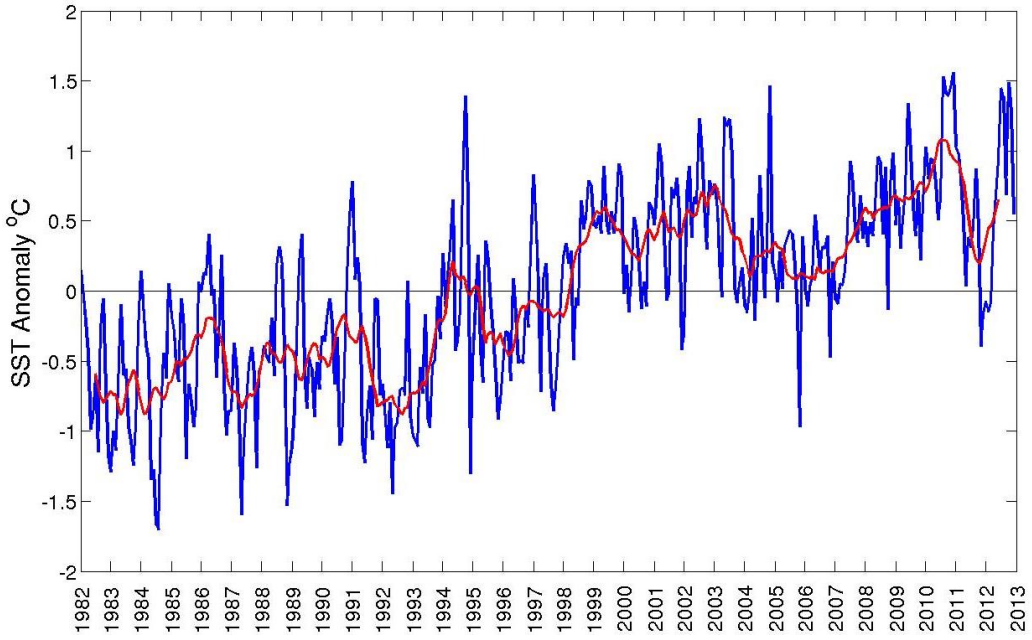

Figure 57 Inter-annual variability of monthly SST anomalies over the Levantine. Red line represents low-pass filtered (moving average with a window of 12 months) SST anomalies.

3.3.5 EOF on SST Anomalies

The majority of variance is explained by 1st EOF mode of SST (Figure 35), which displays the seasonal signal of SST (Figure 36). In order to discriminate processes beyond the seasonal signal, EOF analysis was conducted on SST anomalies. However, the results were dominated by high-frequency signals. Therefore, a low-pass filter (1 year moving average) was applied prior to EOF analysis. The following dataset will hereafter be referred to as the filtered sea surface temperature anomalies (F-SSTA).

The first three modes of F-SSTA explain 92.3% of the total variance. First F-SSTA mode represents 87.5% of total variance. Its spatial structure (Figure 58) exhibits negative magnitudes all over the basin, with maximum negative magnitudes around Rhodes Gyre, Antalya and Latakia regions and around Crete. These regions are more prone to warming/cooling. This might be caused by entrapment of surface waters as a result of mesoscale circulation in these regions.This structure is very similar to the overall (1982-2012) SST trend map (Figure 43). It displays smaller magnitudes mostly around the southern part of the basin. Its temporal evolution (Figure 59) represents a phase transition in magnitude from positive to negative, indicating warming all over the Levantine.

Second F-SSTA mode explains 3% of total variance (38% excluding the first mode). Its spatial structure displays a zonal gradient with greater positive magnitudes in the north and a pronounced negative magnitude at Iera-Petra eddy. The corresponding temporal mode (Figure 61) displays positive and negative magnitudes with a complex interannual variability. Considering Iera-Petra is a wind-driven persistent circulation feature in the Levantine (Amitai et al., 2010), it can be suggested that this mode represents the response of SST to wind regime and also atmospheric conditions influencing on the northern and southern parts.

Third F-SSTA mode represents only 1.75% (or 22% excluding the first mode) of total variance. Its spatial structure (Figure 62) displays a pronounced positive magnitude in Iera-Petra region, a dipole pattern in Rhodes Gyre region, and a fuzzy scheme in the rest of the basin with neutral (around 0 magnitudes) and negative magnitudes. Its corresponding temporal evolution (Figure 63) exhibits both positive and negative magnitudes with three to four year oscillations.

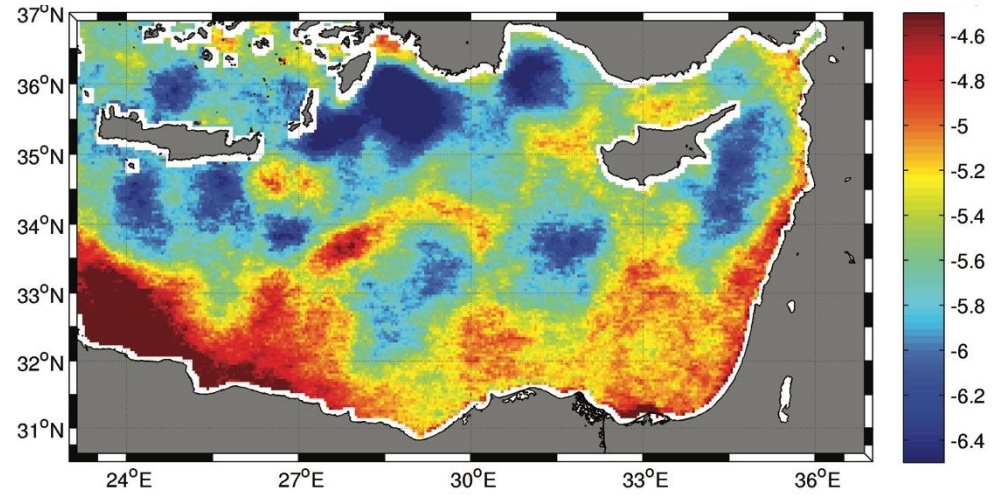

Figure 58 First spatial mode of F-SSTA (x10^{-3}).

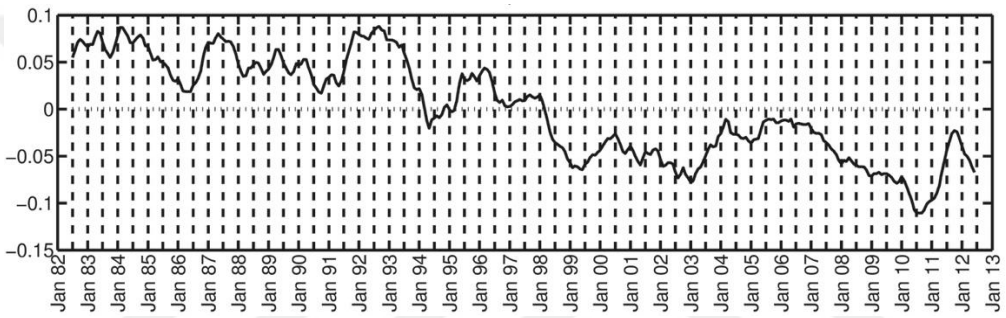

Figure 59 First temporal mode of F-SSTA.

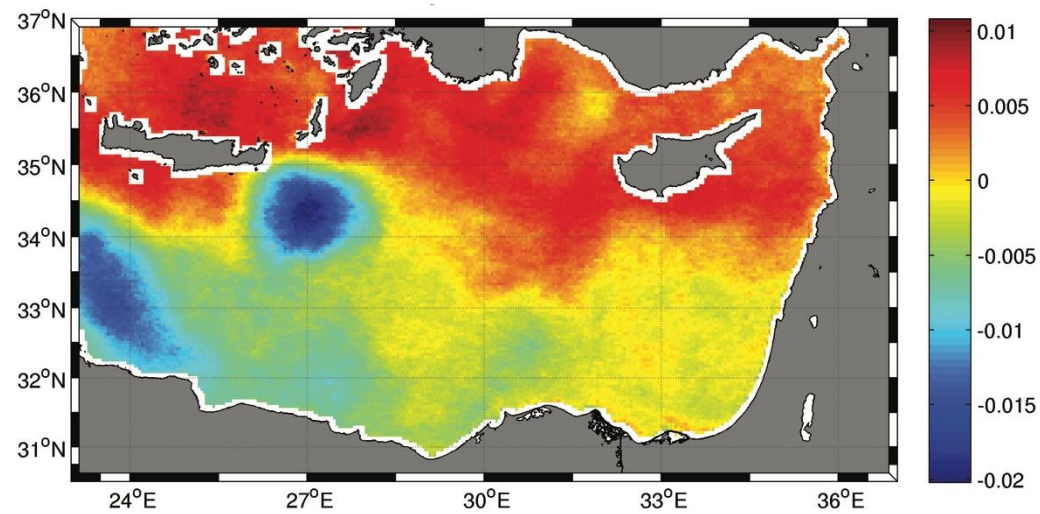

Figure 60 Second spatial mode of F-SSTA.

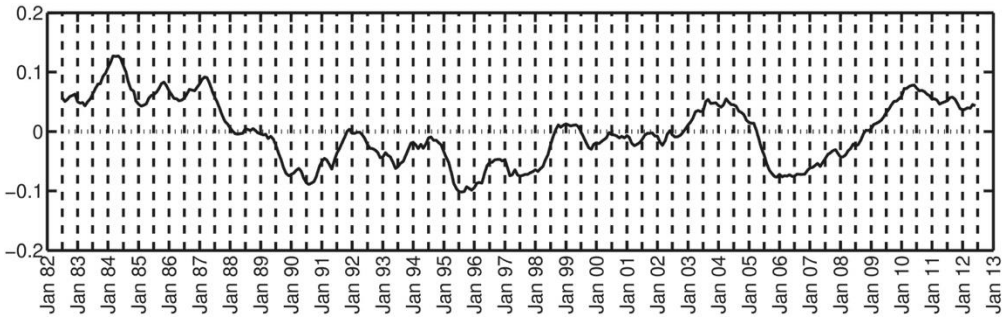

Figure 61 Second temporal mode of F-SSTA.

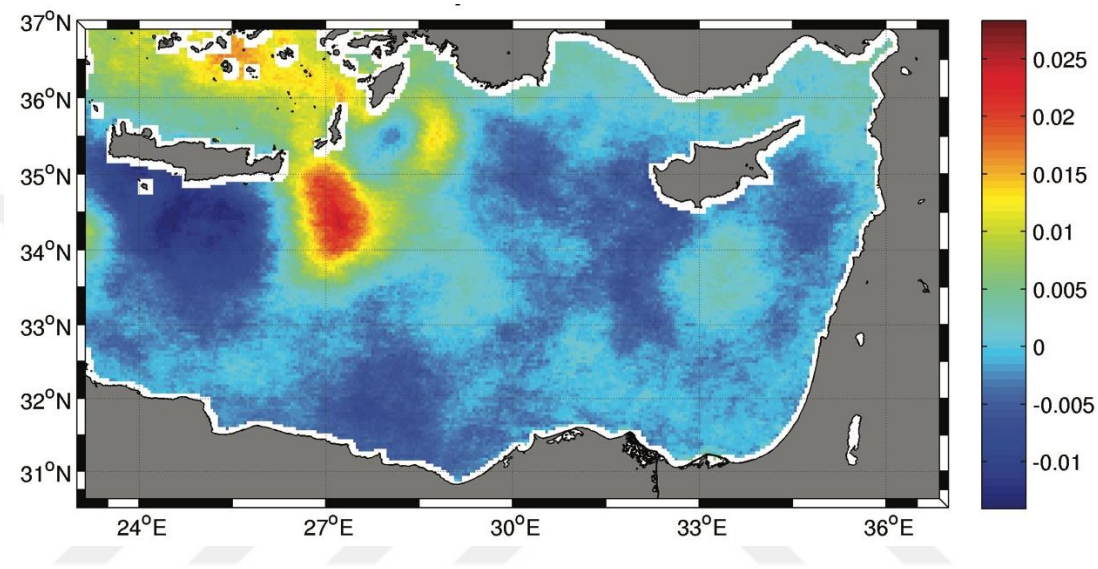

Figure 62 Third spatial mode of F-SSTA

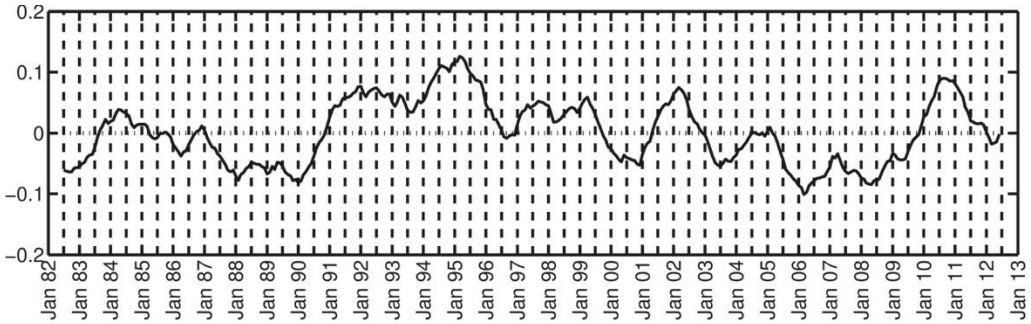

Figure 63 Third temporal mode of F-SSTA

3.3.6 Connections with large-scale atmospheric patterns

In order to assess the response of Levantine to teleconnection patterns of North Atlantic Oscillation (NAO) , East-Atlantic West-Russia (EA-WR) and Atlantic Multidecadal Oscillation (AMO) indices, F-SSTA time series was compared with low-pass filtered (12 month moving average) indices. Positive phase of NAO enhances the meridional sea level pressure (Trigo et al.,2002) results in stronger westerlies around mid-latitudes of the Atlantic onto Europe and anomalous northerly flow across Mediterranean (Hurrell and Deser,2009), producing warmer conditions over Scandinavia and northern Russia, extending to Central Europe. Positive phase of NAO means colder conditions for Eastern Mediterranean region (Trigo et al., 2002). Positive state of the EA-WR index enhances high pressure over the North Sea, opposed by low-pressure centers over West Russia (Josey et al., 2011).Positive state of EA-WR results in northerly airflow over the eastern Mediterranean and a warmer southeasterly flow in the western Mediterranean, constructing a east-west dipole structure in the Mediterranean (Josey et al.,2011). AMO index is defined by the detrended sea surface temperature anomalies averaged over the North Atlantic (Enfield et al., 2001). Oscillations(~70 years) in AMO index and Mediterranean SST were found to be very similar (Marullo et al.,2011).

F-SSTA is negatively correlated with NAO (-0.58) with 10 months lag and negatively correlated to EA-WR (-0.44) with one month time lag. F-SSTA time series is positively correlated to AMO and displays the highest correlation coefficient (0.71 with no lag) among three indices. Evolution of SST versus NAO, EA-WR and AMO indices are given in Figure 64. Spatial distribution of correlations of F-SSTA and NAO display a rather fuzzy pattern with magnitudes ranging from -0.4 to -0.55 (Figure 65). Lowest correlation is observed in Iera-Petra. Distribution of correlations between F-SSTA and EA-WR display a southeast/northwest gradient, with higher correlations on the southeastern part (Figure 66). This map suggests that the area influenced by EA-WR pattern does not reach west of 28^{O} E. Relatively higher correlations around Crete is an exception of EA-WR influence zone. Distribution of correlations between F-SSTA and AMO display highest correlations on the westernmost part of the basin, however the overall distribution of correlations are all higher than 0.6 suggesting influence of AMO index all over the basin.

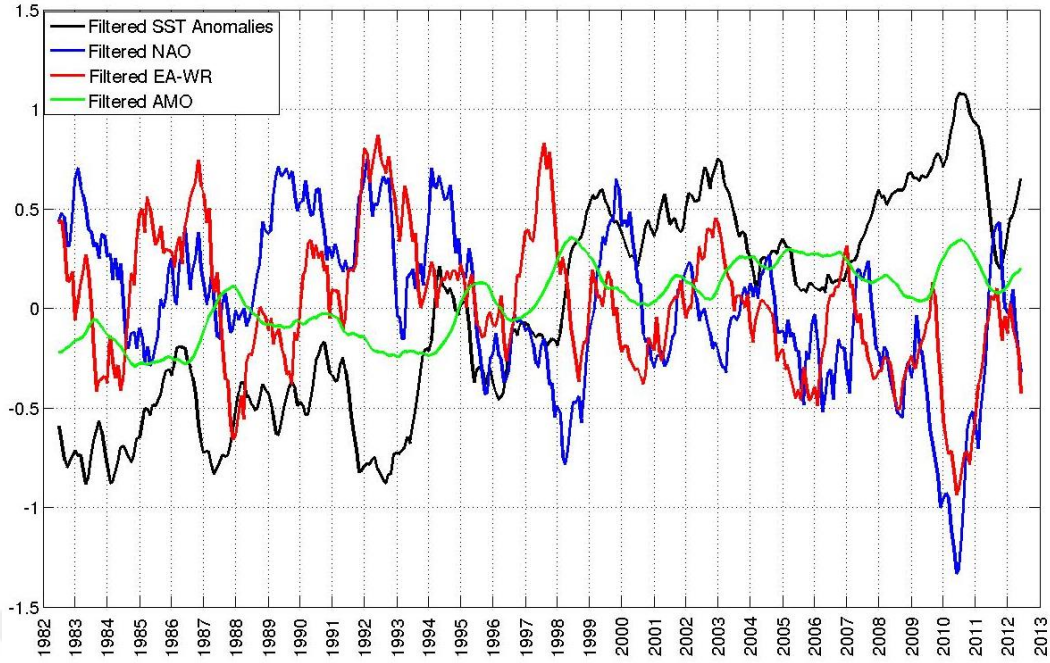

Figure 64 Inter-annual distribution of low-pass filtered SST anomalies, NAO, EA-WR and AMO indices.

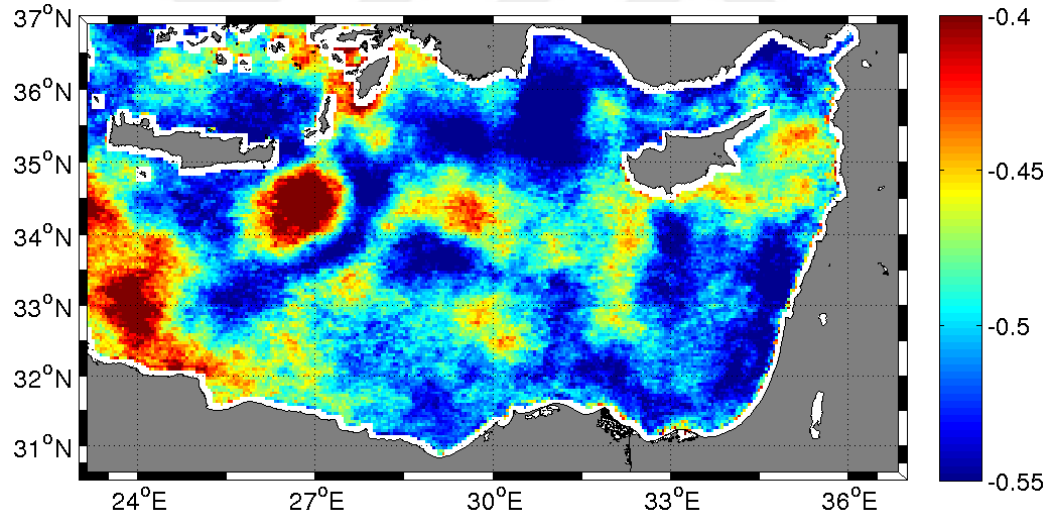

Figure 65 Spatial distribution of correlations between low-pass filtered SST anomalies and NAO for 1982-2012.

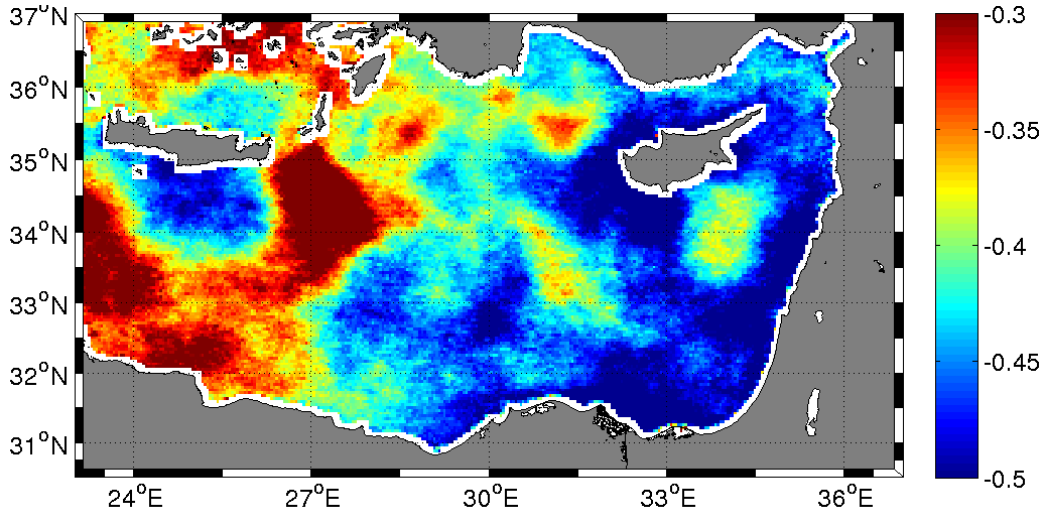

Figure 66 Spatial distribution of correlations between low-pass filtered SST anomalies and EA-WR for 1982-2012.

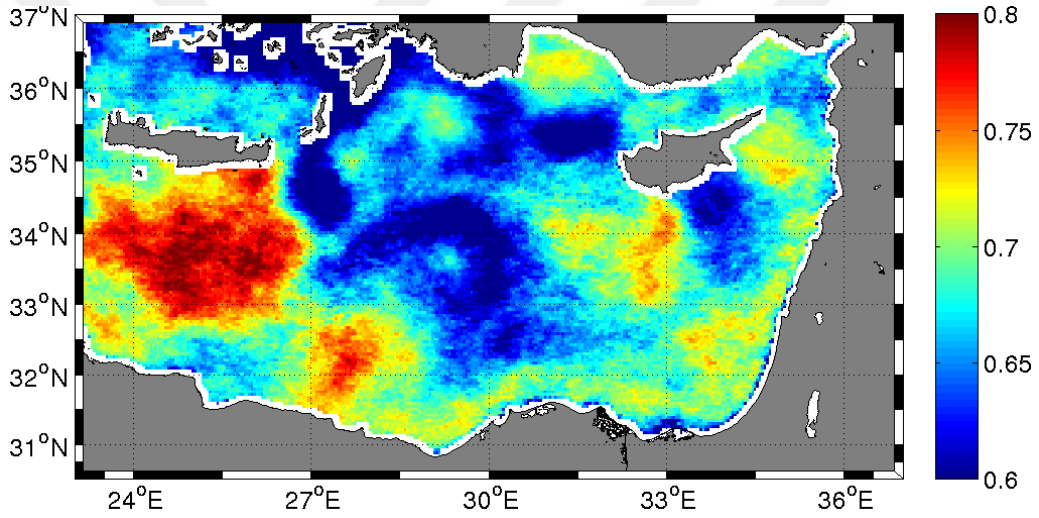

Figure 67 Spatial distribution of correlations between low-pass filtered SST anomalies and AMO for 1982-2012.

3.4 Discussion and conclusions

In this chapter the spatiotemporal variability and recent trends of Levantine SST were investigated by conducting trends analysis and an EOF analysis on the sea surface temperature dataset between 1982 and 2012. Most of the variability was explained by the first EOF mode (92.5%), which represented the seasonal cycle of SST. The signal of Rhodes Gyre and Iera-Petra are clearly seen in EOF modes 2 and 3, which represent smaller portions (4% and 0.5% respectively) of total variance. The existence of these

features in the SST modes emphasizes the dominance of these features in the Levantine Basin.

Trends of SST were calculated using GHRSST, OISST and HadleySST datasets. The basin wide warming trend was estimated as 0.06 ^{o}C/year. OISST and HadleySST trends were relatively lower, 0.04 ^{o}C/year and 0.05 ^{o}C/year respectively. This is an expected result, considering these datasets have different resolutions. The trends calculated here are comparable with previous studies over the Eastern Mediterranean such as 0.15 ^{o}C/year for 1983-1992 period over the Eastern Mediterranean using 18km data (Marullo et al., 1999b), 0.061 ^{o}C/year for the whole Mediterranean for 1992-2005 using optimally interpolated SST data (Criado-Aldeanueva et al., 2008), 0.05 ^{o}C/year for 1985-2006 using 4km monthly dataset (Nykjaer 2009) and 0.042 ^{o}C/year for 1985-2008 using an optimally interpolated dataset (Skliris et al., 2012) or 0.77 ^{o}C/year for 1985-2009 period (Macias et al., 2013). It is important to note at this point that all studies listed above calculated trends for the whole Eastern Mediterranean. Specific calculations for Levantine Basin are limited. Shaltout and Omstedt (2014) calculated the 1982-2012 SST trend for Levantine Basin as 0.042^{o}C/year, using 0.25^{o} data. Considering the low resolution of satellite data used there, the different result to this study is expected.
Spatial distribution of SST trends displayed that the highest warming trend is observed around Rhodes Gyre and Iera-Petra eddy. This might be a result of entrapment of surface waters via dominant circulation features in these areas. Spatial distribution of SST trends for each month exhibit higher warming trends in the western part of the basin during summer (June, July, and August).Previously (Josey et al., 2011) it has been shown that the NAO and EA-WR indices have a small impact on heat loss/gain in the Mediterranean in summer. Therefore intense warming trends observed in summer might be a result of increased radiative fluxes.

The analysis of SST anomalies revealed a clear shift from negative anomalies to positive anomalies in 1997/1998. 1982-1997 is dominated by negative anomalies and 1998-2012 is dominated by positive anomalies. Considering the DINEOF analysis conducted on SST dataset showed that the dominant signal is the seasonal cycle, EOF analysis was conducted on the anomaly dataset to investigate the SST variability beyond the seasonal cycle. The results were filled with high-frequency signals. Therefore EOF analysis was conducted on the low-pass filtered anomaly (F-SSTA) dataset. The spatial structure of the first mode revealed patchy pattern with most negative values around

Rhodes Gyre, Antalya, Latakia and Crete. The corresponding temporal mode denoted a warming trend. Thus, the 1st spatial mode displays the regions of the Levantine with the highest and lowest warming. SST trend map showed similar regions with highest warming rates, consolidating the results. Second and third modes of F-SSTA exhibited pronounced patterns (both uniform and dipole patterns) in Iera-Petra and Rhodes. This is the region of phase transition (cyclonic/anticyclonic) for wind stress curl. Thus it can be claimed that these two modes are influenced by the wind. However, correlations between these modes and wind stress curl were very low. An important correlation exists between the first modes of SST and wind stress curl (0.76 with 1 month lag). However, this is expected considering the first temporal modes of both parameters represent a seasonal pattern. A relation between F-SSTA and zonal and meridional components of wind was found to be 0.71 and 0.50 (both with 2 months lag) respectively. Thus it can be concluded that the wind regime is an extremely important driver of the SST spatio-temporal pattern in the Levantine Basin. Previously, it has been found that the SST response to wind reached a maximum (correlation=~0.6) in 5 months (Kabbara et al., 2002). Our results suggested that this coupling is reached at 8 months with a higher correlation (0.74). However, it is important to note that Kabbara et al. (2002) used a lower resolution SST dataset (18km) with a shorter time span (1985-1997).

In order to identify any links to large-scale atmospheric forcing, correlations between low-pass filtered SST anomalies and low-pass filtered indices (NAO, EA-WR and AMO) were investigated. Temporal distribution of basin averaged SST was found to be negatively correlated with NAO (-0.58) with 10 months lag. However, the spatial distribution of correlations showed that this is the maximum value of correlations. Basin averaged SST was negatively correlated with EA-WR index (-0.44) with one month lag. Correlations vary between -0.3 and -0.5 around the basin. Spatial distribution of correlations between SST and EA-WR suggest that EA-WR index is more influential on the eastern part of Levantine. Highest correlation among climatic indices was found in AMO. SST was positively correlated with AMO (0.71) with no lag. Correlations displayed a patchy pattern around the basin with magnitudes varying 0.6 to 0.8. This suggests the strong influence of Atlantic inflow over the Levantine basin, which was previously suggested by Skrilis et al. (2012). AMO and Mediterranean SST were found to have similar oscillations (Marullo et al., 2011) and it was suggested that AMO

variability is transferred to the Mediterranean through atmospheric processes (Mariotti and Dell'Aquila 2011). Another study suggested that AMO is responsible for more than half of total warming in the Mediterranean (Macias et al., 2013). Previous studies suggested that EA-WR index showed no significant correlation with SST (Skrilis et al., 2012) and lower correlations with NAO index. However, within this study, both indices had significant correlations with higher correlation magnitudes.

This chapter investigated the spatio-temporal variability and warming trends of Levantine SST using high-resolution satellite SST data for 1982-2012. Impacts of wind and heat flux on the SST were investigated as well as atmospheric teleconnections. Rapid warming of Levantine will most likely result in increased stratification, reduced mixing, decline of cold water formation/renewal events and eventually reduced oxygen in deeper layers. It is also important to note that increased SST's will result in perturbations of the ecosystem. Mediterranean is a climate change hotspot (IPCC 2007; Shaltout et al., 2014.) and enhanced warming will result in higher rates of successfully established of tropical species in the Mediterranean (Raitsos et al., 2010; Schmidt et al., 2015).

3.5 Comparison of the sea surface temperature variability in the Black Sea and Levantine Basin

The Black Sea is an enclosed basin with a very shallow mixed layer. Therefore, the SST response to atmospheric forcing in the Black Sea is faster and more amplified than the Eastern Mediterranean which possesses a much deeper mixed layer. Another factor effecting on the warming of these regions may be the impact of atmospheric variability over the region (Krichak et al., 2002; Josey et al.,2011). The Black Sea basin wide warming trend for 1982-2012 was estimated as 0.078 ^{o}C/year, reaching much higher values regionally. On the other hand, Levantine basin average warming was estimated as 0.06 ^{o}C/year also displaying higher rates regionally. The Black Sea displays highest warming with a fuzzy spatial structure, having highest warming rates in the eastern and northeastern parts of the basin, whereas in the Levantine highest warming rates are observed in areas with the well-known circulation field such as Rhodes Gyre. Analysis of thermal anomalies displayed a transition from negative to positive anomalies in both seas. In the Black Sea, 1982-1998 (1999-2012) was dominated by negative (positive) anomalies whereas in the Levantine basin, 1982-1997 (1998-2012) was dominated by negative (positive) anomalies. These transitions were clearly evident in the first

temporal EOF modes, conducted on low-pass filtered SST anomalies. Particularly warmer and colder years were sometimes similar (i.e. 2012) in both seas, however not always, suggesting influence of both common and different large scale atmospheric patterns. Black Sea SST displays a combined response to NAO and EA-WR, whereas SST in the Levantine is mainly regulated by Atlantic influence, displaying the highest correlations with AMO throughout the basin. This is probably caused by the proximity of the two regions to these atmospheric patterns. For example EA-WR index displayed highest correlations with Levantine SST in the eastern part of the basin (Figure 66), highlighting the importance of proximity to atmospheric structures.

CHAPTER 4: Inferring different phytoplankton responses to variability in the Black Sea physical environment from satellite remote sensing: seasonal to interannual time scales.

4.1 Introduction

Over the past decades, significant changes occurred in the Black Sea ecosystem. Combined effects of anthropogenic and climatic changes have led to severe alterations in the ecosystem. Eutrophication, overfishing, outburst of invasive and opportunistic species, climate change and their impacts on the ecosystem have been documented extensively (Zaitsev and Mamaev, 1997; Gucu, 2002; Daskalov, 2002; Shiganova, 1998; Oguz et al., 2003; Oguz, 2005a). Eutrophication has particularly been observed in the northwestern shelf (Mee, 1992; Bodeanu, 1993; Cociasu et al.,1996; Yunev et al.,2007; Oguz and Velikova, 2010). Northwestern shelf has its own characteristics and complex ecosystem dynamics (Tolmazin 1985; Oguz and Gilbert, 2007; Oguz and Velikova, 2010) where the discharge intensity of rivers has a major impact on the ecosystem (Nezlin et al., 1999). Impacts of eutrophication on plankton in the open waters of the Black Sea were not observed until mid1980's (Vinogradov et al., 1999; Yunev et al., 2005), whereas changes in the nutrient profiles were evident (Tugrul et al., 1992; Basturk et al., 1997; Oguz et al., 2000; Konovalov and Murray, 2001; Yunev et al., 2005). One reason may be the partially isolated ecosystem of the open waters by the meandering Rim current (Oguz et al., 1993; Yunev et al., 2002). Basin-wide changes were evident at the second half of the 1980's (Yunev et al., 2005) through various studies (Mikaelyan, 1997; Vedernikov and Demidov, 2002; Yunev et al., 2002).

Eutrophication degraded the ecosystem starting from the 1970's, eventually propagating towards higher trophic levels (Oguz, 2005a). Plankton community structure, intensity and frequency of algal blooms were altered (Bodeanu, 1993; Moncheva and Krastev, 1997; Mikaelyan, 1997; Oguz, 2005a). Recently Black Sea ecosystem displayed positive changes including reduced nutrient input from rivers, increase in diatoms proportion, frequency of algal blooms and a decrease in total phytoplankton biomass (Bodeanu et al.,2004; Yunev et al., 2002; Parr et al.,2005; GEF-UNDP, 2006; TDA ,2007; BSC, 2008; Oguz and Velikova, 2010). Despite Black Sea ecosystem

shows recovery signs in terms of eutrophication, another bottom-up control mechanism (Oguz and Gilbert, 2007), climate forcing, continuously has a negative impact on the ecosystem. Phytoplankton response to increased temperatures has been schematized for the world ocean (Doney, 2006) and Black Sea is no exception. Warming induces stronger stratification and reduced mixing resulting in reduced nutrient input from the nutricline (Nezlin, 2001). Bottom-up flux of nutrients was suggested to be the reason of the observed "regime shifts" in the lower trophic levels of the Black Sea ecosystem (Mikaelyan et al., 2013). Impacts of warming and cooling on the Black Sea ecosystem, especially on the lower-trophic levels have been subject to various studies, (Mikaelyan, 1997; Nezlin et al., 1999; Nezlin, 2001; Oguz et al., 2003; Oguz, 2005b; McQuatters-Gollop et al., 2008). Changes in temperature also regulate the baroclinic and frontal instability of the Rim current, generating filaments, meanders, and other mesoscale and sub-mesoscale features that play an important role in the cross-shelf transport (Oguz et al.,2002). Physical evolutions of cross-shelf transport as well as its biological consequences have been documented all along the Black Sea coast (Sur et al., 1994; Sur et al., 1996; Ozsoy and Unluata, 1997; Gawarkiewicz et al. 1999; Oguz et al., 2002; Ginzburg et al., 2002; Shapiro et al., 2010).

All of the aforementioned factors have important impacts on the Black Sea ecosystem. This study focuses on the impacts of warming and accompanying changes (changing winds, sea level, and circulation) on the ecosystem, by means of investigating the phytoplankton dynamics. Phytoplankton response to changing temperature and circulation is elaborated, particularly in the deeper basin, considering the dynamics of the shelf are rather complex, as previously mentioned.

4.2 Materials and Methods

The Black Sea 1998-2012 time series of sea level anomalies used in this study were obtained from AVISO (Archiving, Validation and Interpretation of Satellite Oceanographic data) Sea Level Anomalies (SLA) regional product for the Black Sea (http://www.aviso.oceanobs.com/en/data/products/sea-surface-height-products/regional/m-sla-black-sea/index.html). They are daily, multi-mission sea surface height anomalies computed with respect to the mean profile over the time frame 1993 to

2012 and gridded on a regular 1/8° x 1/8° grid. The mean dynamic topography data provided by Korotaev et al. (2003) was added to the daily AVISO fields to compute the absolute dynamic height (ADT) of the Black Sea and then the data were averaged into weekly composites of absolute dynamic height. Mean ADT and geostrophic velocities averaged over 1993-2014 period are shown in Figure 68.

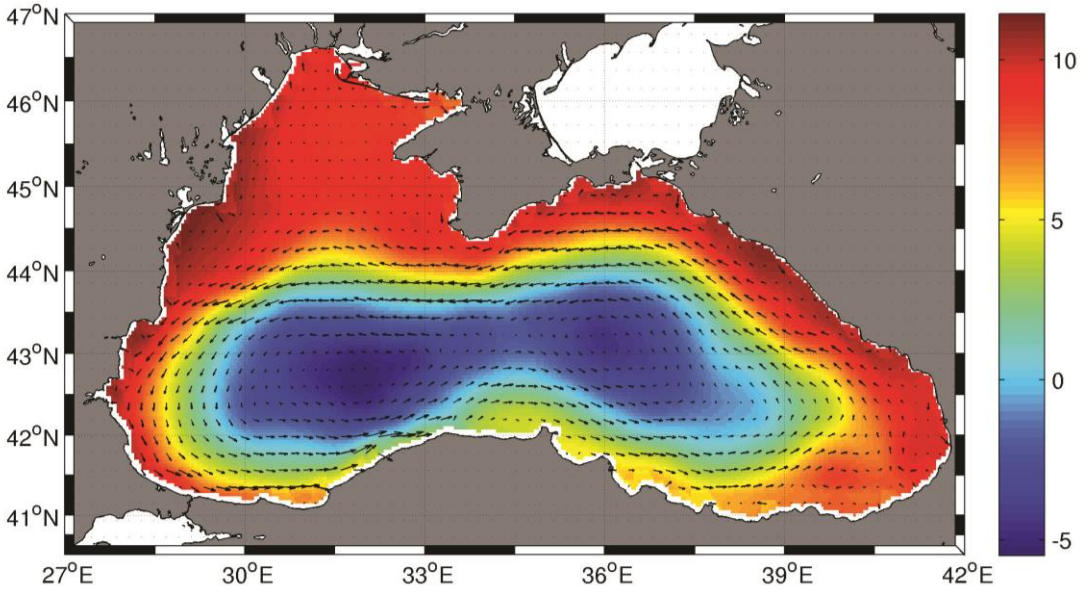

Figure 68 Mean absolute dynamic topography (cm) and geostrophic velocities in the Black Sea (1993-2014).

Sea surface temperature data used in this study is the AVHRR (Advanced Very High Resolution Radiometer) Pathfinder version 5.2 data. Daily images of night-time overpass sea surface temperature data from 1998 to 2012 were obtained, which refers to the temperature of the surface layer of the Black Sea. The data available on a 4km grid were averaged into the same weekly composites as the absolute dynamic height data. This 7-day averaged temperature data still has data gaps in it and hence the missing data was filled in using the Data INterpolating Empirical Orthogonal Functions (DINEOF) technique as detailed below.

Chlorophyll data was obtained from the European Service for Ocean Colour, GlobColour Global 4km product, which includes reprocessed Level 3 data from satellites MERIS, MODIS AQUA, SeaWIFS and VIIRS for the period 1998-2012. Of the different satellite data used to create this product the MERIS data was produced using the OC4Me algorithm, SeaWIFS data was produced with the OC4v5 algorithm, and the MODIS/VIIRS data were produced using the OC3v5 algorithm. The GlobColor data set contains daily maps of near-surface Chl-a concentration (mg/m^3) with a 4 km

resolution dataset merged (all four satellites) using the GSM model (Maritorena and Siegel, 2005). The data were averaged into the same weekly composites. This weekly averaged chlorophyll data has considerable amount of missing data (~30%) and hence this data was also filled in using DINEOF technique as detailed below. While there may be problems associated with any of the algorithms used for detecting chlorophyll a in the Black Sea these are not of importance here, as we are using the compiled data set to analyze for trends and not to compute the absolute biomass of phytoplankton.

All three satellite data sets above were interpolated onto the same 4 x 4km spatial grid and a commom landmask was created that includes all areas where one of the products may have missing or faulty data. For SST data, an instrument noise of 0.6 ^{o} C has been suggested in the Black Sea (Nardelli et al., 2010). Altimetry data has root mean square differences of 4.3-6.7 cm with tide gauge data in the Black Sea (Volkov and Landerer, 2015). Median percentage error of GlobColour chlorophyll data in the open ocean was found as 29.53% when compared to in-situ measurements, whereas this value was found to be 53.04%, 44.08% and 35.77% for MERIS, MODIS and SeaWiFS respectively (Ford et al., 2012).

Surface wind stress data used in the study is the Cross-Calibrated Multi-Platform (CCMP) Ocean Surface Wind Vector L3.0 First-Look Analyses data set retrieved from the Jet Propulsion Lab website (http://podaac.jpl.nasa.gov/Cross-Calibrated_Multi-Platform_OceanSurfaceWindVectorAnalyses).

This data set contains 6-hourly gridded analysis of ocean surface winds on a 0.25° spatial grid, of which an average of the two daily measurements were used in this study. The CCMP dataset combines cross-calibrated satellite winds obtained from Remote Sensing Systems using a Variational Analysis Method and includes cross-calibrated satellite winds derived from SSM/I, SSMIS, AMSR-E, TRMM TMI, QuikSCAT, SeaWinds, and WindSat. The reference height of the surface wind data is 10m. Wind stress (τ) was calculated as $\tau = \rho_a C_D V^2$ with air density ρ_a = 1.293 km m^{-3} and drag coefficient C_D depending on wind speed, V, after Trenberth et al. (1990). In addition the wind stress curl was calculated as $Curl(\tau) = \frac{\partial \tau_y}{\partial x} - \frac{\partial \tau_x}{\partial y}$ where the components of the wind stress vector τ are τ_x and τ_y. The curl expresses the rotation a vertical column of air would experience in a wind field that varies in space.

River discharge data taken from the Ludwig et al. (2003, 2009) river discharge

dataset created from observations and model results for the Black and Mediterranean Seas for the EU 7th framework project PERSEUS is used in this study. This data set was chosen because there are only sparse observations on Black Sea Rivers available for this time frame. A total number of 11 rivers are considered in this study that make up a mean yearly discharge of 320 km^3 yr^{-1}, of which Danube contributes 2/3rd of the discharge and the four major rivers emptying on the northwestern shelf, Danube, Dniepr, Dniestr and Southern Bug, contribute 89% of the water discharge into the Black Sea. These estimates fit well with those made by Volkov and Landerer (2015) using Danube discharge from the Global Runoff Center and discharge data until the 1990's from Dai et al. (2009).

Table 6 Mean water and DIN discharge of eleven largest rivers discharging into the Black Sea during the period 1998-2009 including peak discharge months. Data taken from Ludwig et al. (2003, 2009)

River	Mean discharge 1998-2009 (km^3 yr^{-1})	Mean nutrient discharge 1998-2009 (kt yr^{-1})	Peak discharge (month)
Danube	217.2	408.3	March-April
Dnieper	49.64	92.36	April
Rioni	11.46	5.46	December-January
Dniester	9.86	17.5	March
Chorokhi	7.83	6.43	January, May
Kizilirmak	5.93	11.62	April
Sakarya	4.92	8.94	February-March
Yesilirmak	4.78	17.22	March-April
Kodori	4.32	1.54	April-May
Filyos	2.2	3.67	January, March
Southern Bug	2.03	7.77	March

4.2.1 Emprical Orthogonal Function Analysis

Empirical Orthogonal Function (EOF) analysis was used to decompose satellite CHL, ADT and SST fields into a series of data-based orthogonal functions that can be used to optimally reconstruct the original datasets. Since, often, only a few of these functions are necessary for reconstruction, EOF analysis greatly reduces the size of the problem to be analysed. The temporal and spatial components of the EOFs contain the dominant spatial structures within the dataset as well as by comparing the EOFs of the different datasets to each other and to other observed or derived fields; our aim is to reveal the relationships between different datasets.

All satellite fields to which the EOF analysis was applied are three dimensional fields which contain the value of the field at specific longitudes, latutudes and times. Suppose that the each field contains a total of k maps consisting of n longitudinal and m latitudinal points. The data can be rearranged in a sample matrix X = (x1,x2,…,xk), where each column is reordering of a map and there are a total of k columns. The EOFs are, then, the left and right eigenvectors of the sample matrix.

4.2.2 Data Gaps

Satellite datasets contain gaps due to instrumentation errors or cloud coverage. It is not possible to decompose a matrix into its components using standard approach. Gaps in the data must be filled using a gap-filling algorithm. Data Interpolating Empirical Orthogonal Functions (DINEOF) (Beckers and Rixen 2003) were used to fill the gaps in the data. Data are stored in a matrix; missing data are initially set to zero. Then Singular Value Decomposition (SVD) is conducted to calculate first EOF mode. This first spatial mode is then multiplied by the corresponding temporal amplitude and used to replace the missing data (step A). Then the SVD is performed again (step B). This is an iterative process, where step A and step B are repeated until convergence is reached. This procedure intends to fill data gaps; EOF analysis is a side product of this technique.

4.2.3 Data filtering

The EOF analysis described above was used in two different ways. The direct application of EOF analysis to weekly composited/averaged data was used to reveal the seasonal dynamics. In the second approach, the data was passed through a low pass filter in order to suppress high-frequency signals to reveal interannual variability.

4.2.4 Eddy tracking

An eddy tracking algorithm called "Eddyscan" is used to identify and track eddies (Faghmous et al., 2012). The eddy identification scheme adopts the principle that every eddy should have a single extremum which is defined as a grid cell with the maximum or minimum SLA amongst its 24 neighbors in a 5x5 grid (Faghmous et al., 2015). Eddies are defined as single maxima/minima surrounded by a closed contour SLA (Faghmous et al., 2015). Eddy tracking scheme in Eddyscan is adopted from Chelton et al. (2011).

4.3 Results

4.3.1 Linking climate to ocean physics (1993 -2014)

Average fields of satellite data

Sea surface temperature displays a zonal gradient with the eastern Black Sea being up to 1.5 degrees warmer than the western of the Black Sea, which is about 1 degree warmer than the northwestern shelf (Figure 69). It is at ~38^{o}E where the east starts to be much warmer than the west. This may be a result of intense anticylonic mesoscale activity in the region all year round. The interior basin is colder as a result of permanent cyclonic gyres in the area. It is surrounded by a slightly warmer Rim Current region. The northwestern shelf is the coldest region. It is known that the northwestern shelf experiences intense cold winds and winter convection. The northwestern shelf together with the centers of cyclonic gyres have been suggested to be the location of cold water formation in the Black Sea (Ozsoy and Unluata, 2003). Temporal evolution of SST (Figure 69) is seasonal with lowest mean temperatures in March and highest in August. March 1998, 2003, 2006 and 2012 were especially cold and the August of 2001, 2002, 2007 and 2010 were particularly warm.

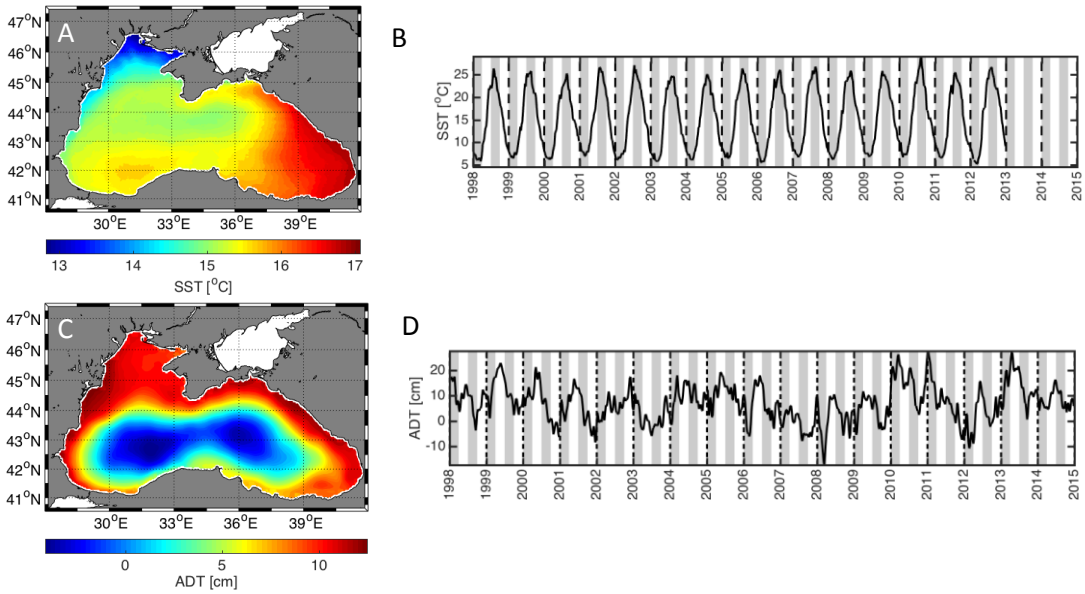

Figure 69 Climatology of satellite derived A) SST (°C) and C) ADT (cm) computed for the time frame 1993-2012 and 1993-2014 respectively, with the corresponding temporal amplitudes for B) SST and D) ADT

The 21-year mean absolute dynamic topography (ADT) map is negative to a minimum of -4.5 cm in the deep basin with its cyclonic gyres, surrounded by a positive periphery with 6 cm representing the Rim Current, and strong positive distribution in the coastal parts. This feature also represents a crude snapshot of the general surface circulation and has already been acknowledged in various studies (Oguz et al. 1993, Korotaev et al. 2003, Capet et al. 2012). The temporal dynamics of ADT does not display an obvious seasonal cycle. Positive fluctuations of ADT are mainly found during summer and negative fluctuations often in winter; however there are exception such as a positive peak in January 2003 and 2011. Largest positive fluctuations of ADT occurred in spring 2010 and winter 2011 and the negative fluctuations occurred in spring 2008. Responsible mechanism for these large fluctuations have been suggested as related to freshwater fluxes dominated by river inflow and Bosphorus outflow (Volkov & Landerer 2015).

First SST mode represents 97 % of the total variability and its temporal pattern follows the seasonal cycle of the SST distribution (Figure 70). The spatial distribution is positive over the Black Sea, with higher values in the Northwestern Shelf, decreasing towards the west. This mode is a representation of the basin wide heating and warming in SSTs. In summer, the temporal mode is positive, indicating stronger warming of SSTs on the

Northwestern Shelf and stronger cooling in winter, due to winter convection. This is a clear demonstration of the shallow water depth and mixed layers on SST distribution. Although the second EOF mode only explains 1.5% and is rather negligible compared to the first mode, it represents the east-west SST gradient observed in the Black Sea. Its temporal distribution is negative throughout almost the whole period. It is mostly negative in fall, increasing SSTs in the eastern basin more and thus establishing the SST zonal gradient. Considering this happens mainly in fall, it suggests increased instability in the circulation system, and thus generation of more anticylones in the region, giving rise to this pattern.

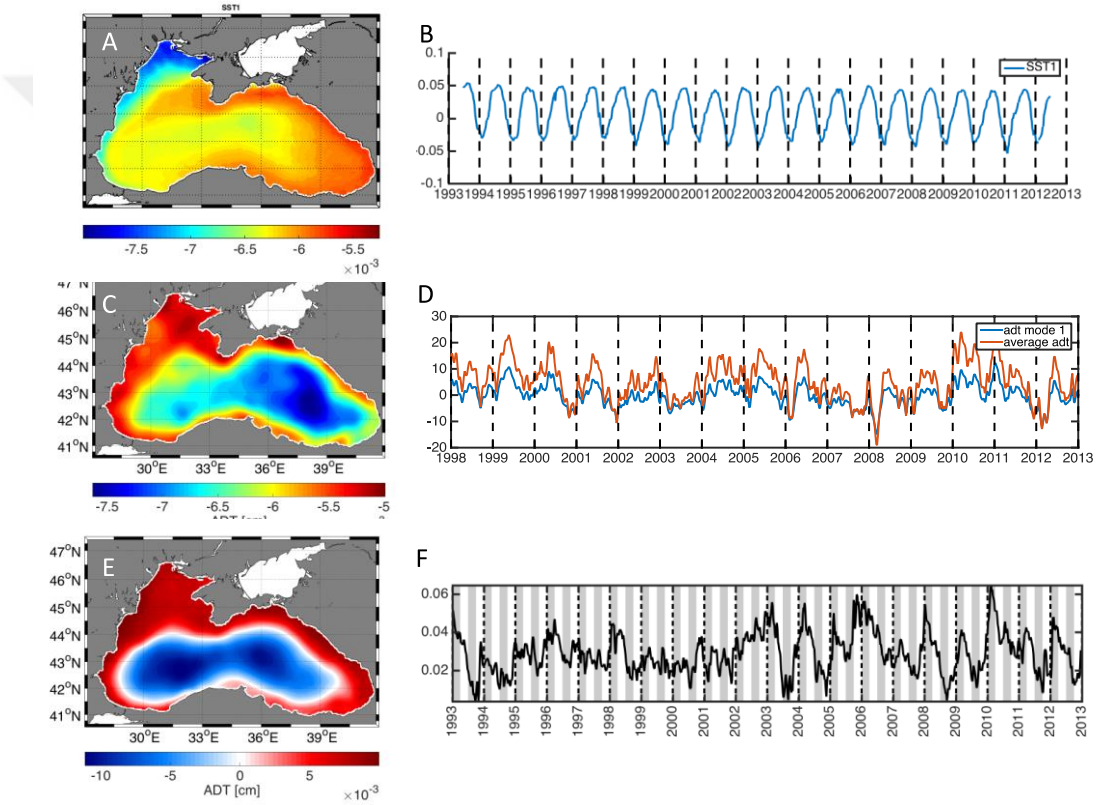

Figure 70 First EOF mode of A) SST and C) ADT computed for the time frame 1993-2912 and 1993-2014 respectively, and E) second EOF mode of ADT. Corresponding temporal amplitudes for B) SST (blue, red for mean SST-1) , D) ADT (blue, red for mean ADT-1) and F) second more of ADT

The first EOF mode of ADT represents 63% of the total variability and the spatial map shows homogeneous negative values across the basin with lower values in the interior. The temporal distribution of this mode follows the average ADT temporal distribution (Figure 70E). This mode corresponds to complex nature of the water budget (river input, air-sea exchange and Bosphorus outflow) of the Black Sea and its distribution

through time, with the change in volume being mainly due to seasonal variability of freshwater in- and outflow as has been noted before (Stanev and Peneva, 2002; Volkov and Landerer 2015).

The second ADT mode represents 28% of the total variability with the spatial map indicating negative values in the interior, slightly positive-neutral at its surrounding and positive at the coastal parts (Figure 70C). The temporal amplitudes are positive at all times with maxima in winter and minima in fall. This mode represents the magnitude of the ADT variation between the cyclonic interior and anticyclonic coastal part, separated by the Rim Current. In early winter the temporal mode is positive, sea level increases in the coastal regions, which is accompanied with compensating sinking of sea level in the open sea. This causes the slope of sea level to increases and results in an intensification of geostrophic currents in winter-to-spring months (Stanev and Peneva, 2002), essentially creating a well pronounced Rim Current and coastal anticyclones whereas when it is weaker, these features weaken. This has previously been also identified by Stanev and Peneva (2002), Grayek et al. (2010) and Capet et al. (2012) where the authors concluded that this mode is associated with the rim current strength.

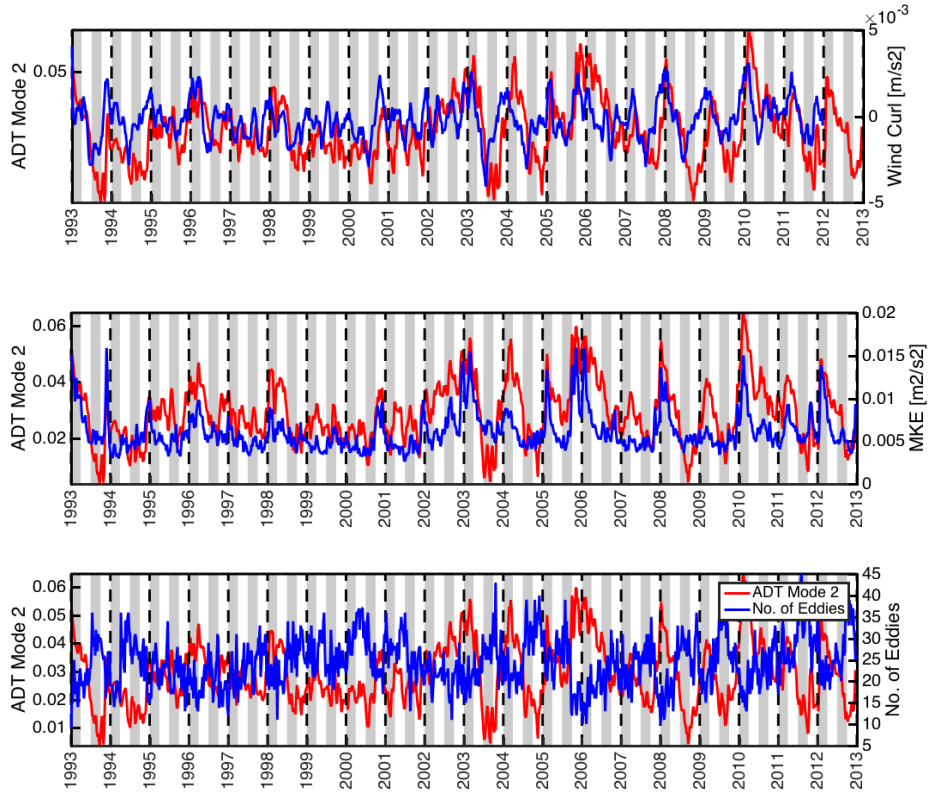

Figure 71 ADT-2 temporal mode (red line) versus A) smoothed wind curl (m/s^2), B) mean kinetic energy (MKE – m^2/s^2) and C) Number of Eddies (blue line).

Hence we conclude that ADT-2 is associated with Rim Current strength and is highly correlated to wind stress curl (r=0.64) with time lag of 4 weeks (Figure 71A). We show here that there is a shift in 2002 from relatively low variability of both wind curl and mean kinetic energy (implying low surface velocity) from 1993-2001 to a much more dynamic system with stronger wind curl variability and currents. The temporal amplitudes of the ADT-2 mode show stronger variability after 2002, with low values in summer and fall and high values in winter and spring. During high values the sea-level increases in the coastal regions (the positive anomalies along the coast) while at the same time the sea level in the open sea is sinking (negative anomalies in the open Black Sea). This indicates a stronger slope of the sea-level and hence leads to stronger geostrophic flow. Therefore, in the time after 2002 the Rim Current is more defined during the winter/spring time than in the years before 2002 when variability is much lower. This effect can also be seen in the Mean Kinetic Energy (MKE) which is seen to increase variability just as the ADT-2 mode (Figure 71B). MKE is highly correlated (r=0.7) to ADT-2. The mean kinetic energy during 1993-2001 was low and the MKE in

the period there after is much higher displaying an almost 2-fold increase in MKE in the system after 2002. After 2002 therefore the Rim Current should be stronger and more defined in winter/spring and less eddies should exist at this time. This is indeed the case as can be seen when correlating ADT-2 with number of eddies computed with an eddy-tracking algorithm (Figure 71C). Correlation is significant at r=-0.64, with no time lag. We conclude that a shift in the circulation that is caused by a significant shift in wind curl occurred in 2002. The effect of this shift is stronger Rim Current System with less eddies (Figure 71).

4.3.2 Linking ocean physics to biological productivity on seasonal time scales

In an effort to link above results to the recent trends in biological productivity, in this study we focus on chlorophyll data derived from GlobColor product in the time frame 1998-2012 and analyze its seasonal variability and correlate it to physical parameters such as SST, ADT, wind curl and river influx.

The mean chlorophyll map displays a strong gradient between the Northwestern Shelf and the rest of the Black Sea (Figure 72A). High production is seen on the shelf, extending south all the way to the Sakarya region, and then to a lesser extent high production is seen along the southern and eastern and northern coastal regions. In contrast, the interior of the Black Sea has significantly lower levels of chlorophyll than the coastal regions. The temporal evolution of chlorophyll concentrations (Figure 72B) correlates well with Sea surface temperature spatial and temporal distribution which has been detailed in previous studies (McQuatters-Gollop et al. 2008). The temporal evolution of chlorophyll concentrations display a shift in regime with maxima in 2001 and a major decline after 2002.

Three major rivers discharge onto the northwestern shelf (Danube, Dniester and Dniepr) and the nutrients they transport into the Black Sea have strong influence on the chlorophyll concentrations on the shelf as has been discussed in many previous studies. The discharge areas of these rivers have the highest chlorophyll concentrations, however it should be kept in mind here that the satellite chlorophyll concentrations on the shelf might be faulty to some extent (see methods above). A clear northwest-southeast

gradient is observed within the northwestern shelf. In the east along the Georgian coast, where the rivers Rioni, Inguri, Kodori and Chorokhi enter the Black Sea higher production than in the surrounding is observed. The mean chlorophyll map gives the impression as if the riverine input alone constitutes the distribution of chlorophyll along the Black Sea. However, if one looks more closely the riverine input alone cannot explain the high coastal phytoplankton concentrations all around the Black Sea compared to the low production in the interior. To show this and because the mean chlorophyll map is dominated by the high production on the Northwestern Shelf, we masked all areas with chlorophyll concentration greater than 0.6 mg/m3 (later referred to as masked Chl-a).

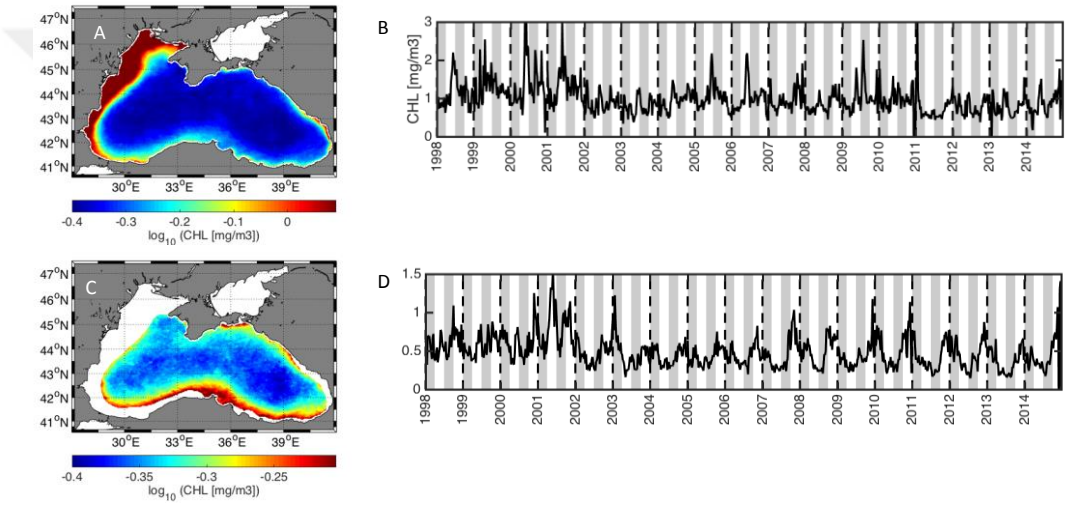

Figure 72 Climatology from 1998-2014 of A) Chl a and B) Chl a where areas with concentrations greater than 0.6 are masked, with the respective data time series (C, D).

First Chl-a EOF mode explains 42% of the total variance and the spatial distribution shows a zonal gradient with positive values in the southwest Black Sea that are decreasing towards the east (Figure 73A). Values around zero are found in an eddy-like feature of Crimea and the interior of the eastern Black Sea shows slight positive values. The temporal distribution of this mode is mainly positive until 2002, with negative values in spring and summer and then changes to being mainly negative in the following years after 2002, with positive values appearing in fall and winter (Figure 73B). Thus this mode increases the difference between the western Black Sea. This mode follows the mean chlorophyll concentration (Figure 73B) and hence captures the anomalous year 2001 and the clear decrease in mean Chl-a biomass beginning 2002. The first Chl-a EOF

mode is negatively correlated (r=-0.6) to the first SST EOF mode with a 5 weeks' time lag, which shows that chlorophyll concentrations are influenced by seasonal heating and cooling and the zonal differences of it across the Black Sea. This suggests that seasonal stratification is an important factor controlling the variability in the deep Black Sea (Vinogradov et al., 1999).

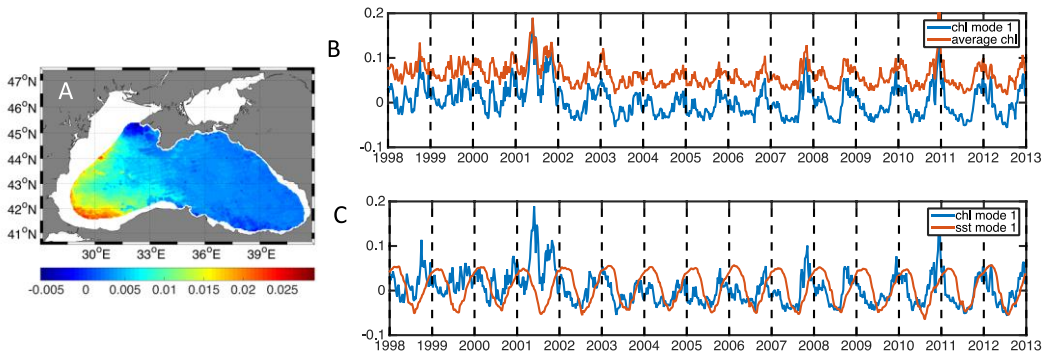

Figure 73 A) First EOF mode of chl a computed over the time frame 1998-2014. Corresponding temporal amplitudes for B) first CHL mode and average chl concentration (red line) and C) first CHL mode and SST-1 mode (red line).

The second Chl-a mode map (18% of total variance) displays a rather zonal distribution compared to 1st mode (Figure 74C). A dipole pattern exists between negative values along the western Black Sea until about 32° and then positive values in the eastern Black Sea, particularly along the southern coast. Temporal distribution of this mode is mostly positive until the end of 2001 and afterwards mostly negative, with positive peaks often occurring in fall or winter and positive values during the rest of the year. Third mode of Chl-a explain 8% of the variation, while the fourth mode of Chl-a explains 4% of the total variance. The spatial map of the third mode shows a band of positive values along the southern-southeastern coast of the Black Sea and negative values in the remaining part. The fourth mode shows a band of high values all around the deep Black Sea, and slight negative values in the interior. This spatial pattern very much resembles the mean ADT spatial pattern.

However, the patterns within these modes suggest the rather complex nature of Chl-a distributions within this region. Here in this study we investigate the relationship of Chl-a to abiotic factors. However it is important to note the impact of biotic factors on Chl-a. Top-down control by gelatinous predators on zooplankton is one factor resulting in significant alterations in the phytoplankton distribution and evolution (Oguz et al.,2000;

Chu et al.,2005) . Another important biotic factor to note is the shifts in the plankton composition of the Black Sea. Shifts in phytoplankton species composition from diatoms to coccolithophores and dinoflagellates have been documented in a number of studies (Cokoacar et al.,2004; Mikaelyan 1997; Yunev et al.,2007). Considering satellite Chl-a gives information only on the first optical depth, subsurface chlorophyll-a maximum , which has 15m-40m variability (Chu et al.,2005) can not be observed. This can be a major reason for low correlation between the ADT and CHL-A.

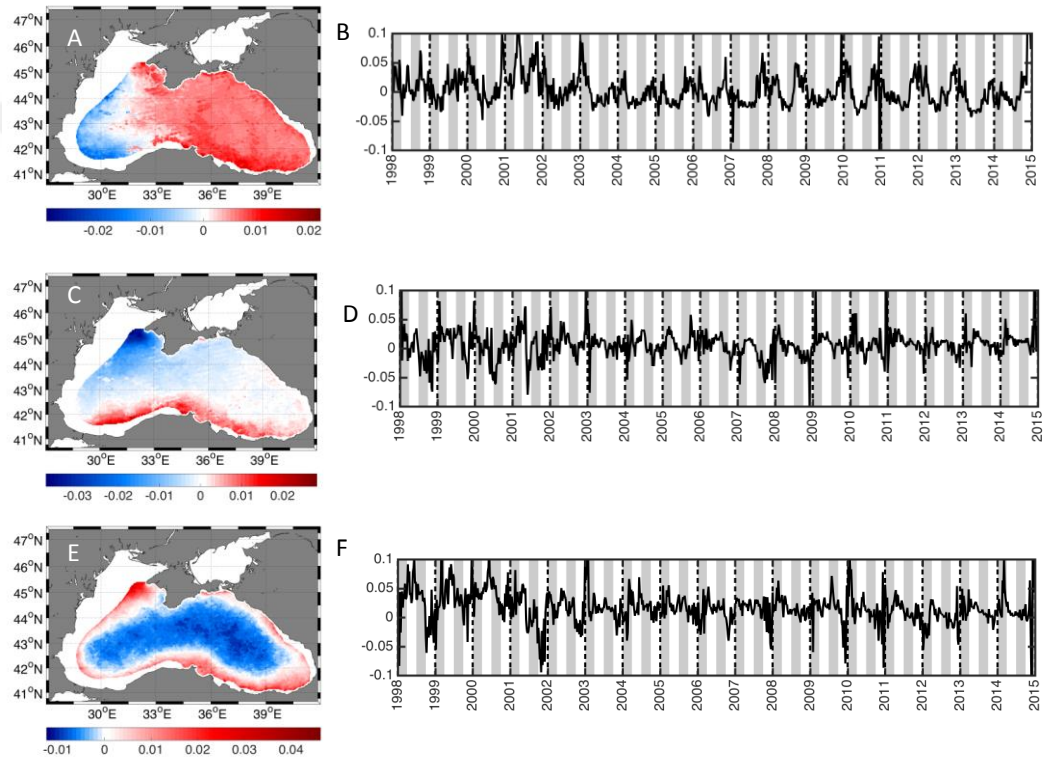

Figure 74 A) Second EOF mode, C) third EOF mode and E) fourth EOF mode of chl a computed over the time frame 1998-2014. Corresponding temporal amplitudes for B) second, D) third, and F) fourth mode.

4.3.3 Linking ocean physics to biological productivity on inter-annual time scales

Results obtained up to this point mainly contain the seasonal dynamics. In order to address the biological response to changing ocean physics at inter-annual time scales, an additional analysis is conducted. In order to eliminate seasonal dynamics, data have

been low-pass filtered using a moving average with 1 year window.

First EOF mode (Figure 75) of filtered ADT (F-ADT) represents 52% of total variability. Its spatial structure is the same as the second ADT mode, displaying a phase separation between the interior and the coastal basin throughout the study period (Figure 76). Second F-ADT mode (Figure 77) represents 44% of total variability and its spatial structure is the same as the first ADT mode showing the sea surface height dynamics (water budget) of the whole basin. This clearly shows that the Rim current circulation mode and the water budget mode have changed roles. Rim Current mode explains more of the total variability than the water-budget mode inter-annually. Basin wide oscillations of the second F-ADT mode (Figure 78) display the large sea level anomalies of the Black Sea, as discussed elsewhere (Volkov and Landerer, 2015).

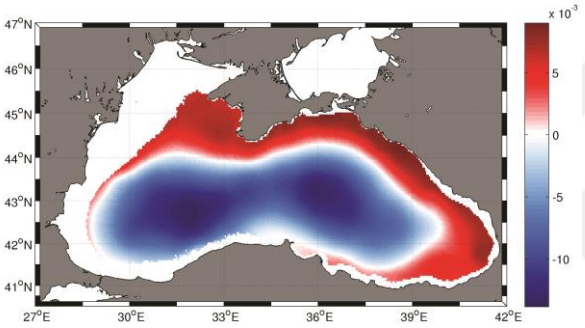

Figure 75 First EOF mode of F-ADT.

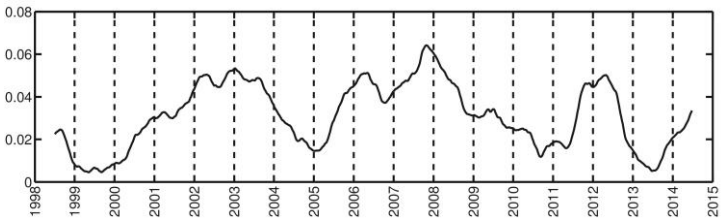

Figure 76 First temporal EOF mode of F-ADT.

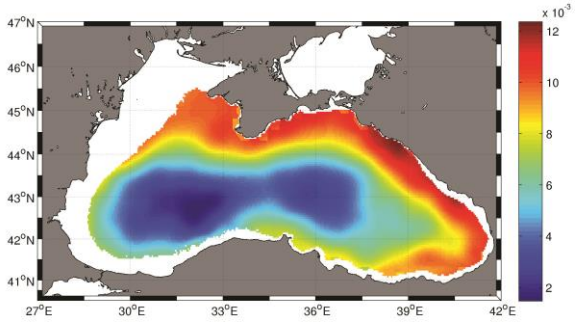

Figure 77 Second EOF mode of F-ADT.

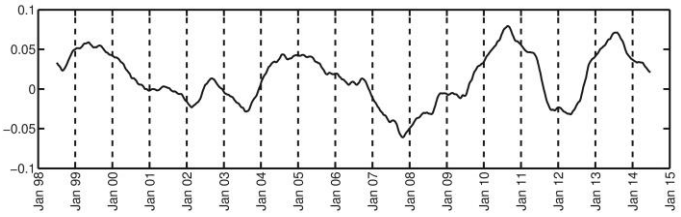

Figure 78 Second temporal EOF mode of F-ADT.

First EOF mode (Figure 79) of filtered Chlorophyll-a (F-CHL) represents 67% of total variability. Its spatial structure shows positive values all around the masked region with higher magnitudes at the south eastern part. Its temporal evolution (Figure 80) shows positive values until 2001. A major bloom is observed in 2011. After 2001, F-CHL suddenly declines, keeping low values until the end of the time-series. This mode represents the basin wide interannual variability of phytoplankton. Its temporal mode also shows negative values, suggesting decreasing phytoplankton in the basin.

Second EOF mode of F-CHL (Figure 81) represents 16% of total variability. Its spatial structure displays a dipole pattern with negative magnitudes in the offshore waters and positive magnitudes at the coast with a neutral line in the middle representing the Rim current zone. Its temporal evolution (Figure 82) displays negative values in 2001 and positive values at the rest of the time. This mode clearly depicts phytoplankton blooms at coastal parts in 1998-2001 and blooms in the deep interior basin in 2001. Following 2001, the phytoplankton blooms at coastal parts are less in magnitude than 1998-2001. Second F-CHL mode is negatively correlated with the first F-ADT mode (r=-0.6 with 8 weeks lag) and positively correlated with the second F-ADT mode (r=0.5 with 7 weeks lag). This clearly shows the phytoplankton response to changing circulation. First F-ADT mode represents the Rim current and second F-ADT mode represents the water budget (rivers). This means that when Rim current is more pronounced, chlorophyll-a decreases and when there is more contribution from rivers, the chlorophyll-a increases. Rim current associated mode of ADT (F-ADT mode 1) controls the interannual phytoplankton variability, especially at the deep interior basin, suggesting that the Rim current acts as a barrier between the coastal waters and the deep interior, regulating the extent of cross-shelf material transport relative to its intensity. Spatial correlations of chlorophyll-a and 1st mode of F-ADT (Figure 83) also consolidates this hypothesis, displaying high negative correlations particularly at the Rim current boundary in the

west.

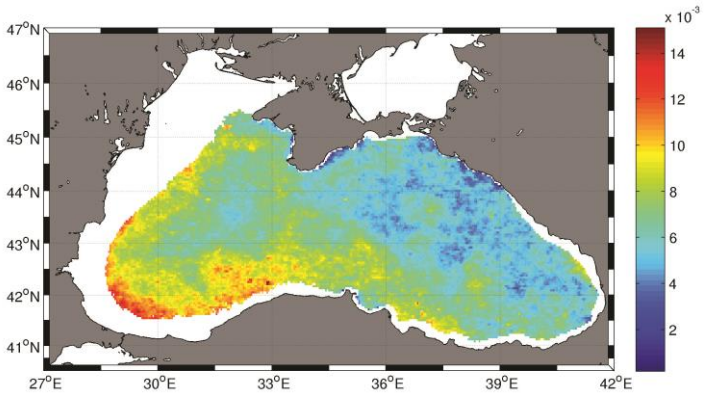

Figure 79 First EOF mode of F-CHL.

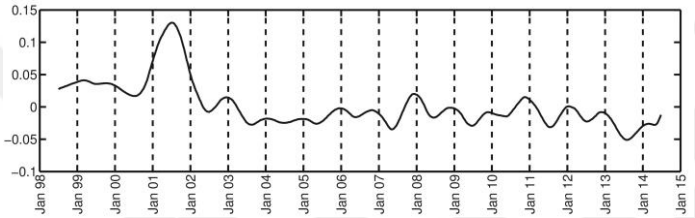

Figure 80 First temporal EOF mode of F-CHL.

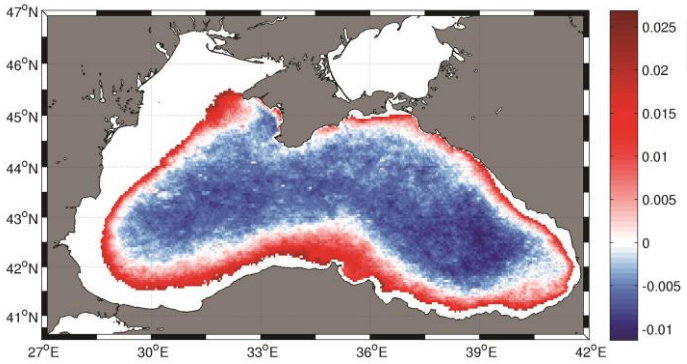

Figure 81 Second EOF mode of F-CHL.

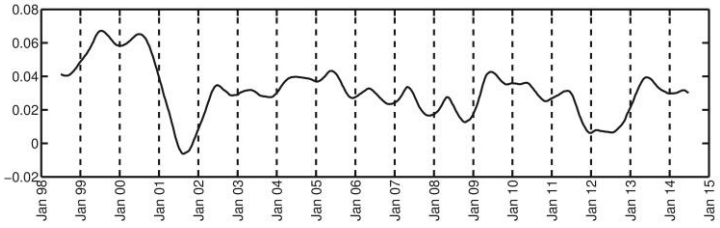

Figure 82 Second temporal EOF mode of F-CHL.

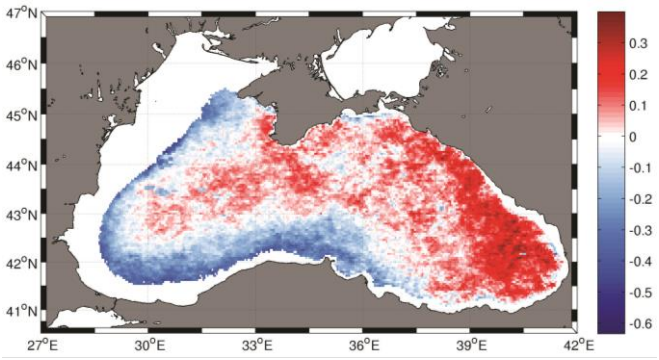

Figure 83 Spatial distribution of Chlorophyll-a and first mode of F-ADT correlations.

4.4 Discussion and Conclusions

Satellite era provided synoptic measurements of ocean productivity. Overall assessment of Black Sea chlorophyll was done using first generation sensors for 1978-1986 (Kopelevich et al., 2002). Utilizing continuous data from next generation sensors, this study investigated the chlorophyll-a variability for 1998-2014. During this period, Black Sea is gradually warming with an increase in sea-level and decreasing chlorophyll-a. Previous studies have already suggested warming causes decreased nutrient loading eventually decreasing chlorophyll (Oguz and Gilbert, 2007), and the extraordinary changes in chlorophyll-a have been regarded as a regime shift (McQuatters-Gollop et al., 2008). Therefore, in order to interpret the chlorophyll-a dynamics better, changes in the physical environment were inspected first.

EOF analysis on ADT revealed that the second mode was associated with the Rim current intensity, as confirmed by previous studies (Stanev and Peneva, 2002; Grayek et al., 2010; Capet et al., 2012). Second ADT mode was well-correlated (0.64 with 4 weeks lag) with wind stress curl. Considering this mode represents the variability of Rim current intensity, accompanying changes should also be evident in the geostrophic velocity (mean kinetic energy) and the number of mesoscale features generated by the instability of the Rim current. Analysis of MKE and eddies provided expected results. MKE and number of eddies were well correlated with the 2nd ADT mode; 0.7 and -0.64 respectively. 1993-2001 period displayed low MKE and after 2002 MKE increased substantially. Similarly, period following 2002 corresponded to less eddy variability. Thus, we concluded that the observed change in wind stress curl in 2002 resulted in a stronger Rim current, higher MKE and less eddies.

In order to investigate the link between the observed changes in physics and

phytoplankton, 1998-2012 period was investigated where CHL-A, SST and ADT data co-exist. Chlorophyll-a variability was dominated by the major rivers. In order to investigate the variability beyond river impact, regions under river impact were masked out. Resulting 1st CHL mode was negatively correlated with the first mode of SST (-0.6 with 5 weeks lag), emphasizing the influence of mixing/stratification on open water blooms. Relatively low correlation was found between ADT and CHL at seasonal time scales.

In order to assess the interannual phytoplankton response to physics, seasonal dynamics were removed using a low-pass filter on the datasets. EOF results conducted on the filtered datasets documented that Rim current mode of ADT is the dominant mode at interannual time scales. Second CHL mode was negatively correlated (-0.6) with the Rim current mode and positively correlated (0.5) with the riverine mode of ADT. Rim current mode of ADT also displayed high spatial correlation with the CHL time-series dataset, especially at the western and southwestern parts of the deep basin. These results suggest that the despite the CHL-A dynamics in the Black Sea depend on SST seasonally, the interannual signal of CHL-A is directly associated with the circulation. At seasonal scale, intensity of winter convection drives spring/summer time phytoplankton bloom intensity, previously documented by CZCS data for 1978-1986 period (Nezlin et al., 1999). On the other hand, interannual variability of the CHL-A was linked to the intensity of Rim current that is driven by the wind stress curl. Intensity of the boundary current defines the extent of cross-shelf material transport. An intensified Rim current acts as a barrier between coastal and offshore waters, decreasing eddy variability and preventing transport of nutrients and biota.

This analysis documented the physical mechanism responsible for the sharp decline in CHL-A after 2001. Despite this decline has various other reasons such as phytoplankton species composition and top-down control, here it is documented that the decline in CHL-A was associated to the physical environment: an intensified Rim current driven by the changing wind stress curl. Periods with intense Rim current corresponded to an increase in MKE and a decrease in eddy variability and possibly decreased cross-shelf exchange.

Other mechanisms leading to the observed chlorophyll-a variability may be: changes in the regional wind induced upwelling, intensity and duration of mesoscale activity or upwelling generated by ageostrophic frontal processes.

Investigating the variability of the physical environment as well as of phytoplankton, this study provides an insight on both the physical and chlorophyll-a dynamics as well as the phytoplankton response to changing physics. Previous studies have investigated the phytoplankton variability and its connections to temperature variabililty (Oguz et al., 2003; Oguz, 2005b; McQuatters-Gollop et al., 2008). Less attention was paid to circulation impact. However the results of this study suggest that circulation has a major impact on interannual phytoplankton variability in the Black Sea.

This study clearly documented phytoplankton response at the surface to changing variability in physical environment. However, information on phytoplankton below the surface layer is missing. In order to fully investigate the phytoplankton response to changing physical environment, this study should be supported by in-situ measurements of chlorophyll-a, documenting the deep chlorophyll maximum and its variability. Another important tool to support such studies at this point might be modelling. This study can be used complemented with modelling studies to enhance the mechanistic understanding where in-situ measurements are insufficient. Decrease in phytoplankton levels are crucially important for the recovery of the Black Sea ecosystem. However extensive decrease in phytoplankton may have negative impacts, such as decrease in zooplankton and eventually in fish. Therefore modelling these lower trophic levels might introduce a perspective for the future scenarios of the phytoplankton and the Black Sea ecosystem.

CHAPTER 5: Inferring different phytoplankton responses to variability in the physical environment from satellite remote sensing: Levantine Basin and analysis of similarities and differences with the Black Sea.

5.1 Introduction

Satellite data provide the opportunity to determine the variability of chlorophyll over the world ocean at fine spatial and temporal resolution, and also the chance to link this variability to environmental factors. Phytoplankton production depends on the availability of nutrients and sunlight which can be altered by various factors such as: ocean circulation, mixed layer dynamics, atmospheric dust deposition, upwelling and solar cycle.

Some of these factors are regulated by temperature which is becoming more of an issue on the last few decades. Warming of the world ocean (Levitus et al., 2005) increases stratification and decreases nutrient supply resulting in decreased plankton (Doney, 2006). An inverse relationship between net primary production and temperature has been observed over most of the world ocean (Behrenfeld et al., 2006). Chlorophyll decline is shown through various studies on the world ocean (Behrenfeld et al., 2006; Boyce et al., 2010; Gregg and Rousseaux, 2014). Variability of chlorophyll is commonly associated with environmental parameters such as sea surface height (as a proxy for ocean circulation), wind, sea surface temperature (proxy for stratification) over the global ocean (Uz and Yoder, 2004; Demarcq, 2009; Wilson and Coles, 2005) as well as different regions: Peru-Chile Current System (Correa-Ramirez et al., 2012), southern Caribbean upwelling system (Rueda-Roa and Muller-Karger, 2013), North Pacific (Palacios et al., 2006), Adriatic Sea (Mauri et al., 2007) and the whole Mediterranean Sea (Volpe et al., 2012). Chlorophyll variability is commonly associated with mesoscale and submesoscale variability in the oceans (Morales et al., 2012; Liu et al., 2013; Jose et al., 2014; Levy et al., 2012; Piontkovski and Nezlin, 2012; Oschlies and Garcon, 1998; Piontkovski et al.,2012; Kouketsu et al.,2015; Gaube et al.,2013; Mahadevan et al.,2012).

Similar to other parts of the world ocean, the Mediterranean Sea is also rapidly warming (Belkin, 2009; Nykjaer, 2009). Response of Mediterranean chlorophyll to changing environmental conditions is yet to be addressed considering the vulnerability of plankton to environmental and climatic perturbations.

The Mediterranean Sea is considered to be the largest oligotrophic area in the world (Crise et al., 1999). Average chlorophyll values indicate that oligotrophy increases from west to east (Santoleri et al., 2008). This trophic regime is a result of the inverse estuarine circulation as the bottom layers at Gibraltar export more nutrients than they import from the surface Atlantic waters. Increased oligotrophy towards eastern Mediterranean is caused by depletion of nutrient richer Atlantic waters in the west and mixing of these waters with ambient nutrient depleted Mediterranean surface waters (Crise et al., 1999). Another factor contributing to the inclination of oligotrophy towards east is the deeper averaged mixed layer depth in the eastern Mediterranean (D'Ortenzio et al., 2005).

In offshore waters of the ultraoligotrophic Levantine basin, Rhodes Gyre is denoted as the only intermittently blooming region whereas the remaining parts of the basin were found to be non-blooming (D'ortenzio and Ribera d'Alcala, 2009). Rhodes Gyre is denoted as an area of active deep water formation (Levantine Intermediate Water (LIW)) site, where the strength of formation depends on the intensity of winter convection (Ovchinnikov, 1984; Lascaratos et al., 1993). Blooms in the Rhodes Gyre are triggered following the winter convection as various studies have shown (D'ortenzio et al., 2003; Ediger and Yilmaz, 1996; Napolitano et al., 2000).

In order to investigate the variability of chlorophyll and its coupling to the physical forcing at all timescales, empirical orthogonal functions (EOF) analysis is used. Volpe et al. (2012) followed a similar analysis on the entire Mediterranean Sea (1998-2006) particularly focusing on the central and western Mediterranean dynamics. Mauri et al. (2007) investigated the chlorophyll variability in the Adriatic Sea using the same technique, where convection regulates the spring phytoplankton bloom (Gacic et al., 2002), similar to the Rhodes Gyre. The current study intends to give an up to date overview of the chlorophyll variability in the Levantine Basin and its regulatory physical mechanisms.

5.2 Material and Methods

Sea surface height data used in this study were obtained from AVISO (Archiving, Validation and Interpretation of Satellite Oceanographic data) absolute dynamic topography regional product for the Mediterranean Sea (http://www.aviso.altimetry.fr/index.php?id=1275). They are daily, delayed time multi-mission absolute dynamic topography data computed with respect to the mean dynamic topography (Rio et al., 2014) and gridded on a regular 1/8° x 1/8° grid. Daily ADT data were averaged into weekly composites. Mean ADT and geostrophic velocities averaged over 1993-2014 period are shown in Figure 84.

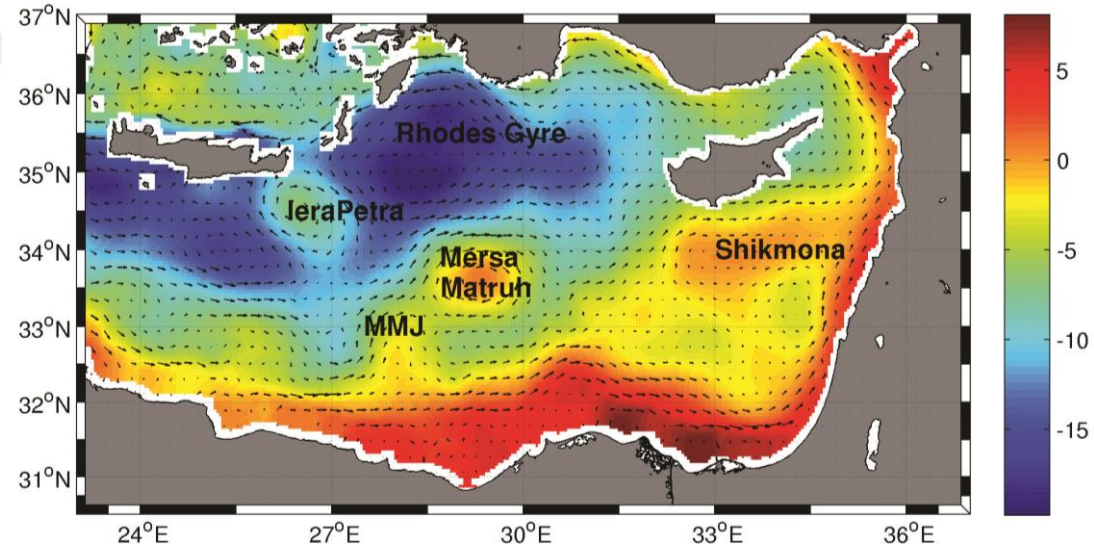

Figure 84 Mean absolute dynamic topography (cm) and geostrophic velocities in the Levantine Basin (1993-2014).

Sea surface temperature data used in this study is the AVHRR (Advanced Very High Resolution Radiometer) Pathfinder version 5.2 data. Daily night time sea surface temperature data for 1998 to 2012 were obtained. 4km daily dataset was averaged into weekly. Weekly averaged temperature data still had data gaps in it which was eventually filled in using the Data INterpolating Empirical Orthogonal Functions (DINEOF) technique as described below. Filling data gaps is not the aim in this study; it is a necessary step to conduct EOF analysis.

Chlorophyll data was obtained from the European Service for Ocean Colour, GlobColour Global 4km product, which includes reprocessed Level 3 data from

satellites MERIS, MODIS AQUA, SeaWIFS and VIIRS for the period 1998-2012. The GlobColor data set consists of daily Chl-a concentration (mg/m^3) data with a 4 km resolution constructed using the GSM (Garver-Siegel-Maritorena) model (Maritorena and Siegel, 2005) to combine the data of all four satellite products. Chl-a dataset was averaged into weekly dataset. Missing data in the weekly dataset was filled in within the DINEOF procedure to successfully complete the EOF analysis.

All three satellite data sets above were interpolated onto the same 4 x 4km spatial grid and a commom landmask was created that excludes the first pixels at the land/sea boundary (which are commonly erroneous in all datasets). For SST data comparisons with in-situ measurements showed root mean square $0.51 \pm 0.01\ ^{o}C$ in the Mediterranean Sea (Pisano et al., 2016). Regional altimetry products for the Mediterranean Sea are suggested to have a noise error of 1.75-3.13 cm (Copernicus Product User Manual: http://marine.copernicus.eu/documents/PUM/CMEMS-SL-PUM-008-017-033.pdf). Rio et al. (2007) found a root mean square error of 3cm for the Gulf of Lions. For chlorophyll data, median percentage error of GlobColour chlorophyll data in the open ocean was found as 29.53% when compared to in-situ measurements, whereas this value was found to be 53.04%, 44.08% and 35.77% for MERIS, MODIS and SeaWiFS respectively (Ford et al., 2012), emphasizing the advantage of the merged product.

Surface wind stress data is calculated from Cross-Calibrated Multi-Platform (CCMP) Ocean Surface Wind Vector L3.0 First-Look Analyses data set obtained from the Jet Propulsion Lab website (http://podaac.jpl.nasa.gov/Cross-Calibrated_Multi-Platform_OceanSurfaceWindVectorAnalyses). This data set contains 6-hourly gridded analysis of ocean surface winds on a 0.25° spatial grid, of which an average of the two daily measurements were used in this study. The CCMP dataset combines cross-calibrated satellite winds utilizing a Variational Analysis Method and includes cross-calibrated satellite winds derived from SSM/I, SSMIS, AMSR-E, TRMM TMI, QuikSCAT, SeaWinds, and WindSat. The reference height of the surface wind data is 10m. Wind stress (τ) was calculated as $\tau = \rho_a C_D V^2$ with air density ρ_a = 1.293 km m^{-3} and drag coefficient C_D depending on wind speed, V, after Trenberth et al. (1990). In addition the wind stress curl was calculated as $Curl(\tau) = \frac{\partial \tau_y}{\partial x} - \frac{\partial \tau_x}{\partial y}$ where the components of the wind stress vector τ are τ_x and τ_y. The curl expresses the rotation a vertical column of air would experience in a wind field that varies in space.

Heat flux data was retrieved from Era-Interim reanalysis dataset (http://www.ecmwf.int/en/research/climate-reanalysis/era-interim) as semi-daily fields. Total heatflux was obtained as a sum of four fields: surface latent heat flux, surface sensible heat flux, surface net solar radiation and surface net thermal radiation. Total heatflux data was then averaged into daily and monthly fields for the study period.

River fluxes were obtained from Ludwig et al. (2003, 2009) river discharge dataset created from observations and model results for the Black and Mediterranean Seas for the EU 7th framework project PERSEUS. All rivers in the study domain are considered for this study.

Coastal and offshore waters criteria mentioned in the study refer to shallower and deeper than 500m respectively, which is determined using the bathymetry data obtained from GEBCO

(http://www.gebco.net/data_and_products/gridded_bathymetry_data/). Rhodes Gyre bloom area definition was accomplished by first selecting a box over the Rhodes area and secondly identifying regions with average chlorophyll-a values larger than 0.09mg/m^3 in the time-averaged (1998-2012) map. The resulting coastal, offshore and Rhodes gyre area definitions are given in (Figure 85).

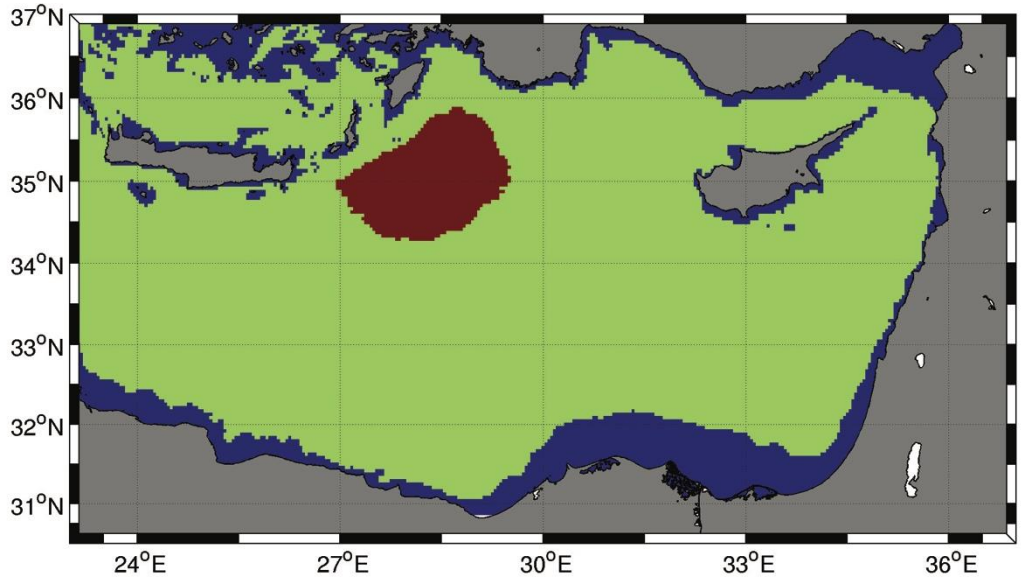

Figure 85 Definition of coastal, offshore and Rhodes Gyre regions in this study. Regions marked with blue denote the coastal waters, red area displays Rhodes Gyre and the sum of the green and red areas represent offshore waters.

5.3 Results

The analysis of chlorophyll-a in the Levantine Basin is presented here with a focus on the seasonal and temporal variability. Relationships of chlorophyll with physical drivers (sea surface temperature, sea surface height, wind and heatflux) are also discussed.

5.3.1 Recent Chlorophyll-a distribution in the Levantine Basin

Chlorophyll in the Levantine Basin has a seasonal cycle, with late winter/early spring blooms. The basin averaged temporal distribution of monthly chlorophyll-a data is given in Figure 86 . Starting with 2007, there is a decline in chlorophyll-values until 2012. This period is again followed by a decrease until 2014. Considering wind data is available until end of 2011 and sea surface temperature data is available until end of 2012, analysis of chlorophyll-a data will be limited with 1998-2012 for consistency.

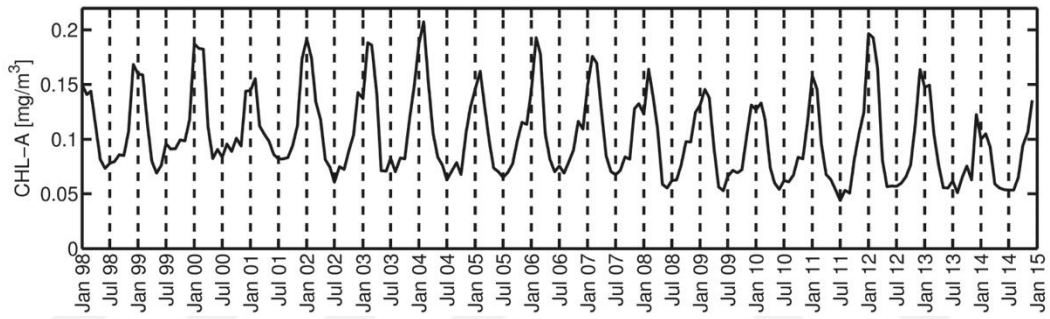

Figure 86 Basin averaged monthly Chlorophyll-a distribution 1998-2014.

Considering its nutrient poor nature, it is expected to see highest chlorophyll values at the coast. Figure 87 displays the general distribution of chlorophyll-a in the Levantine Basin. As expected, the dominant feature of the basin is the area under Nile discharge impact. Second most important feature is the Cilician Basin. There is a sharp gradient between the coastal waters and the oligotrophic offshore waters. The only feature in the offshore waters with relatively higher chlorophyll is the Rhodes Gyre, which can be barely seen in the map due to order of magnitude.

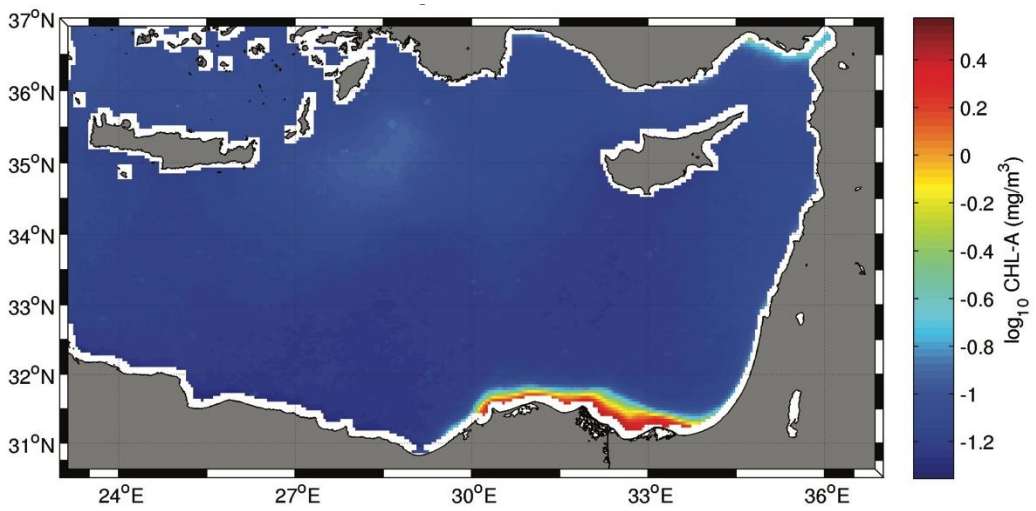

Figure 87 Temporally averaged Chlorophyll-a (in logarithmic scale) map of the Levantine Basin.

In order to get a general understanding of the interannual variability of the basin wide chlorophyll in the Levantine basin, a low pass filter (with a moving average of 53 weeks) is applied on the weekly dataset. Chlorophyll values oscillate until show a significant decline after 2007 (Figure 88). Decline in chlorophyll is observed in the coastal waters (Figure 89) as well as the offshore waters (Figure 90). Chlorophyll in coastal waters display a gradual decline first in 2004 and then in 2007 whereas in chlorophyll in offshore waters decline after 2007.

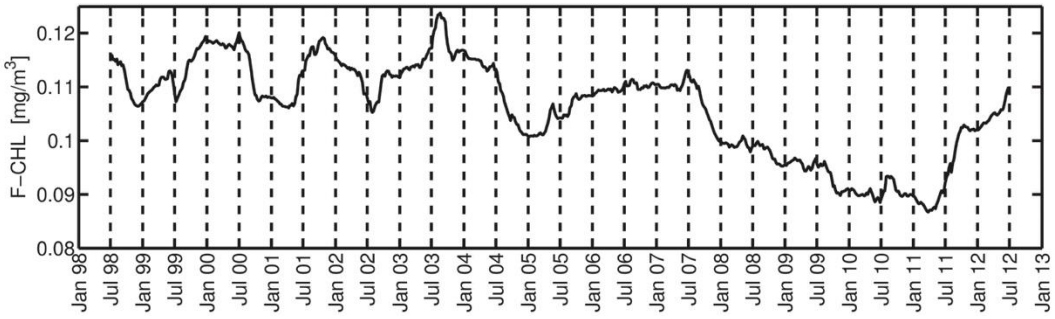

Figure 88 Basin averaged low-pass filtered Chlorophyll-a time series

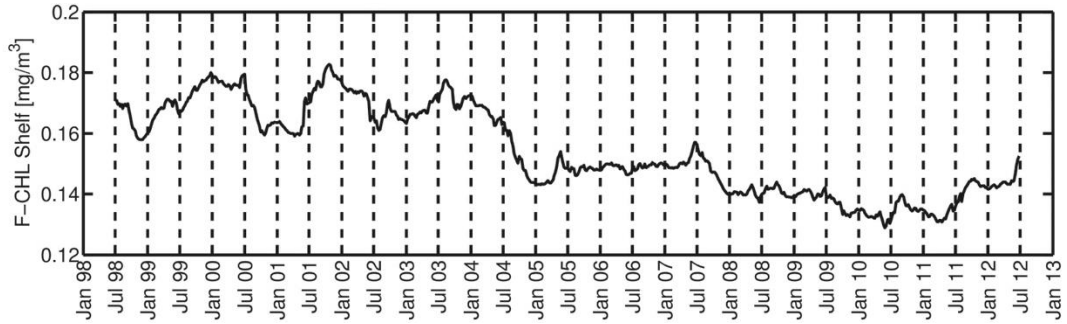

Figure 89 Low-pass filtered Chlorophyll-a time series of coastal waters

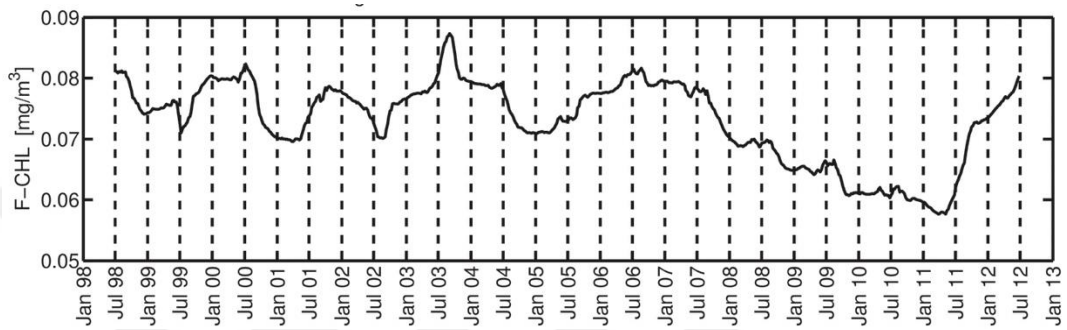

Figure 90 Low-pass filtered Chlorophyll-a time series of offshore waters.

Total discharge rates all rivers in the Levantine are given in Figure 91. Decline of discharge rates in 2003/2004 and also in 2007/2008 corresponds to declines in chlorophyll in coastal waters (Figure 89). Similarly the elevated levels of river discharge correspond to increasing chlorophyll-a values in 2003 however not in shelf waters but offshore waters (Figure 90) and this increase is also amplified in the basin averaged time series (Figure 88). Increased river discharges in 2009 however, do not correspond to any increase in chlorophyll (also not in the years to follow.).

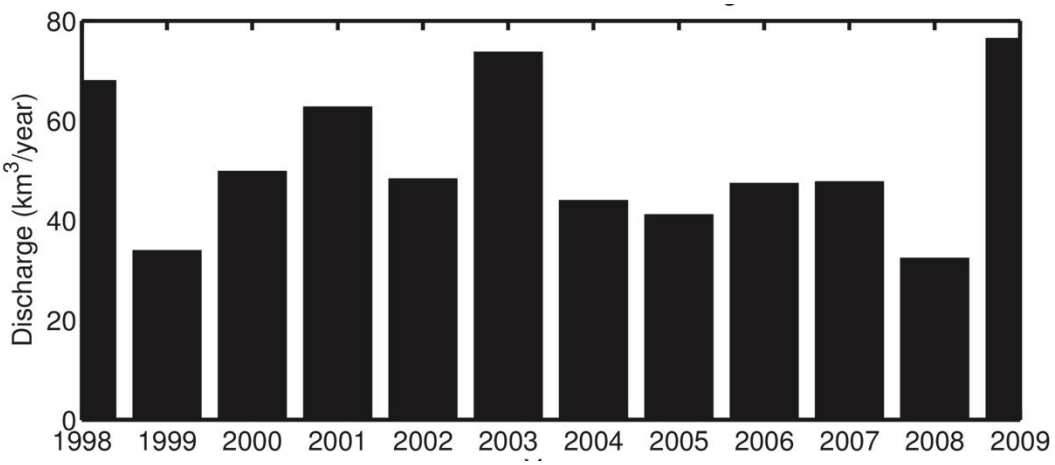

Figure 91 Total Yearly change of all rivers in the Levantine

5.3.2 Physical-biological interactions at seasonal time scale

In order to identify variability at any spatiotemporal scale, EOF analysis was conducted on the weekly chlorophyll-a dataset as well as sea surface temperature and absolute dynamic topography.

Temporal average of SST and ADT are given in Figure 92 and Figure 93 respectively to give an overview of the physical parameters in the basin. SST map displays east-west partition around 31^{o}N. Rhodes Gyre and Iera-Petra eddy are clearly evident. Asia minor current is clearly observed as a thermal front just north of Rhodes Gyre. Similar to the SST map, ADT average map also displays many of the well-known circulation fields: Rhodes Gyre, Iera-Petra , Mersa-Matruh and Shikmona eddies. The controversial path of the Atlantic water is also evident; one flank following the Egyptian coast and the other flank entering from 34^{o}N as part of the cyclonic cell which also contains Rhodes Gyre.

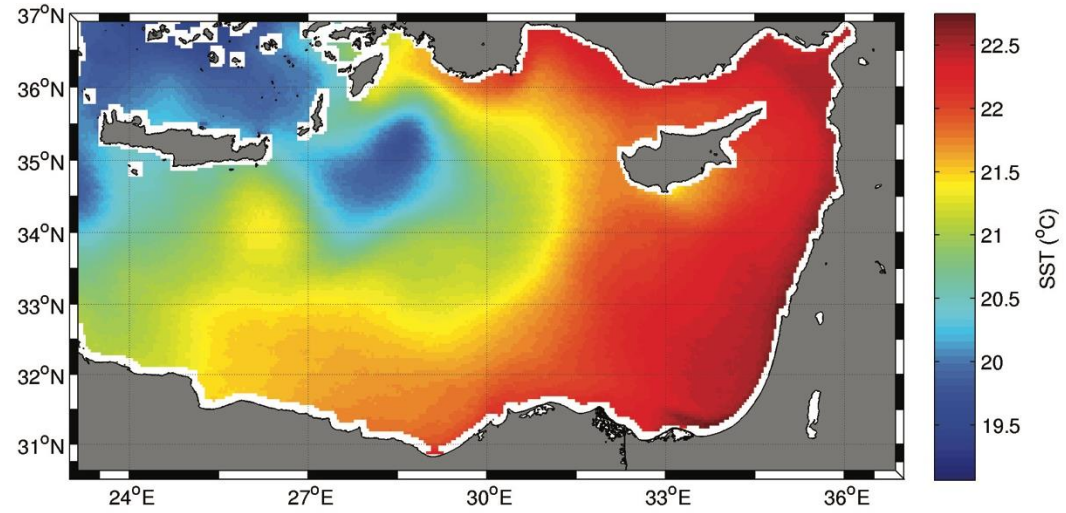

Figure 92 Temporal average of sea surface temperature

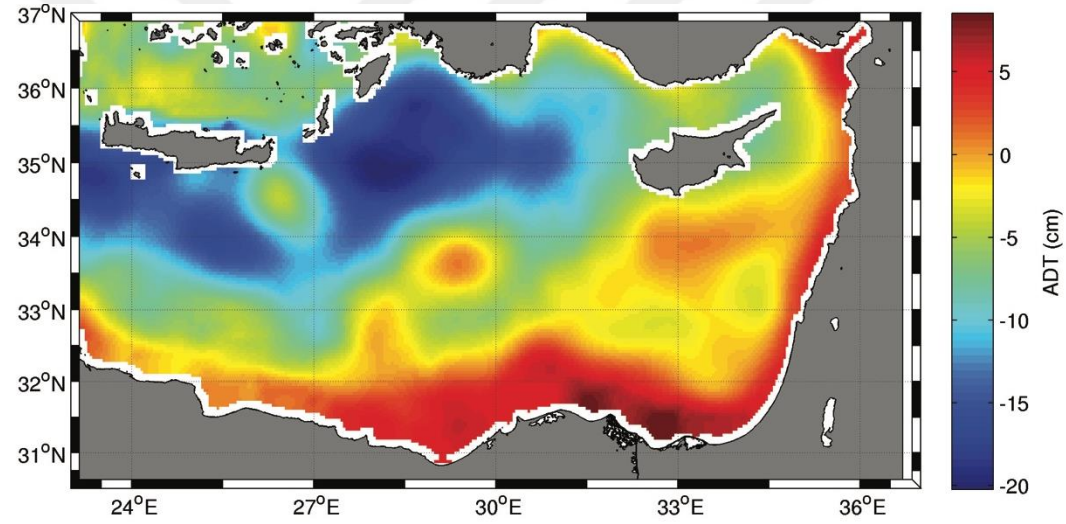

Figure 93 Temporal average of absolute dynamic topography.

First Chl-a mode represents 70% of the total variability (Figure 94) and mainly represents the fuzzy phytoplankton dynamics of the river discharge area most probably related to the rate of water and related nutrient flux (Figure 95). Considering the lack of proper river flux data, physical meaning of this mode could only be speculated.

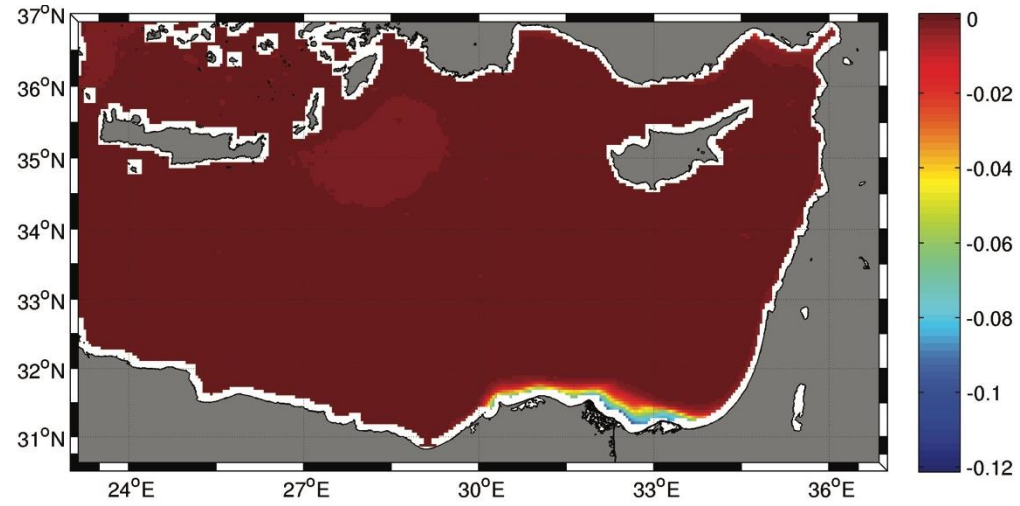

Figure 94 First spatial EOF mode of Chlorophyll-a

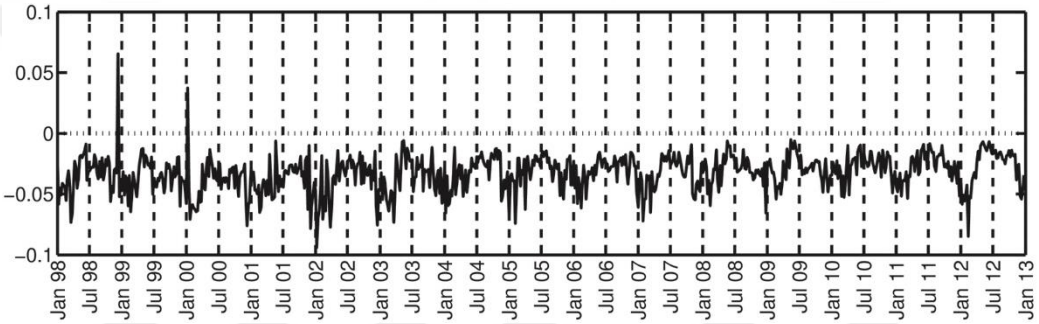

Figure 95 First temporal EOF mode of Chl-a

Considering the space-time variability of the Levantine basin chlorophyll-a can't be distinguished from Nile area dynamics (70% of total variability) and it has been previously shown that the offshore chlorophyll is also decreasing (Figure 90), waters deeper than 500m were chosen to reapply the EOF analysis.

First EOF mode of offshore chlorophyll-a (Figure 96) explains 34% of total variability. It clearly displays dynamics of the Rhodes Gyre. A very small area in Antalya Bay displays the same magnitudes as Rhodes Gyre. Considering the shelf is steep around this region, it is clear that the coastal impact reaches beyond 500m bathymetry contour. Its temporal evolution (Figure 97) displays a seasonal cycle with late winter/early spring blooms. Largest temporal magnitudes are observed in 1999, 2006, 2007 and 2012. This mode proves that the most dominant features of the Levantine basin in terms of chlorophyll magnitude are the Nile discharge area, Cilician basin, Antalya basin and finally the Rhodes Gyre.

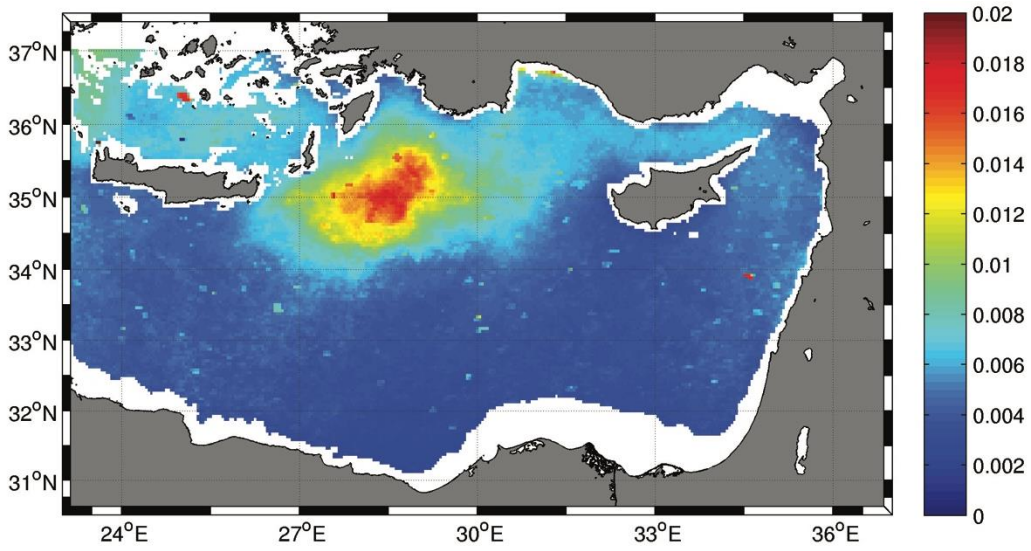

Figure 96 First spatial EOF mode of offshore chlorophyll.

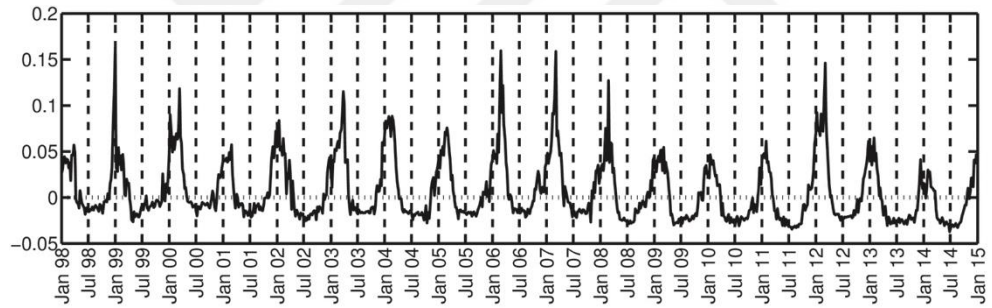

Figure 97 First temporal EOF mode of offshore chlorophyll.

Second (Figure 98) and third (Figure 99) EOF mode of offshore chlorophyll-a explain 9% (each) of total variability. Second mode displays a dipole pattern between Rhodes Gyre and other parts (especially in Antalya basin and Lebanon/Israel coast). Third mode displays the Rhodes Gyre and its influence area. Corresponding temporal evolution of both modes contain huge spikes most probably caused by the fuzzy structure of the spatial maps caused by large anomalies of short time periods (1-2 weeks) or the errors caused by the filling algorithm. Therefore the temporal evolutions of these modes are not shown. These two modes do not display any significant correlation with SST or ADT modes.

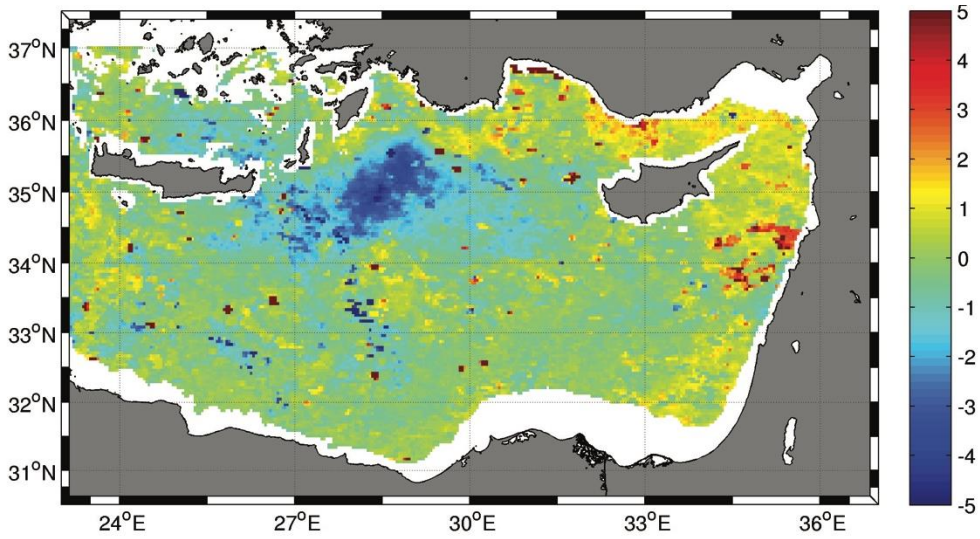

Figure 98 Second spatial EOF mode of offshore chlorophyll (x10^{-3}).

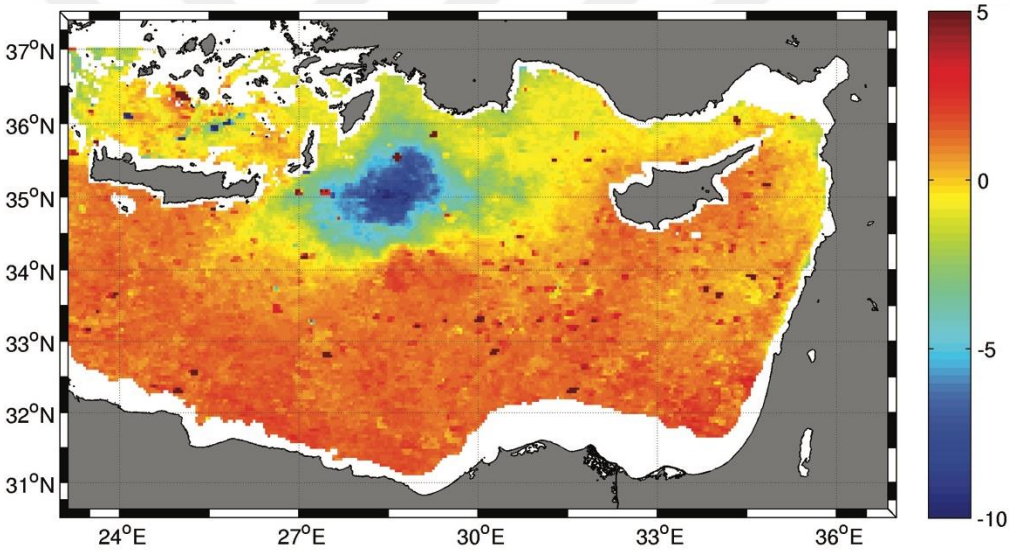

Figure 99 Third spatial EOF mode of offshore chlorophyll (x10^{-3}).

First EOF mode of SST (Figure 100) explains 94% of total variability and its temporal evolution (not shown) clearly displays the seasonal cycle with negative magnitudes in summer and positive magnitudes in winter. This mode suggests that the Turkish coast (around Antalya basin) is more prone to warming (cooling) during summer (winter). Second EOF mode of SST (Figure 101) explains 4% of total variability (66% excluding the first mode). This mode is very similar to the basin average SST distribution (Figure 92), displaying positive magnitudes around Cretan Sea and Rhodes Gyres and negative magnitudes in the eastern parts of the basin. Its temporal evolution (Figure 102) displays

only negative values with large negative magnitudes generally in late autumn. This mode represents the SST gradient between Rhodes Gyre and the eastern part of the basin, as well as the convection events. Cretan Sea and Rhodes Gyre display the largest cooling during autumn which is the preconditioning time for deep water formation. 2007 displays the largest negative magnitude.

Second mode of SST and first mode of CHL are both spatially (-0.57) and temporally (-0.52 with 10 weeks lag) correlated. The correlations between these modes suggest the impact of winter mixing and re-stratification in spring. Preconditioning of winter convective mixing/deep water formation starts in late autumn/early winter depending on atmospheric conditions. 10 weeks (~2.5 months) lag between the temporal modes represent the period between mixing of the water column in winter and its re-stratification in spring.

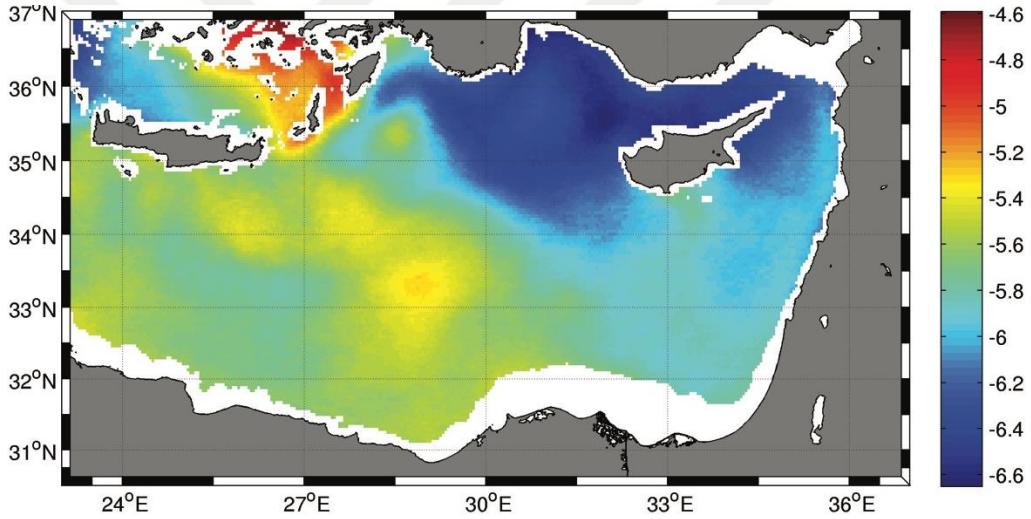

Figure 100 First spatial EOF mode of SST ($x10^{-3}$).

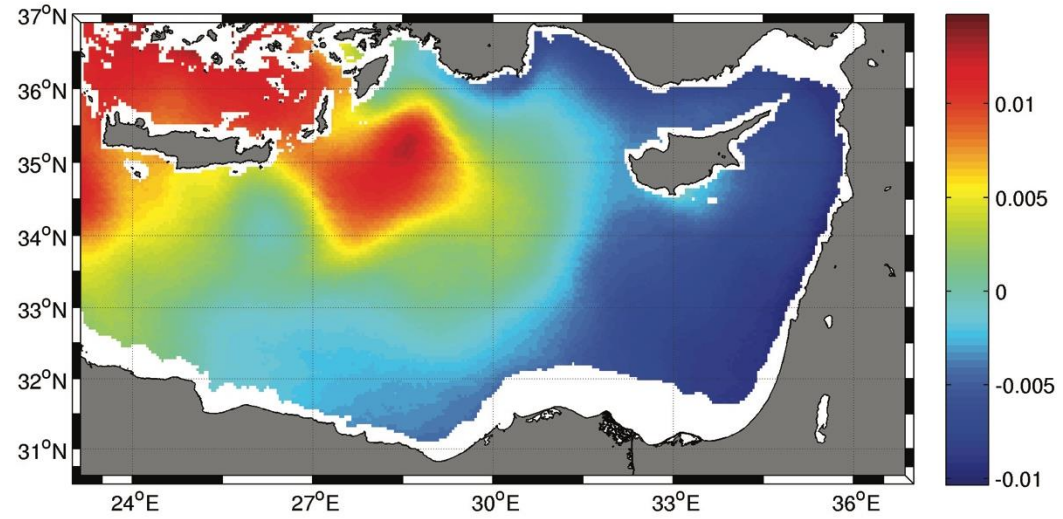

Figure 101 Second spatial EOF mode of SST.

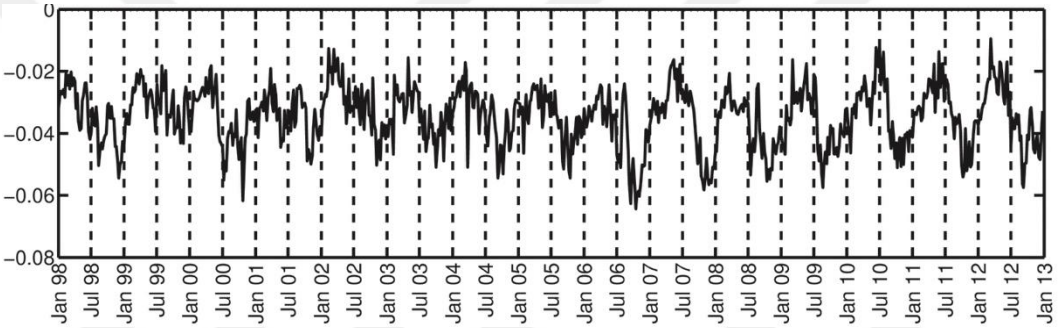

Figure 102 Second temporal EOF mode of SST.

First mode of ADT (Figure 103) explains 46% of total variability. It represents various circulation patterns clearly such as the Rhodes Gyre and IeraPetra eddy. This mode displays only negative values with smaller negative magnitudes around Rhodes Gyre and south of Crete. Its temporal evolution (Figure 104) displays a seasonal cycle with negative magnitudes in late autumn/early winter and positive magnitudes in spring. This mode represents the strength of cyclonic circulation in the basin. Largest magnitudes are observed in 2010 and 2011. First mode of ADT is spatially (-0.62) and temporally (-0.65 with 8 weeks lag) correlated with the first mode of chlorophyll-a (Figure 96). These correlations represent the circulation impact on chlorophyll-a. Intensification of the boundary current (enhancing the intensity of Rhodes Gyres and coastal anticyclones) in late autumn and its weakening in spring. Temporal evolution of this mode is also well correlated (r=0.5) with the MKE in the basin, with time lag of 3 weeks.

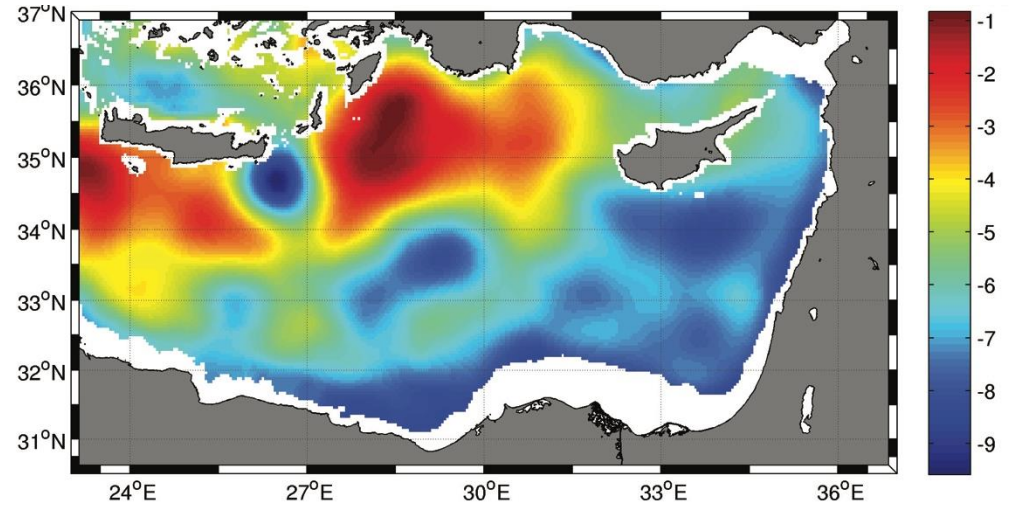

Figure 103 First spatial EOF mode of ADT.

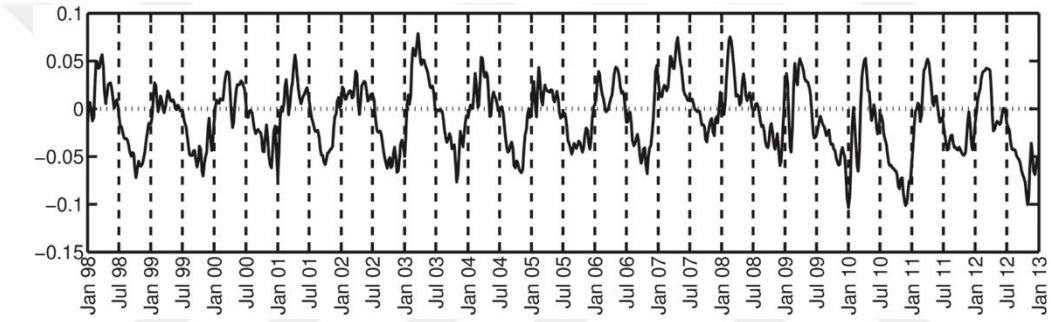

Figure 104 First temporal EOF mode of ADT.

Second EOF mode of ADT (Figure 105) explains 37% of total variability and displays a very similar pattern with the first mode. In fact they are almost identical (with spatial correlation of 0.96). However their physical meaning is rather different. The first mode signals increased or decreased sea surface height all over the basin with different magnitudes, whereas in the second mode, regions have different phases. The second temporal mode (Figure 106) displays positive values only. This means that regions denoted with positive and negative magnitudes show a phase separation. The Rhodes Gyre and the area south of Crete exhibit declining sea surface height whereas the eastern coastal boundary displays an increasing sea surface height. It can be said that the second mode displays the seasonal evolution of the cyclonic circulation (Rhodes Gyre) and anticyclonic patterns caused by the instability along the path of the Atlantic waters. This mode represents the cyclonic/anticyclonic phase separation within the basin with its strength changing in time (with a seasonal cycle). This mode is spatially (0.65) and

temporally (-0.56 with 7 weeks lag) correlated with offshore chlorophyll mode 1 (Figure 96).

Despite looking very similar in spatial structure ADT mode 1 and mode 2 represent different patterns. They represent the intensity of the general cyclonic character of the basin and the intensity of the jet encircling the basin (leading to stronger/weaker cyclones and anticyclones in the basin) respectively. Both of these modes, in the end, are related with the intensity of cyclonic circulation in Rhodes Gyre. Considering their good correlations with 1st Chlorophyll-a mode they clearly represent the circulation impact on chlorophyll in offshore waters.

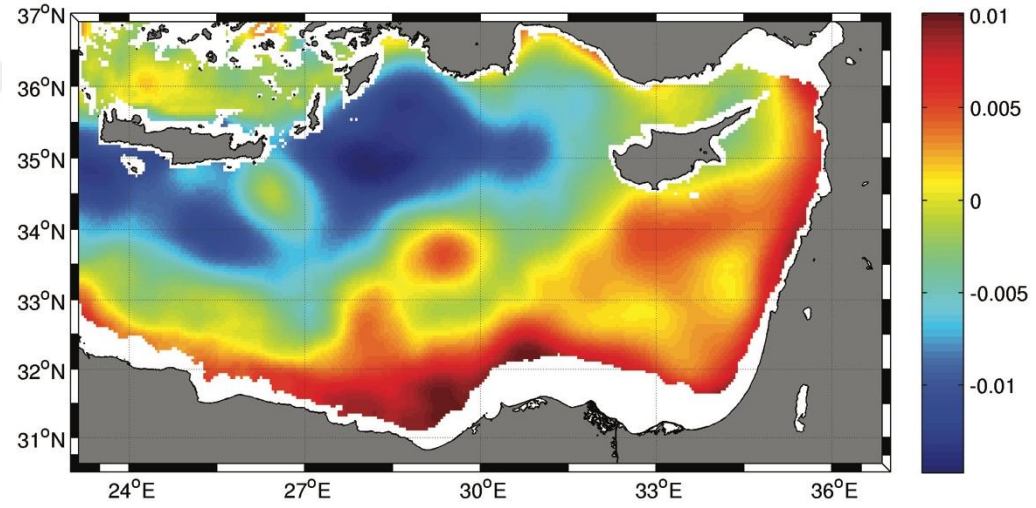

Figure 105 Second spatial EOF mode of ADT.

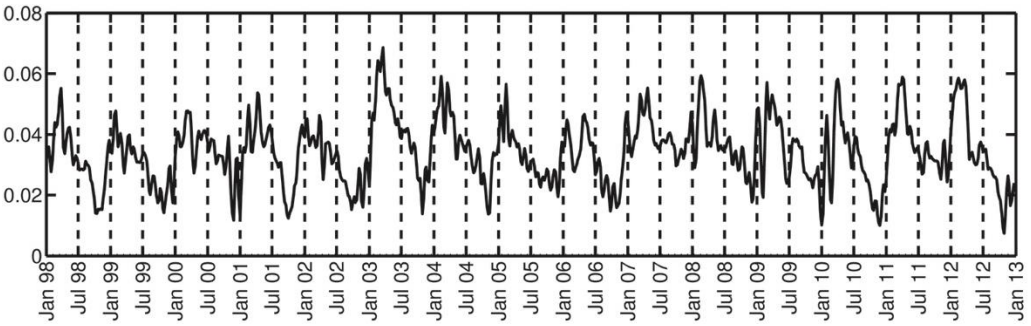

Figure 106 Second temporal EOF mode of ADT.

5.3.3 Interannual physical-biological interactions

Results of the EOF analysis presented in (5.3.2 Physical-biological interactions at seasonal time scale) interprets the processes regulating most of the chlorophyll-a variability at seasonal time scales. There is a strong seasonal component within all three datasets and this signal dominates most of the explained variability. In order to identify the dynamics of chlorophyll-a at longer time periods, and its coupling to physical forcing, the seasonal cycle and the high frequency signals were filtered out from the datasets and EOF analysis was conducted again on these filtered anomaly datasets.

The first F-CHL mode (Figure 108) represents 45% of total variability. It displays negative values all over the basin, with larger magnitudes focused on the Rhodes Gyre. Its temporal evolution (Figure 109) displays positive negative fluctuations. This mode displays that the only dominant feature in the offshore waters is the Rhodes Gyre. Chlorophyll increase in 2006-2007 suggests blooming of Rhodes Gyre intensely during these years.This is confirmed by Rhodes Gyre averaged (following Figure 85) chlorophyll distribution (Figure 107).

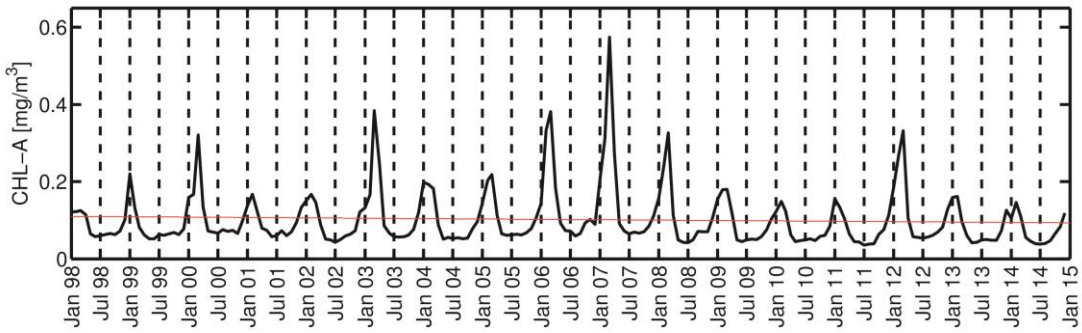

Figure 107 Averaged Chlorophyll-a distribution in Rhodes Gyre 1998-2014.

The second F-CHL mode (Figure 110) represents 16% of total variability and its spatial structure is very similar to the first mode, however displaying a more concentrated impact area of Rhodes Gyre. Its temporal evolution (Figure 111) shows both negative and positive magnitudes. Similar to the first mode it displays intermittent blooms of Rhodes Gyre. The main difference between the two modes is that the first mode shows the increase/decrease of chlorophyll in the whole Levantine is derived by Rhodes Gyre, whereas in the second mode during periods of decreasing chlorophyll in Rhodes Gyre

(i.e. 2001-2002 and 2004), the basin displays a very minor chlorophyll increase. These may be caused by regional upwelling, dust events, or impacts of increased cross-shelf transport due to weaker boundary current.

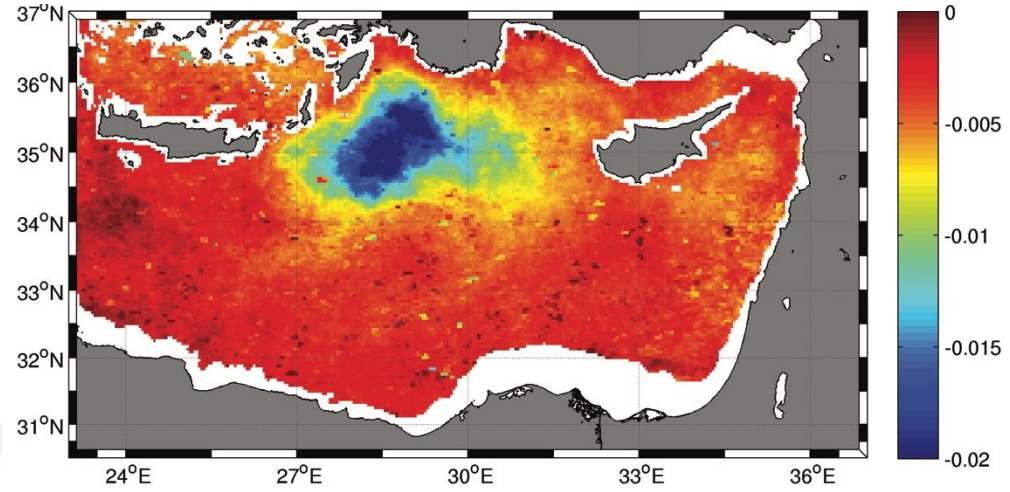

Figure 108 First spatial EOF mode of F-CHL.

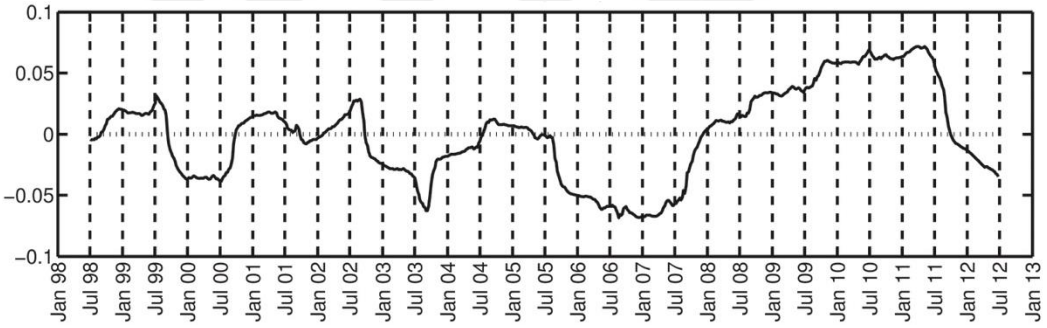

Figure 109 First temporal EOF mode of F-CHL.

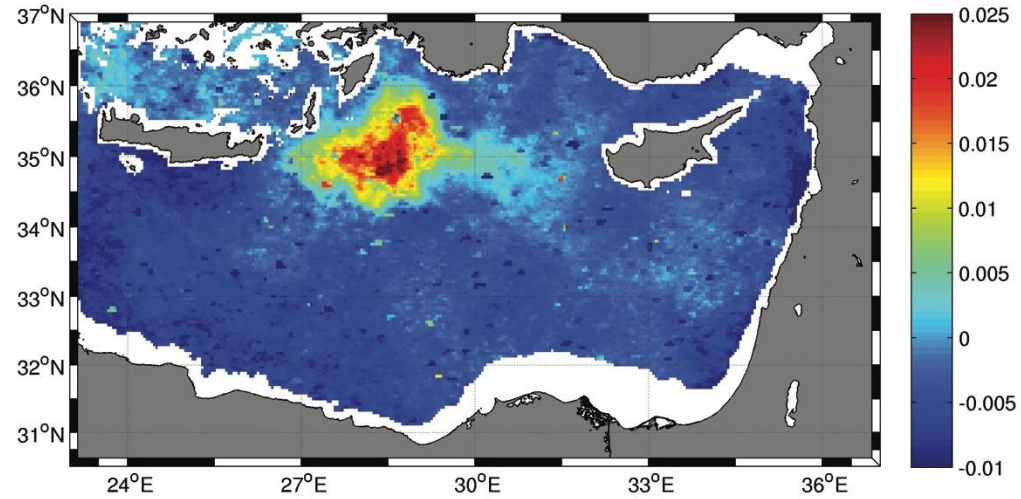

Figure 110 Second spatial EOF mode of F-CHL.

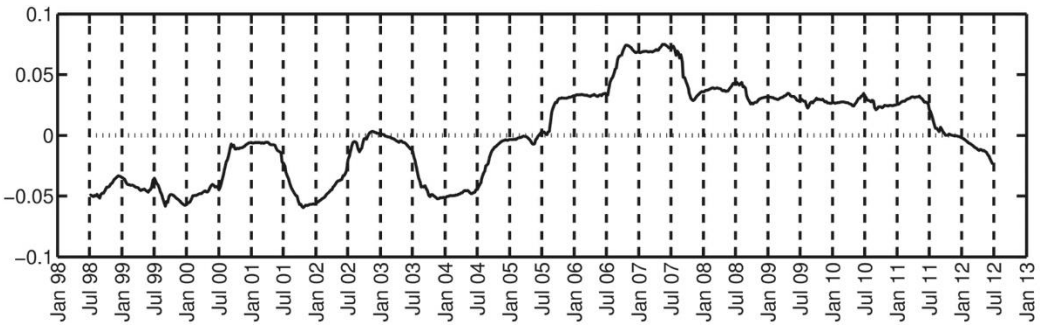

Figure 111 Second temporal EOF mode of F-CHL.

Third spatial mode of F-CHL explains (Figure 112) 7% of total variability and displays a different spatial pattern than the first two modes. This mode represents a dipole pattern between the Iera-Petra eddy and the Rhodes Gyre area. Its temporal mode (Figure 113) exhibits positive and negative magnitudes. This mode is rather interesting, because during certain years (i.e 2003), it displays increased values of chlorophyll around IeraPetra eddy.

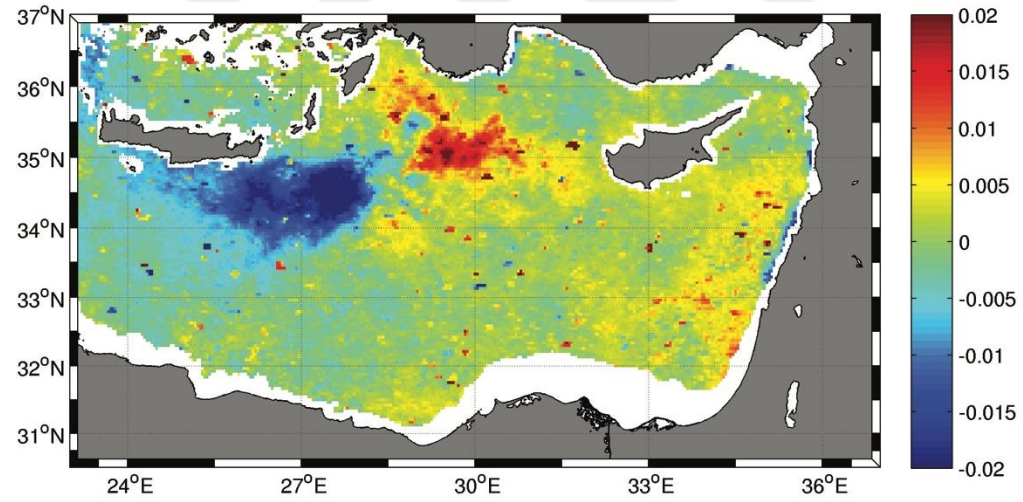

Figure 112 Third spatial EOF mode of F-CHL.

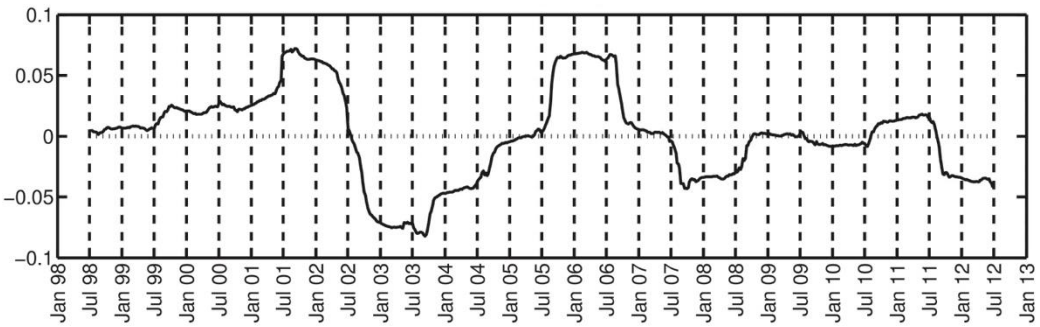

Figure 113 Third temporal EOF mode of F-CHL.

First spatial mode of F-SST represents 70% of total variability. Its spatial structure (Figure 114) displays negative magnitudes all over the basin with intense negative magnitudes around Rhodes Gyre and south of Cyprus (Cyprus eddy). Corresponding temporal mode (Figure 115) suggests that Levantine starts warming rapidly in 2007. After 2007, the only cooling in the basin is observed in 2012. This mode is both spatially (0.5) and temporally (-0.73 with 6 weeks lag) correlated with the first F-CHL mode. First mode of F-SST represents warming of the entire basin, with intense warming around Cretan Sea and Rhodes Gyre. Considering high correlations with the first F-CHL mode, 1st F-SST mode represents the weakening of winter convection in the region. As a consequence of reduced winter convective mixing, reduced spring blooms are observed in Rhodes Gyre (Figure 108 and Figure 109).

Second spatial mode of F-SST explains 7% of total variability. It displays negative values around the Cretan Sea and the Rhodes Gyre and positive magnitudes south of the basin. The spatial symbolizes the Mid-Mediterranean Jet. Its temporal distribution (Figure 117) displays warming starting in 2004. It suggests warming of the southern basin after 2004 and cooling at the core of the Rhodes Gyre. This mode is spatially (Rather low -0.3) and temporally (0.64 with 6 weeks lag) correlated with the 2nd F-CHL mode (Figure 110 and Figure 111).

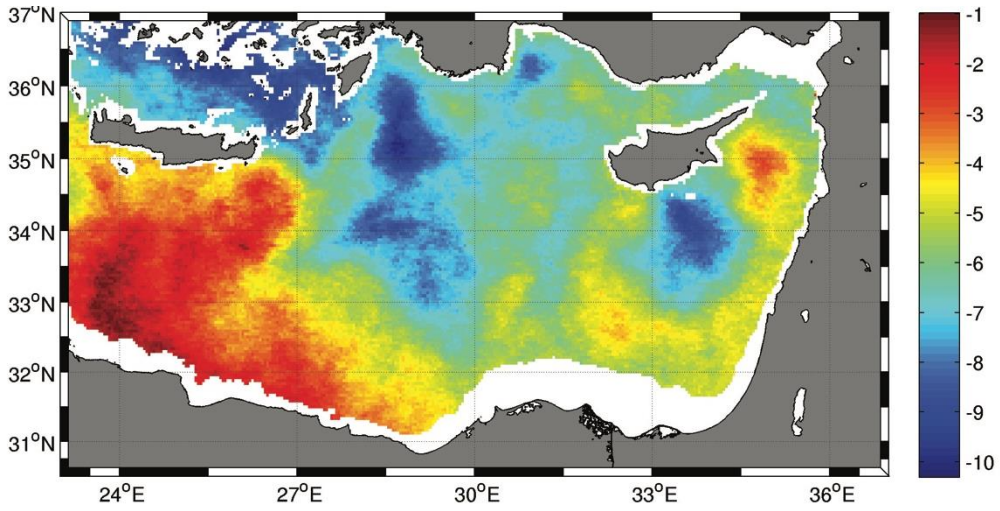

Figure 114 First spatial EOF mode of F-SST (x10^{-3}).

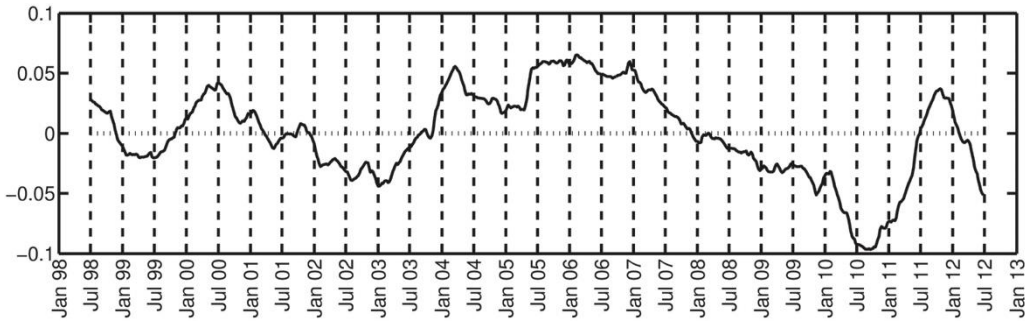

Figure 115 First temporal EOF mode of F-SST.

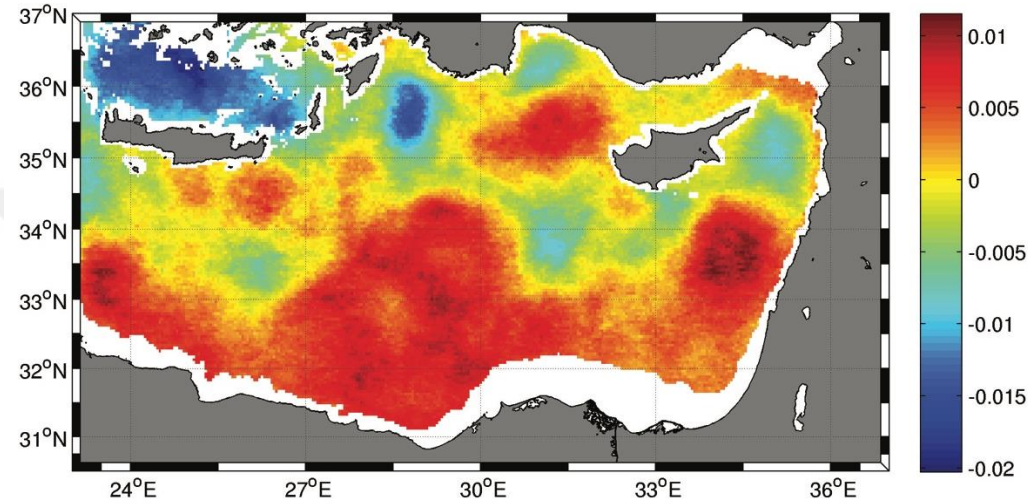

Figure 116 Second spatial EOF mode of F-SST.

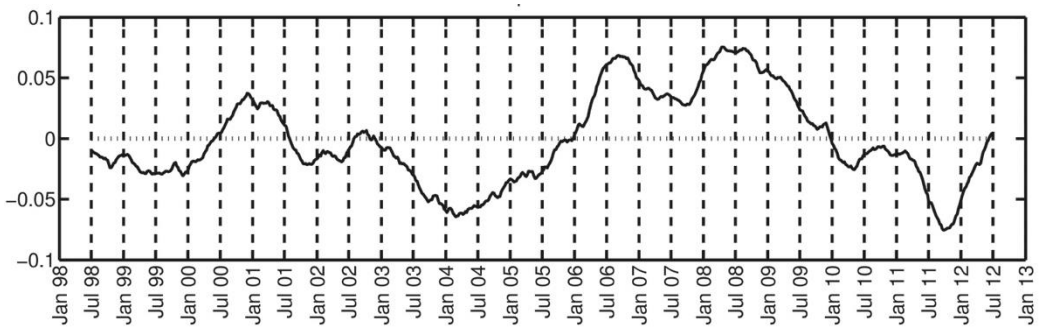

Figure 117 Second temporal EOF mode of F-SST.

First F-ADT mode (Figure 118) explains 46% of total variance. It displays dipole patterns (mainly as mesoscale formations) with only positive magnitudes south of Crete. Rest of the basin displays negative magnitudes. Its temporal evolution (Figure 119) exhibits an increase in the sea surface height starting in 2007, suggesting a decrease in cyclonic nature of the Levantine basin circulation. First F-ADT mode is temporally (-0.74 with 6 months lag) correlated with the first F-CHL mode (Figure 109). This

coupling suggests the decreasing cyclonic circulation in the Levantine basin reduces upwelling intensity around Rhodes Gyre and results in decreased bloom intensity.

Second F-ADT mode represents 17% of total variability. Spatially, this mode (Figure 120) represents clearly the most dominant mesoscale feature in the Levantine basin: IeraPetra eddy. Its temporal evolution (Figure 121) suggests that the anticyclonic intensity of IeraPetra eddy is reduced during 2003. Second F-ADT mode is both spatially (-0.49) and temporally (0.74 with 9 weeks lag) correlated with the third F-CHL mode (Figure 112 and Figure 113). This mode suggests an extraordinary situation in the basin, high chlorophyll values in the most dominant anticyclone of the basin.

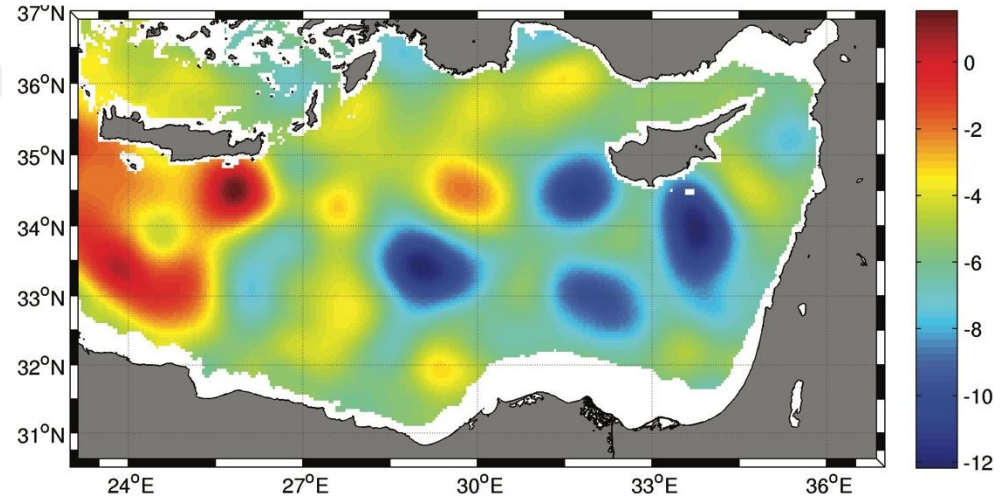

Figure 118 First spatial EOF mode of F-ADT (x10^{-3}).

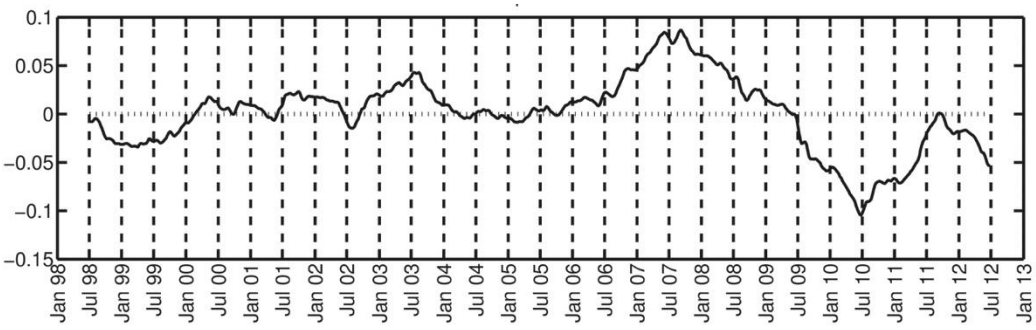

Figure 119 First temporal EOF mode of F-ADT.

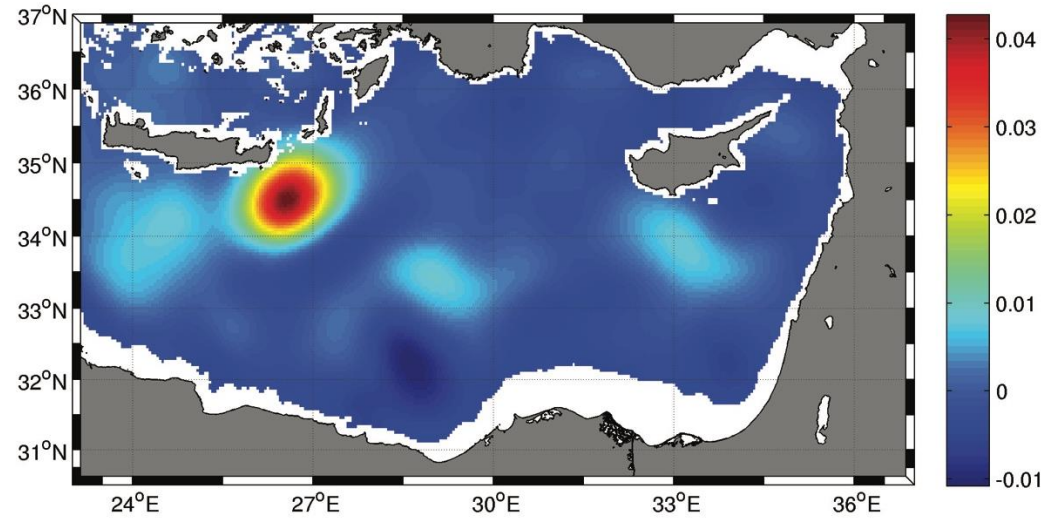

Figure 120 Second spatial EOF mode of F-ADT.

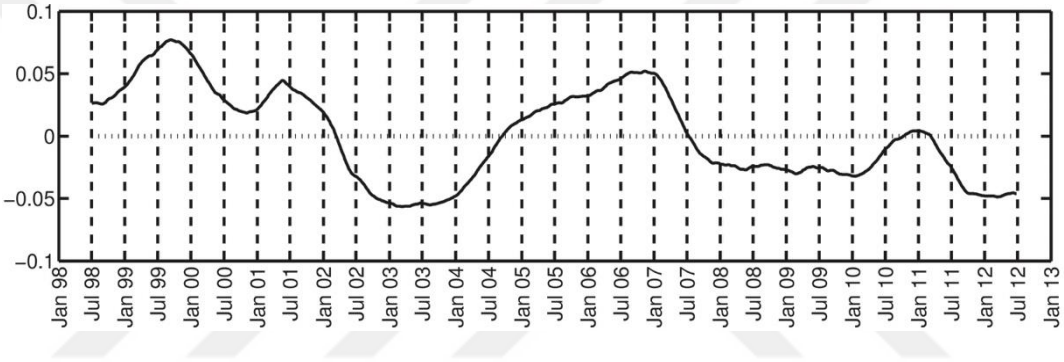

Figure 121 Second temporal EOF mode of F-ADT.

5.4 Discussion and Conclusions

This analysis shows that the most dominant chlorophyll-a sources (in order of magnitude) are the Nile discharge area, Cilician Basin, Antalya Basin (and other coastal waters) and finally Rhodes Gyre in the offshore waters. The remaining Levantine basin does not display any blooms that are recurrent or strong enough to be observed in the space-time decomposition through EOF analysis. Blooms related to regional upwelling or dust events may be observed on individual spatial maps of chlorophyll-a in very short time periods (i.e 1-7 days), however the dataset used in this study is weekly and the aim was not to observe these high-frequency. The aim was to address any seasonal to decadal variability in the chlorophyll-a dynamics. Areas called as "remaining of the Levantine Basin" above, do not display any blooms and were also called "non-blooming" through cluster analysis (D'Ortenzio and Ribera d'Alcala 2009).

Rhodes Gyre is the most productive area in the offshore waters of the Levantine basin which can clearly be seen from the results given above. The current results suggest that Rhodes Gyre bloom depends on winter convection and intensity of the cyclonic circulation in the gyre. Interannual Chlorophyll-a distribution (low-pass filtered with a moving window of 1 year) in Rhodes Gyre (Rhodes Gyre averaged) displays significantly high correlation (-0.63 with 4 months lag) with heat flux anomaly data (not shown) in the gyre. This result is reasonable considering the time starting from convective mixing (preconditioning of deep water formation) to re-stratification of the water column.

Starting in 2007, the Levantine basin underwent rapid warming and an increase in sea surface height. These changes corresponded to a decline in offshore chlorophyll-values. Shelf waters also display a decrease in chlorophyll-a after 2007, however this decrease is minor. A major decrease in the shelf waters chlorophyll-a is observed starting in 2004, which coincides to a major decline in total freshwater fluxes (yearly) into the basin.

The increase in temperature can suppress phytoplankton blooms through two different ways. Firstly, increased temperature enhances stratification and also decreases winter convective mixing which result in decreased phytoplankton blooms in the Rhodes Gyre. Temporal distribution of chlorophyll-a clearly displays this phenomena. Colder years correspond to increased levels of biomass through intense blooms (i.e. 2007 and 2012). The secondary impact of increased temperature on chlorophyll-a is through its impact on circulation. Increased temperatures contribute to steric component of the sea level, which corresponds to 55% of total sea level trend (Criado-Aldeanueva et al., 2007), resulting in alterations of the circulations field.

Sea surface height however is not only influenced by thermal expansion. Through modelling (Fukumori et al., 2007), zonal wind stress over the Strait of Gibraltar and Atlantic Ocean was suggested to be the reason for non-seasonal sea level fluctuations in the Mediterranean Sea. Extreme sea level anomalies during winter of 2009/2010 and 2010/2011 were shown to be correlated with the wind stress anomalies (Landerer and Volkov, 2013), practically proving previous theoretical model study. The first mode of zonal wind stress (not shown) was found to be correalated (0.58) with the first mode of ADT. This result is lower than the findings of Landerer and Volkov

(2013), however this is probably because the domain of the current study is limited with Levantine and satellite wind data is used instead of reanalysis data.

Another result of this study is that decreasing cyclonic circulation in the basin (Figure 118 and Figure 119) corresponds to decreased chlorophyll values in the basin. Interannual variability of F-ADT and F-CHL first modes displayed this relation with a correlation of (-0.74 with 6 months lag). Another impact of the circulation on chlorophyll was through strengthening of the cyclonic circulation, just opposite of the first case. One of the most persistent mesoscale features in the Levantine basin is the IeraPetra eddy, which is driven by the Etesian winds over the region (Amitai et al.,2010). Third mode of chlorophyll (explaining 7% of total variance) displayed increased chlorophyll values in 2003-2004. Weekly circulation maps (not shown) suggested a very weak (or non-existing) IeraPetra eddy during the time period. Considering this is a eddy-driven persistent eddy, its nonexistence may have caused increased cyclonic circulation on this location, advecting higher chlorophyll concentration waters from adjacent Rhodes Gyre upwelling area, or causing blooms in the area itself. Temporal evolution of wind stress curl averaged over the IeraPetra eddy (box average 33.5^{o} N - 35^{o} N and 25^{o} E - 27^{o} E) display an extreme fluctuation towards positive wind stress curl in the area (Figure 122). This alteration in wind stress curl resulted in weakening/disappearance of the eddy resulting in enhanced chlorophyll values. Changes in the Etesian winds in the region during this time period may be related to the exceptional heat wave anomaly that affected Europe in 2003 (Schar and Jendritzky, 2004).

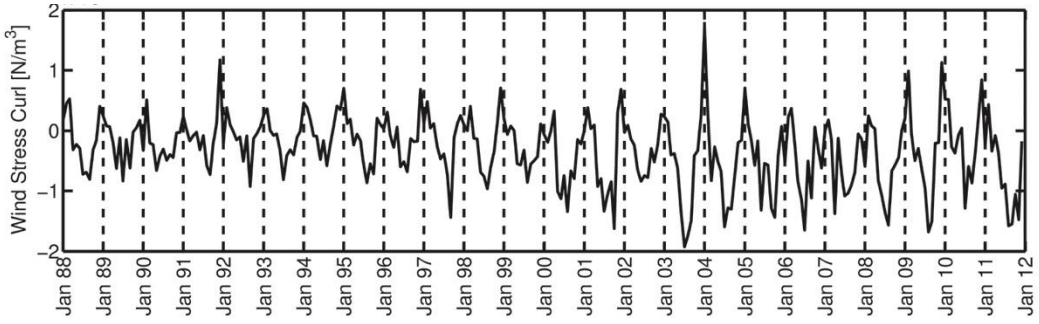

Figure 122 Temporal evolution of wind stress curl ($N/m^3 x10^{-7}$) averaged over Iera-Petra eddy.

Assuming the similar (but opposite sign of wind stress curl) mechanism, wind stress curl was averaged over Rhodes Gyre, expecting to find direct relations to F-CHL

increases/decreases. Although the results show largest positive wind stress curl in 2007 (which is the most pronounced bloom in Rhodes Gyre), the correlations with chlorophyll (averaged over the Rhodes Gyre) were low. This suggests that although the intensity of positive wind stress curl and cyclonic circulation have an impact on Rhodes Gyre chlorophyll signals, the main driver of Rhodes Gyre blooms is the winter convective mixing. High correlation between heat flux anomalies and chlorophyll values (-0.63) in Rhodes Gyre and even higher correlations between F-SST and F-CHL first modes over the whole deep basin support this result. Cold years (i.e. 2007 and 2012) were found to be concurrent with intense blooms in the Rhodes Gyre. Thus it can be stated that, except for the coastal/shelf waters, which are modulated by complex riverine/nutrient flux dynamics, the remaining contribution to chlorophyll-a comes from Rhodes Gyre upwelling area which mainly depends on intensity of winter convection and secondly on strength of cyclonic circulation in the basin. A minor contribution (in space-time decomposition) is observed in offshore waters close to the shelf boundary, which can be caused by increased cross-shelf transport during weaker cyclonic circulation. Finally, as the dipole pattern (positive around Rhodes Gyre and negative around IeraPetra eddy) of wind stress curl is disturbed most probably as a consequence of heat waves (ocean-atmosphere coupling), IeraPetra area displays a surprisingly high contribution to chlorophyll in the basin.

This study clearly documented phytoplankton response at the surface to changing variability in physical environment in the Levantine Basin. However, information on deep chlorophyll is missing. Deep chlorophyll maximum is an important feature in the Levantine basin and such information from in-situ measurements may complement the satellite data, providing a better understanding of the phytoplankton response to variability in the physical environment.

5.5 Comparison of the chlorophyll-a response to physics in the Black Sea and Levantine Basin

Similar to most of the large marine ecosystems in the world (Belkin, 2009), Black Sea and Levantine basin are exposed to warming. As a consequence of warming and response of phytoplankton to accompanying physical changes, chlorophyll is decreasing in most of the world ocean (Behrenfeld et al., 2006; Gregg and Rousseaux 2014; Doney 2006). Black Sea and Levantine basin are no exception. As demonstrated in this study both of them exhibit a decline in total chlorophyll-a in time.

In both the Black Sea and Levantine, discharge areas of major rivers are the most productive areas: northwestern shelf in the Black Sea and Nile discharge area and Cilician basin in the Levantine. A major difference between the two basins is the trophic state. Levantine offshore waters are completely (except Rhodes Gyre) non-blooming (D'Ortenzio and Ribera d'Alcala 2009), whereas Black Sea deep basin displays blooms.

In the Black Sea, chlorophyll-a significantly decreases after 2001. Previous studies (McQuatters-Gallop et al., 2008) called it a regime-shift and stated that it may be a related to climate, nutrient loading or even food web structure. In the current study it was shown that the decline after 2001 corresponded to changes in the Rim Current intensity, which was represented by the 2^{nd} mode of ADT. This cyclonic basin wide circulation is driven by the wind stress curl. Changes in rim current intensity were related to changes in wind stress curl. The period following 2002 displays a stronger rim current and lower number of eddies. Thus it can be stated that an intensifying rim current resulted in decreased cross-shelf transport of nutrients and resulted in decreased chlorophyll.

In the Levantine Basin however, chlorophyll significantly decreases after 2007. The chlorophyll variability in the offshore Levantine basin directly depends on the Rhodes Gyre bloom, which is triggered by winter convective mixing. Thus it can be stated that the chlorophyll interannual variability depends on the interannual variability of winter convective mixing. Cold years tend to display more chlorophyll in offshore waters (i.e.2007, 2012). Despite the fact that wind stress curl and mean kinetic energy did not reveal significant correlations with ADT modes, there are clues hinting at a similar process as was observed in the Black Sea. Individual weekly maps (not shown) display patches of high chlorophyll areas suggesting cross-shelf transport for example

between Turkey and Cyprus and between Turkey and Rhodes Gyre. These cold years correspond to years with more positive ADT (less cyclonic circulation). One reason of low correlation between the wind stress curl and circulation fields may be related to the basin averaging. Temporal evolution along the path of the main cyclonic circulation may yield better results. However, the path of this flow is under debate itself (Hamad et al., 2005; Millot and Gerin, 2010; Ciappa 2014). Therefore, this analysis should be part of a future study. One other fact suggests that a change in the wind stress curl was driving the changes observed in IeraPetra eddy in 2002-2004. Caused by sign change in wind stress curl, the IeraPetra eddy weakened and disappeared temporarily. Similar changes in wind stress curl are therefore expected in other locations. Considering SST frontal regions display strong coupling of the wind stress curl and SST (atmosphere-ocean coupling) (Castelao 2012; Chelton et al., 2007), it is expected that these changes occurring in wind stress curl in the Black Sea and Levantine are possibly a result of increased temperatures. However, this needs to be verified with a more detailed study.

Offshore waters of the Black Sea and Levantine display a similar decline in chlorophyll, however resulting from different physical origins. The Black Sea chlorophyll decline was found to be mainly dependent on the reduction of shelf-open ocean transport as a result of intensified boundary current (resulting from change in wind stress curl). While the chlorophyll decline in the Levantine was found to be mainly dependent on the decline in winter convection (caused by warming).

CHAPTER 6: Thesis Conclusions

This thesis investigated the spatio-temporal variability of sea surface temperature warming utilizing simple linear regressions and empirical orthogonal functions analysis and also the response of phytoplankton to physical dynamics and their spatial temporal variability in the Black Sea and Levantine. The second and third chapters of this thesis were dedicated to the extensive analysis of sea surface temperature variability in the Black Sea and Levantine basin respectively. Fourth and fifth chapters focused on identifying the phytoplankton response to environmental conditions in the Black Sea and Levantine basin respectively.

Chapter two focused on the analysis of sea surface temperature in the Black Sea and found it to be warming rapidly with a trend of 0.078 ^{o}C/year for 1982-2012. In this study the Black Sea was divided into nine basins utilizing the results of the EOF analysis. Eastern and northeastern parts of the basin displayed highest warming trends over the time period with the highest warming rates especially in autumn season, whereas the other regions trends were very close to the general basin trend. A detailed analysis on the thermal anomalies and their interannual distribution displayed two different periods during the study period. 1982-1998 was dominated by negative thermal anomalies whereas the following period, 1999-2012 was dominated by positive thermal anomalies. EOF analysis conducted on the low-pass filtered SST anomalies (F-SSTA) documented that the whole basin is warming, however more rapidly on the eastern, northeastern and northwestern parts, which are also shown by regional warming trends (Table 1, Table 3). Black Sea SST was negatively correlated with both NAO (-0.49) and EA-WR (-0.53 with 1 month lag) indices showing a complex relationship to large scale atmospheric changes.

Chapter three was dedicated to the analysis of sea surface temperature in the Levantine basin and a positive warming trend was found to be 0.06 ^{o}C/year over the entire basin, whereas regional warming trends reached as high as 0.08 ^{o}C/year. Warming trend maps of each month for 1982-2012 period showed large variability, however the

regions with the highest warming in all of these maps were similar pointing to Rhodes Gyre, Antalya and Latakia basins as the regions with the highest warming. Analysis of thermal anomalies differntiated two periods, 1982-1997 dominated by negative anomalies and 1998-2012 by positive anomalies. EOF analysis conducted on the low-pass filtered thermal anomalies displayed a similar spatial structure of warming as the simple linear regressions analysis, showing highest warming in the Rhodes Gyre region. Among large-scale patterns, SST showed highest correlations with AMO index. Basin averaged correlations were estimated as EA-WR (-0.44 with 1 month lag), NAO (-0.58 with 10 months lag) and AMO (0.71, no lag) whereas regionally correlations with AMO reached as high as 0.8.

In conclusion, Black Sea was found to be much rapidly warming compared to the Levantine basin, due to Black Sea being an enclosed basin with a very shallow mixed layer depth. In the Black Sea areas with highest warming were around the eastern and northeastern parts displaying fuzzy spatial structure, whereas in the Levantine basin the highest warming areas were the ones with well-known characteristics, such as the Rhodes Gyre. These patterns suggest that the Black Sea warming is mainly dues to decreased cooling from northeast, considering northeasterlies are one of the two most pronounced wind regimes in the Black Sea, whereas the Levantine Basin warming is due to increasing heatflux. The Black Sea responds almost equally with NAO and EA-WR whereas the Levantine seems to be dominated by impact from the Atlantic (AMO).

Chapter four focused on the response of phytoplankton to changing physical mechanisms in the Black Sea. Physical biological interactions at both seasonal and interannual time scales were investigated utilizing results of univariate EOF analysis for 1998-2012. Chlorophyll-a data clearly displayed a decrease after 2001. The same period coincided with an increase in the intensity of the cyclonic boundary current, which resulted from changes in the wind stress curl. The same period also displayed an increase in the mean kinetic energy and a decrease in the number of eddies. It is concluded here that the increased intensity of the cyclonic boundary current decreased the cross shelf transport of nutrients which led to a decrease in chlorophyll.

Chapter five was dedicated to the investigation of spatio-temporal variability of phytoplankton and its response to physical parameters. Chlorophyll in the Levantine basin displayed a significant decrease both over the shelf waters and offshore waters.

Chlorophyll dynamics in the coast are regulated mainly by dynamics of riverine fluxes. In order to investigate the chlorophyll variability beyond riverine controls, space-time decompositions of variables were interpreted with a specific focus on offshore waters. In the offshore waters of the Levantine basin, a clear decline in chlorophyll was evident after 2007, which was accompanied with an increasing sea surface temperature and sea surface height. Increased temperature reduced winter convective mixing events, which then reduced Rhodes Gyre circulation. The observed decrease in cyclonic circulation also contributed to reduction in Rhodes Gyre bloom intensity due to less upwelling of nutrient rich waters during these times. Increased chlorophyll was observed in the vicinity of IeraPetra eddy during 2003-2004. At this time, IeraPetra eddy was rather weak or absent. In this period, the wind stress curl over IeraPetra region was modified, which led to the weakening of its anticyclonic activity and hence resulted in increased phytoplankton. Considering that the high atmospheric temperature during 2003 were considered a heat wave in Europe, it is likely that predominant winds were modified winds during this period, causing the weakening of the eddy. This suggest a strong ocean-atmosphere coupling, however this remains to be investigated in more detail.

This study investigated the phytoplankton response to physical mechanisms in both the Black Sea and Levantine basin. Over the time period of investigation major changes in phytoplankton in the Black Sea after 2001 were most likely driven by wind and its influence on the basin wide circulation (rim current), whereas in the Levantine basin the observed changes in phytoplankton were taking place later in time (2007) and seem to have been regulated by convection.

REFERENCES

Alvera-Azcárate, A., Barth, A., Rixen, M., and Beckers, J. M. (2005). Reconstruction of incomplete oceanographic data sets using empirical orthogonal functions: Application to the Adriatic Sea surface temperature. *Ocean Modelling*, *9*(4), 325–346.

Amitai, Y., Lehahn, Y., Lazar, A., and Heifetz, E. (2010). Surface circulation of the eastern Mediterranean Levantine basin: Insights from analyzing 14 years of satellite altimetry data. *Journal of Geophysical Research: Oceans*, *115*(10), 1–11. http://doi.org/10.1029/2010JC006147

Basturk, O., Tugrul, S., Konovalov, S., Salihoglu, I., (1997). Variations in the vertical structure of water chemistry within the three hydrodynamically di!erent regions of the Black Sea. In: Ozsoy, E., Mikaelyan, A. (Eds.), Sensitivity to Change: Black Sea, Baltic Sea and North Sea, NATO ASI Series 2, Environment, Vol. 27. Kluwer Academic Publishers, Dordrecht, pp. 183-196.

Beckers, J. M., and Rixen, M. (2003). EOF calculations and data filling from incomplete oceanographic datasets. *Journal of Atmospheric and Oceanic Technology*, *20*(12), 1839–1856. http://doi.org/10.1175/1520-0426(2003)020<1839:ECADFF>2.0.CO;2

Behrenfeld, M. J., O'Malley, R. T., Siegel, D. a, McClain, C. R., Sarmiento, J. L., Feldman, G. C., … Boss, E. S. (2006). Climate-driven trends in contemporary ocean productivity. Nature, 444(7120), 752–755. http://doi.org/10.1038/nature05317

Belkin, I. M. (2009). Rapid warming of Large Marine Ecosystems. *Progress in Oceanography*, *81*(1-4), 207–213. http://doi.org/10.1016/j.pocean.2009.04.011

Belokopytov, V. N. (2011). Interannual variations of the renewal of waters of the cold intermediate layer in the Black Sea for the last decades. *Physical Oceanography*, *20*(5), 347-355.

Bodeanu, N. (1993). Microalgal blooms in the Romanian area of the Black Sea and contemporary eutrophication conditions. In: Smayda TJ, Shimizu Y (eds) Toxic phytoplankton blooms in the sea. Elsevier, Amsterdam, p 203–209.

Bodeanu, N., Andrei, C., Boicenco, L., Popa, L., Sburlea, A., (2004). A new trend of the phytoplankton structure and dynamics in the Romanian marine waters. Cercetari Marine 35, 77–86.

Boyce, D. G., Lewis, M. R., and Worm, B. (2010). Global phytoplankton decline over the past century. Nature, 466(7306), 591–596. http://doi.org/10.1038/nature09268

BSC (2008). State of the environment of the Black Sea (2001–2006/7). Oguz, T. (ed) The Commission on the Protection of the Black Sea Against Pollution publication, Istanbul.

Capet, A., Barth, A., and Beckers, J. (2012). Deep-Sea Research II Interannual variability of Black Sea ' s hydrodynamics and connection to atmospheric patterns, 80, 128–142. http://doi.org/10.1016/j.dsr2.2012.04.010

Capet, A., Stanev, E. V., Beckers, J. M., Murray, J. W., and Grégoire, M. (2016). Decline of the Black Sea oxygen inventory. *Biogeosciences*, *13*(4), 1287-1297.

Casey, K. S., Brandon, T. B., Cornillon, P., and Evans, R. (2010). The past, present, and future of the AVHRR pathfinder SST program. In *Oceanography from Space: Revisited* (pp. 273–287). http://doi.org/10.1007/978-90-481-8681-5_16

Castelao, R. (2012). Sea surface temperature and wind stress curl variability near a cape. Journal of Physical Oceanography, 120816073618001. http://doi.org/10.1175/JPO-D-11-0224.1

Chashchin, A. K. (1996). The Black Sea populations of anchovy. Scientia Marina, 60(2), 219-255.

Chelton, D. B., Schlax, M. G., Samelson, R. M. (2007). Summertime Coupling between Sea Surface Temperature and Wind Stress in the California Current System. Journal of Physical Oceanography, 37(3), 495–517. http://doi.org/10.1175/JPO3025.1

Chelton, D. B., Schlax, M. G., Samelson, R. M. and R. A. de Szoeke (2007). Global observations of large oceanic eddies, Geophys. Res. Lett., 34, L15606, doi:10.1029/2007GL030812.

Chu, P. C., Ivanov, L. M., and Margolina, T. M. (2005). Seasonal variability of the Black Sea chlorophyll- a concentration, 56, 243–261. http://doi.org/10.1016/j.jmarsys.2005.01.001

Ciappa, A. C. (2014). The controversial path of Atlantic Water in the Eastern Mediterranean. Progress in Oceanography, 123, 74–83. http://doi.org/10.1016/j.pocean.2014.02.001

Cociasu, A., Dorogan, L., Humborg, C., Popa, L. (1996). Long-term ecological changes in Romanian coastal waters of the Black Sea. Mar Pollut Bull 32:32–38.

Cociasu, A., Popa, L.,(2005). Significant changes in Danube nutrient loads and their impact on the Romanian Black Sea coastal waters. Cercet Mar 35, 25–37.

Cokacar, T., Oguz, T., and Kubilay, N. (2004). Satellite-detected early summer coccolithophore blooms and their interannual variability in the Black Sea. Deep-Sea Research Part I: Oceanographic Research Papers, 51(8), 1017–1031. http://doi.org/10.1016/j.dsr.2004.03.007

Correa-Ramirez, M. A., Hormazabal, S. E., Morales, C. E. (2012). Spatial patterns of annual and interannual surface chlorophyll-a variability in the Peru-Chile Current System. Progress in Oceanography, 92-95, 8–17. http://doi.org/10.1016/j.pocean.2011.07.008

Criado-Aldeanueva, F., Del Río Vera, J., and García-Lafuente, J. (2008). Steric and mass-induced Mediterranean sea level trends from 14 years of altimetry data. *Global and Planetary Change*, *60*(3-4), 563–575. http://doi.org/10.1016/j.gloplacha.2007.07.003

Crise, A., Allen, J. I., Baretta, J., Crispi, G., Mosetti, R., Solidoro, C. (1999). The Mediterranean pelagic ecosystem response to physical forcing. Progress in Oceanography, 44(1-3), 219–243. http://doi.org/10.1016/S0079-6611(99)00027-0

D'Ortenzio, F., Ribera d'Alcalà, M. (2009). On the trophic regimes of the Mediterranean Sea: a satellite analysis. Biogeosciences Discussions, 5(4), 2959–2983.

D'Ortenzio, F., Ragni, M., Marullo, S., Ribera d'Alcala, M. (2003). Did biological activity in the Ionian Sea change after the Eastern Mediterranean Transient? Results

from analysis of remote sensing observations. Journal of Geophysical Research-Oceans, 108(C9), 8113, doi:10.1029/2002JC001556. http://doi.org/10.1029/2002JC001556

Dai, A. G., Qian, T. T., Trenberth, K. E. and Milliman, J. D. (2009). Changes in continental freshwater discharge from 1948 to 2004. J. Clim. 22, 2773–2792

Daskalov, G. M., 2002. Overfishing drives a trophic cascade in the Black Sea. Mar Ecol Prog Ser 225, 53–63.

Demarcq, H. (2009). Trends in primary production, sea surface temperature and wind in upwelling systems (1998-2007). Progress in Oceanography, 83(1-4), 376–385. http://doi.org/10.1016/j.pocean.2009.07.022

Ding, Y., Wei, Z., Mao, Z., Wang, X., and Pan, D. (2009). Reconstruction of incomplete satellite SST data sets based on EOF method. *Acta Oceanologica Sinica*, *28*(2), 36–44.

Doney, S. C. (2006). Plankton in a warmer world. Nature, 444, 695–696.

D'Ortenzio, F., Iudicone, D., de Boyer Montegut, C., Testor, P., Antoine, D., Marullo, S., et al. (2005). Seasonal variability of the mixed layer depth in the Mediterranean Sea as derived from in situ profiles. Geophysical Research Letters, 32, L12605, doi: 10.1029/2005GL022463.

Ediger, D., Yilmaz, A. (1996). Characteristics of deep chlorophyll maximum in the northeastern Mediterranean with respect to environmental conditions, J. Mar. Syst., 9, 291 – 303.

Enfield, D. B., Mestas-Nuñez, A. M., and Trimble, P. J. (2001). The Atlantic multidecadal oscillation and its relation to rainfall and river flows in the continental US. Geophysical Research Letters, 28(10), 2077-2080.

Faghmous, J. H., Frenger, I. , Yao, Y. , Warmka, R. , Lindell, A., Kumar, V. (2015). A daily global mesoscale ocean eddy dataset from satellite altimetry, Sci. Data , 2, 150028. doi: 10.1038/sdata.2015.28.

Faghmous, J. H., L. Styles, V. Mithal, S. Boriah, S. Liess, V. Kumar, F. Vikebo, and M. D. S. Mesquita (2012), EddyScan: A physically consistent ocean eddy monitoring application, in Proc. Conf. Intel. Data Under., pp. 96–103, IEEE, Boulder, Colo.,

doi:10.1109/ CIDU.2012.6382189. [Available at http://ieeexplore.ieee.org/xpls/abs_all.jsp?arnumber=6382189andtag=1.]

Ford, D. A., Edwards, K. P., Lea, D., Barciela, R. M., Martin, M. J., and Demaria, J. (2012). Assimilating GlobColour ocean colour data into a pre-operational physical-biogeochemical model. Ocean Science, 8(5), 751-771.

Fukumori, I., D. Menemenlis, and T. Lee (2007). A near-uniform basinwide sea level fluctuation of the Mediterranean Sea, J. Phys. Oceanogr., 37(2), 338–358.

Gačić, M., Civitarese, G., Miserocchi, S., Cardin, V., Crise, A., Mauri, E. (2002). The open-ocean convection in the Southern Adriatic: A controlling mechanism of the spring phytoplankton bloom. Continental Shelf Research, 22(14), 1897–1908. http://doi.org/10.1016/S0278-4343(02)00050-X

Gaube, P., Chelton, D. B., Strutton, P. G., Behrenfeld, M. J. (2013). Satellite observations of chlorophyll, phytoplankton biomass, and Ekman pumping in nonlinear mesoscale eddies. Journal of Geophysical Research: Oceans, 118(12), 6349–6370. http://doi.org/10.1002/2013JC009027

Gawarkiewicz, G., Korotaev, G., Stanichny, S., Repetin, L., Soloviev, D. (1999). Synoptic upwelling and cross-shelf transport processes along the Crimean coast of the Black Sea. Cont. Shelf Res., 19, 977–1005.

GEF-UNDP (2006). Trends in nutrient loads from the Danube River and trophic status of the Black Sea. Joint Report of the GEF-UNDP Black Sea Ecosystem Recovery Project and the GEF-UNDP Danube Regional Project, Istanbul.

Ginzburg, A. I., Kostianoy, A. G., and Sheremet, N. A. (2004). Seasonal and interannual variability of the Black Sea surface temperature as revealed from satellite data (1982-2000). *Journal of Marine Systems*, *52*(1-4), 33–50.

Ginzburg, A.I., Kostianoy, A.G., Sheremet, N.A., (2008). Sea surface temperature variability. Kostianoy, A.G., Kosarev, A.N. (Eds.), The Black Sea Environment, Springer, Berlin/Heidelberg (2008), pp. 255–275.

Ginzburg, A.I., Kostianoy, A.G., Krivosheya, V.G., Nezlin, N.P., Soloviev, D.M., Stanichny, S.V., Yakubenko, V.G. (2002). Mesoscale eddies and related processes in the northeastern Black Sea. J. Mar. Syst., 32, 71–90.

Grayek, S., Stanev, E. V. (2010). On the response of Black Sea level to external forcing : altimeter data and numerical modelling, 123–140. http://doi.org/10.1007/s10236-009-0249-7

Gregg, M. C., and Yakushev, E. (2005). Surface ventilation of the Black Sea's cold intermediate layer in the middle of the western gyre. *Geophysical Research Letters*, *32*(3), 1–4.

Gregg, W. W., and Rousseaux, C. S. (2014). Decadal trends in global pelagic ocean chlorophyll: A new assessment integrating multiple satellites, in situ data, and models. Journal of Geophysical Research C: Oceans, 119(9), 5921–5933. http://doi.org/10.1002/2014JC010158

Gregg, W. W., Casey, N. W., and McClain, C. R. (2005). Recent trends in global ocean chlorophyll. *Geophysical Research Letters*, *32*(3), 1–5.

Gucu, A.C., (2002). Can overfishing be responsible for the successful establishment of Mnemiopsis leidyi in the Black Sea? Estuarine, Coastal and Shelf Science 54, 439–451.

Hamad, N., Millot, C., Taupier-Letage, I. (2005). A new hypothesis about the surface circulation in the eastern basin of the Mediterranean sea. Progress in Oceanography 66, 287–298.

Hurrell, J. W., and Deser, C. (2010). North Atlantic climate variability: the role of the North Atlantic Oscillation. Journal of Marine Systems, 79(3), 231-244.

IPCC, (2007). Climate change 2007: synthesis report. Contribution of working groups I-III to the Fourth assessment report of the Intergovernmental panel on climate change, Cambridge Univ. Press, Cambridge.

Ivanov, L. I., Backhaus, J. O., Özsoy, E., and Wehde, H. (2001). Convection in the Black Sea during cold winters. *Journal of Marine Systems*, *31*(1-3), 65–76.

Jose, Y. S., Aumont, O., Machu, E., Penven, P., Moloney, C. L., Maury, O. (2014). Influence of mesoscale eddies on biological production in the Mozambique Channel:

Several contrasted examples from a coupled ocean-biogeochemistry model. Deep-Sea Research Part II: Topical Studies in Oceanography, 100, 79–93. http://doi.org/10.1016/j.dsr2.2013.10.018

Josey, S. A., Somot, S., and Tsimplis, M. (2011). Impacts of atmospheric modes of variability on Mediterranean Sea surface heat exchange. Journal of Geophysical Research: Oceans, 116(C2).

Kabbara, N., Yan, X. H., Klemas, V. V, and Pan, J. (2002). Temporal and spatial variability of the surface temperature anomaly in the Levantine Basin of the Eastern Mediterranean. *International Journal of Remote Sensing*, *23*(18), 3745–3761. http://doi.org/Doi 10.1080/01431160110070663

Kazmin, A. S., and Zatsepin, A. G. (2007). Long-term variability of surface temperature in the Black Sea, and its connection with the large-scale atmospheric forcing. *Journal of Marine Systems*, *68*(1-2), 293–301.

Kazmin, A. S., Zatsepin, A. G., and Kontoyiannis, H. (2010). Comparative analysis of the long-term variability of winter surface temperature in the Black and Aegean seas during 1982-2004 associated with the large-scale atmospheric forcing. *International Journal of Climatology*, *30*(9), 1349–1359.

Kilpatrick, K. A., Podesta, G. P., & Evans, R. (2001). Overview of the NOAA/NASA advanced very high resolution radiometer Pathfinder algorithm for sea surface temperature and associated matchup database. J. Geophys. Res, 106(C5), 9179-9197.

Klein, B., Roether, W., Manca, B. B., Bregant, D., Beitzel, V., Kovaceriv, V., and Luchetta, A. (1999). The large deep water transiet in the eastern Mediterranean. *Deep Sea Research*, *46*(1999), 371–414.

Konovalov, S.K., Murray, J.W. (2001). Variations in the chemistry of the Black Sea on a time scale of decades (1960–1995). J Mar Syst 31:217–243.

Korotaev, G., Oguz, T., Nikiforov, A., and Koblinsky, C. (2003). Seasonal, interannual, and mesoscale variability of the Black Sea upper layer circulation derived from altimeter data. J. Geophys. Res., 108(C4), 3122. http://doi.org/10.1029/2002jc001508

Kouketsu, S., Kaneko, H., Okunishi, T., Sasaoka, K., Itoh, S., Inoue, R., Ueno, H. (2015). Mesoscale eddy effects on temporal variability of surface chlorophyll a in the Kuroshio Extension. Journal of Oceanography. http://doi.org/10.1007/s10872-015-0286-4

Krichak, S. O., and P. Alpert (2005). Decadal trends in the east Atlantic- west Russia pattern and Mediterranean precipitation, Int. J. Climatol., 25, 183–192, doi:10.1002/joc.1124

Krivosheya, V. G., I. M. Ovchinnikov, and A. Y. Skirta, (2002). Interannual variability of the Cold Intermediate Layer renewal in the Black Sea, in Multidisciplinary Investigations of the North-East Part of the Black Sea (in Russian), edited by A. Zatsepin, and M. Flint, pp. 27–39, Nauka, Moscow.

Landerer, F. W., and D. L. Volkov (2013). The anatomy of recent large sea level fluctuations in the Mediterranean Sea, Geophys. Res. Lett., 40, 553–557, doi:10.1002/GRL.50140.

Lascaratos, A., W. Roether, K. Nittis, and B. Klein (1999). Recent changes in deep water formation and spreading in the eastern Mediterranean Sea: A review, Prog. Oceanogr., 44, 5–36.

Levitus, S., Antonov, J., and Boyer, T. (2005). Warming of the world ocean, 1955-2003. Geophysical Research Letters, 32(2), 1–4. http://doi.org/10.1029/2004GL021592

Levy, M., Iovino, D., Resplandy, L., Klein, P., Madec, G., Trguier, A. M., … Takahashi, K. (2012). Large-scale impacts of submesoscale dynamics on phytoplankton: Local and remote effects. Ocean Modelling, 43-44, 77–93. http://doi.org/10.1016/j.ocemod.2011.12.003

Li, Y., and He, R. (2014). Spatial and temporal variability of SST and ocean color in the gulf of maine based on cloud-free SST and chlorophyll reconstructions in 2003-2012. *Remote Sensing of Environment*, *144*, 98–108.

Liu, F., Tang, S., and Chen, C. (2013). Impact of nonlinear mesoscale eddy on phytoplankton distribution in the northern south china sea. Journal of Marine Systems, 123-124, 33–40. http://doi.org/10.1016/j.jmarsys.2013.04.005

Ludwig, W., Dumont, E., Meybeck, M., and Heussner, S. (2009). Progress in Oceanography River discharges of water and nutrients to the Mediterranean and Black Sea : Major drivers for ecosystem changes during past and future decades ? Progress in Oceanography, 80(3-4), 199–217. http://doi.org/10.1016/j.pocean.2009.02.001

Ludwig, W., Meybeck, M., Abousamra, F., 2003. Riverine transport of water, sediments, and pollutants to the Mediterranean Sea. UNEP MAP Technical report Series 141, UNEP/MAP Athens, 111 pp. Available from: < http://www.unepmap.org/ >.

Macias, D., Garcia-Gorriz, E., and Stips, A. (2013). Understanding the causes of recent warming of mediterranean waters. How much could be attributed to climate change? *PLoS ONE*, *8*(11). http://doi.org/10.1371/journal.pone.0081591

Mahadevan, a., D'Asaro, E., Lee, C., and Perry, M. J. (2012). Eddy-Driven Stratification Initiates North Atlantic Spring Phytoplankton Blooms. Science, 337(6090), 54–58. http://doi.org/10.1126/science.1218740

Malanotte-Rizzoli, P., Manca, B. B., D'alcala, M. ., Theocharis, A., Brenner, S., Budillon, G., Ozsoy, E. (1999). The Eastern Mediterranean in the 80s and in the 90s:the big transition in the intermedieta and deep circulations. *Dynamics of Atmospheres and Oceans*, *29*, 365–395.

Mariotti, A., and Dell'Aquila, A. (2012). Decadal climate variability in the Mediterranean region: Roles of large-scale forcings and regional processes. *Climate Dynamics*, *38*(5-6), 1129–1145. http://doi.org/10.1007/s00382-011-1056-7

Maritorena, S., Siegel, D. A. (2005). Consistent merging of satellite ocean color data sets using a bio-optical model, 94, 429–440. http://doi.org/10.1016/j.rse.2004.08.014

Marullo, S. (1999). The sea surface temperature field in the Eastern Mediterranean from advanced very high resolution radiometer (AVHRR) data Part II. Interannual variability. *Journal of Marine Systems*, *20*(1-4), 83–112. http://doi.org/10.1016/S0924-7963(98)00072-4

Marullo, S., Artale, V., and Santoleri, R. (2011). The SST multidecadal variability in the Atlantic-Mediterranean region and its relation to AMO. *Journal of Climate*, *24*(16), 4385–4401. http://doi.org/10.1175/2011JCLI3884.1

Marullo, S., Santoleri, R., Malanotte-Rizzoli, P., and Bergamasco, A. (1999). The sea surface temperature field in the Eastern Mediterranean from advanced very high resolution radiometer (AVHRR) data: Part I. Seasonal variability. *Journal of Marine Systems*, *20*(1-4), 63–81. http://doi.org/10.1016/S0924-7963(98)00071-2

Mauri, E., Poulain, P. M., Juznic-Zonta, Z. (2007). MODIS chlorophyll variability in the northern Adriatic Sea and relationship with forcing parameters. Journal of Geophysical Research: Oceans, 112(3), 1–14. http://doi.org/10.1029/2006JC003545

Mauri, E., Poulain, P. M., Notarstefano, G. (2008). Spatial and temporal variability of the sea surface temperature in the Gulf of Trieste between January 2000 and December 2006. *Journal of Geophysical Research*, *113*(C10), C10012.

McQuatters-Gollop, A., Mee, L. D., Raitsos, D. E., and Shapiro, G. I. (2008). Non-linearities, regime shifts and recovery: The recent influence of climate on Black Sea chlorophyll. *Journal of Marine Systems*, *74*(1-2), 649–658.

Mee, L.D., (1992). The Black-Sea in crisis — a need for concerted international action. Ambio 21 (4), 278–286.

Meredith, E. P., Semenov, V. a., Maraun, D., Park, W., and Chernokulsky, A. V. (2015). Crucial role of Black Sea warming in amplifying the 2012 Krymsk precipitation extreme. *Nature Geoscience*, *8*(8), 615–619.

Mikaelyan, A.S., (1997). Long-term variability of phytoplankton communities in open Black Sea in relation to environmental changes. In: Ozsoy, E., Mikaelyan, A. (Eds.), Sensitivity to Change: Black Sea, Baltic Sea and North Sea. NATO-ASI Series, Environment, vol. 27. Kluwer Academic Publishers, Dordrecht, pp. 105–116

Mikaelyan, A.S., Zatsepin, A.G., Chasovnikov, V.K., (2013). Long-term changes in nutrient supply of phytoplankton growth in the Black Sea. J. Mar. Syst. 117-118, 53-64.

Millot, C., and Gerin, R. (2010). The mid-mediterranean jet artefact. Geophysical Research Letters, 37(12), 1–6. http://doi.org/10.1029/2010GL043359

Moncheva, S., Krastev, A. (1997). Some aspects of phytoplankton long-term alterations off Bulgarian Black Sea Shelf. In: Sensitivity to Change: Black Sea, Baltic Sea and

North Sea, E. Ozsoy, A. Mikaelyan, eds. NATO ASI Series, Vol. 27. Kluwer Academic Publishers, Dordrecht, pp. 79–94.

Morales, C. E., Hormazabal, S., Correa-Ramirez, M., Pizarro, O., Silva, N., Fernandez, C., Torreblanca, M. L. (2012). Mesoscale variability and nutrient-phytoplankton distributions off central-southern Chile during the upwelling season: The influence of mesoscale eddies. Progress in Oceanography, 104, 1–16. http://doi.org/10.1016/j.pocean.2012.04.015

Napolitano, E., Oguz, T., Malanotte-Rizzoli, P., Yilmaz, A., Sansone, E. (2000). Simulations of biological production in the Rhodes and Ionian basins of the eastern Mediterranean, J. Mar. Syst., 24, 277 – 298.

Nardelli, B. B., Colella, S., Santoleri, R., Guarracino, M., and Kholod, A. (2010). A re-analysis of Black Sea surface temperature. *Journal of Marine Systems, 79*(1-2), 50–64.

Nezlin, N.P., (2001). Unusual phytoplankton bloom in the Black Sea during 1998–1999: analysis of remotely sensed data. Oceanology 41 (3), 375–380.

Nezlin, N.P., Kostianoy, A.G.and Gregoire, M. (1999). Patterns of seasonal and interannual changes of surface chlorophyll concentrations in the Black Sea revealed from the remore sensed data, Remote Sens. Environ., 69, 43-55.

Nykjaer, L. (2009). Mediterranean Sea surface warming 1985-2006. *Climate Research, 39*(1), 11–17. http://doi.org/10.3354/cr00794

Oguz, T. (2005a) Long term impacts of anthropogenic and human forcing on the reorganisation of the Black Sea ecosystem. Oceanography, 18(2), 112-121.

Oguz, T. (2005b). Black Sea Ecosystem Response to Climatic Teleconnections. *Oceanography, 18*(2), 122–133.

Oguz, T., Dippner, J. W., and Kaymaz, Z. (2006). Climatic regulation of the Black Sea hydro-meteorological and ecological properties at interannual-to-decadal time scales. Journal of Marine Systems, 60(3), 235-254.

Oguz, T. and Gilbert, D. (2007). Abrupt transitions of the top-down controlled Black Sea pelagic ecosystem during 1960-2000: evidence for regime-shifts under strong fishery exploitation and nutrient enrichment modulated by climate-induced variations.

Deep Sea Res.I, 54,220-242.

Oguz, T., and Velikova, V. (2010). Abrupt transition of the northwestern Black Sea shelf ecosystem from a eutrophic to an alternative pristine state. *Marine Ecology Progress Series*, *405*, 231–242.

Oguz, T., Cokacar, T., Malanotte-Rizzoli, P., and Ducklow, H. W. (2003). Climatic warming and accompanying changes in the ecological regime of the Black Sea during 1990s. *Global Biogeochemical Cycles*, *17*(3).

Oguz, T., Deshpande, A. G. and Malanotte-Rizzoli, P. (2002). On the Role of Mesoscale Processes Controlling Biological Variability in the Black Sea: Inferrences From SeaWIFS-derived Surface Chlorophyll Field. Continental Shelf Research, 22, 1477–1492.

Oguz, T., Ducklow, H. W., Malanotte-Rizzoli, P. (2000) "Modeling distinct vertical biogeochemical structure of the Black Sea: Dynamical coupling of the oxic, suboxic and anoxic layers". Global Biogeochemical Cycles, 14(4), 1331-1352.

Oguz, T., Latun, V.S., Latif, M.A., Vladimirov, V.V., Sur, H.I., Markov, A.A., Ozsoy, E. , Kotovshchikov, B.B., Eremeev, V.V. and Unlulata, U. (1993) Circulation in the surface and intermediate layers of the Black Sea. Deep-Sea Res., I 40, 1597–1612

Oguz, T., Salihoglu, B., (2000). Simulation of eddy-driven phytoplankton production in the Black Sea. Geophysical Research Letters 27 (14), 2125-2128, 27(14). http://doi.org/10.1029/1999GL011083

Oschlies, A., and Garcon, V. (1998). Eddy-induced enhancement of primary production in a model of the North Atlantic Ocean ´. Nature, 394(July), 266–269. http://doi.org/10.1038/28373

Ovchinnikov, I. M., Plakhin, A. (1984). The formation of Intermediate Water in the Mediterranean. Oceanology, 24, 168–173.

Ovchinnikov, I., and Y. I. Popov (1987). Evolution of cold intermediate layer in the Black Sea, Oceanology, Engl. Transl., 27, 555 – 560.

Ozsoy, E., and Unluata, U. (1997). Oceanography of the Black Sea: a review of some recent results. *Earth-Science Reviews*, *42*(4), 231–272.

Ozsoy, E., Hecht, A., and Unluata, U. (1989). Circulation and hydrography of the Levantine Basin. Results of POEM coordinated experiments 1985-1986. *Progress in Oceanography*. http://doi.org/10.1016/0079-6611(89)90004-9

Ozsoy, E., Hecht, A., Unluata, U., Brenner, S., Oguz, T., Bishop, J., Rozentraub, Z. (1991). A review of the Levantine Basin circulation and its variability during 1985-1988. *Dynamics of Atmospheres and Oceans*, *15*(3-5), 421–456. http://doi.org/10.1016/0377-0265(91)90027-D

Ozsoy, E., Hecht, A., Unluata, U., Brenner, S., Sur, H. I., Bishop, J., Oguz, T. (1993). A synthesis of the Levantine Basin circulation and hydrography, 1985-1990. *Deep-Sea Research Part II*, *40*(6), 1075–1119. http://doi.org/10.1016/0967-0645(93)90063-S

Palacios, D. M., Bograd, S. J., Foley, D. G., and Schwing, F. B. (2006). Oceanographic characteristics of biological hot spots in the North Pacific: A remote sensing perspective. Deep-Sea Research Part II: Topical Studies in Oceanography, 53(3-4), 250–269. http://doi.org/10.1016/j.dsr2.2006.03.004

Parr, W., Volovik, Y., Nixon, S., Lipan, I. (2005). Improving the understanding of the Danube River impact on the status of the Black Sea. UNDP-GEF Black Sea Ecosystem Recovery Project Report to the Black Sea-Danube Technical Working Group, Istanbul.

Piontkovski, S. A., Nezlin, N. P., Al-Azri, A., Al-Hashmi, K. (2012). Mesoscale eddies and chlorophyll variability in the Sea of Oman. International Journal of Remote Sensing, 33(17), 5341–5346. http://doi.org/10.1080/01431161.2012.661096

Piontkovski, S., Nezlin, N. (2012). Mesoscale eddies of Arabian Sea: physical–biological interactions. International Journal of Marine Science 2 (7), 51–56. http://dx.doi.org/10.5376/ijms. 2012.02.0007.

Pisano, A., Nardelli, B. B., Tronconi, C., and Santoleri, R. (2016). The new Mediterranean optimally interpolated pathfinder AVHRR SST Dataset (1982–2012). Remote Sensing of Environment, 176, 107-116.

Raitsos, D. E., Beaugrand, G., Georgopoulos, D., Zenetos, A., Pancucci-Papadopoulou, A. M., Theocharis, A., and Papathanassiou, E. (2010). Global climate change amplifies the entry of tropical species into the eastern Mediterranean Sea. *Limnology and Oceanography*, *55*(4), 1478–1484. http://doi.org/10.4319/lo.2010.55.4.1478

Rayner, N. A., Parker, D. E., Horton, E. B., Folland, C. K., Alexander, L. V., Rowell, D. P., Kaplan, A. (2003). Global analyses of sea surface temperature, sea ice, and night marine air temperature since the late nineteenth century. *Journal of Geophysical Research*, *108*(D14), 4407. http://doi.org/10.1029/2002JD002670

Reynolds, R. W., (2009): What's New in Version 2. OISST Webpage.http://www.ncdc.noaa.gov/sites/default/files/attachments/Reynolds2009_oisst_daily_v02r00_version2-features.pdf

Reynolds, R. W., Smith, T. M., Liu, C., Chelton, D. B., Casey, K. S., and Schlax, M. G. (2007). Daily High-Resolution Blended Analyses for Sea Surface Temperature. *Journal of Climate*, *20*, 5473–5496. http://doi.org/10.1175/2007JCLI1824.1

Rio, M. H., Poulain, P. M., Pascual, A., Mauri, E., Larnicol, G., & Santoleri, R. (2007). A mean dynamic topography of the Mediterranean Sea computed from altimetric data, in-situ measurements and a general circulation model. Journal of Marine Systems, 65(1), 484-508.

Rio, M. H., Pascual, A., Poulain, P. M., Menna, M., Barceló, B., and Tintoré, J. (2014). Computation of a new mean dynamic topography for the Mediterranean Sea from model outputs, altimeter measurements and oceanographic in situ data, Ocean Sci., 10, 731–744, doi:10.5194/os-10-731-2014

Rueda-Roa, D. T., and Muller-Karger, F. E. (2013). The southern Caribbean upwelling system: Sea surface temperature, wind forcing and chlorophyll concentration patterns. Deep-Sea Research Part I: Oceanographic Research Papers, 78, 102–114. http://doi.org/10.1016/j.dsr.2013.04.008

Santoleri, R., Volpe, G., Marullo, S., and Buongiorno Nardelli, B. (2008). Open waters optical remote sensing of the Mediterranean Sea. In V. Barale, and M. Gade (Eds.), Remote sensing of the European seas (pp. 103–116). Springer

Schär, C., Jendritzky, G. (2004). Climate change: Hot news from summer 2003. Nature, 432(7017), 559–560.

Schmidt, C., Morard, R., Almogi-Labin, A., Weinmann, A. E., Titelboim, D.,

Abramovich, S., and Kucera, M. (2015). Recent invasion of the symbiont-bearing foraminifera pararotalia into the eastern mediterranean facilitated by the ongoing warming trend. *PLoS ONE*, *10*(8), 1–25. http://doi.org/10.1371/journal.pone.0132917

Schrum, C., Staneva, J., Stanev, E., and Ozsoy, E. (2001). Air-sea exchange in the Black Sea estimated from atmospheric analysis for the period 1979-1993. *Journal of Marine Systems*.

Shulman, G. E. (2002). Anchovies of the Sea of Azov and the Black Sea: Regularities of wintering migrations (brief review).

Shaltout, M., Omstedt, A. (2014). Recent sea surface temperature trends and future scenarios for the Mediterranean Sea. *Oceanologia*, *56*(3), 411–443. http://doi.org/10.5697/oc.56-3.411

Shapiro, G. I., Stanichny, S. V., and Stanychna, R. R. (2010). Anatomy of shelf-deep sea exchanges by a mesoscale eddy in the North West Black Sea as derived from remotely sensed data. *Remote Sensing of Environment*, *114*(4), 867–875.

Shiganova, T.A., (1998). Invasion of the Black Sea by the ctenophore Mnemiopsis leidyi and recent changes in pelagic community structure, Fish. Oceanogr., 7, 305–310.

Skliris, N., Sofianos, S., Gkanasos, A., Mantziafou, A., Vervatis, V., Axaopoulos, P., and Lascaratos, A. (2012). Decadal scale variability of sea surface temperature in the Mediterranean Sea in relation to atmospheric variability. *Ocean Dynamics*, *62*(1), 13–30. http://doi.org/10.1007/s10236-011-0493-5

Stanev, E. V, and Peneva, E. L. (2001). Regional sea level response to global climatic change : Black Sea examples . Glob Planet Change Regional sea level response to global climatic change : Black Sea examples, (August 2016). http://doi.org/10.1016/S0921-8181(01)00148-5

Staneva, J. V., and Stanev, E. V. (2002). Water mass formation in the Black Sea during 1991-1995. *Journal of Marine Systems*, *32*(1-3), 199–218.

Sur, H. I., Ozsoy, E., and Unluata, U. (1994). Boundary current instabilities, upwelling, shelf mixing and eutrophication processes in the Black Sea.*Progress in Oceanography*, *33*(4), 249-302.

Sur, H.I., Ozsoy, E., Ilyin, Y.P., Unluata, U. (1996). Coastal/deep ocean interactions in the Black Sea and their ecological/environmental impacts. J. Marine Systems, 7, 293–320, 1996.

TDA (2007). Black Sea transboundary diagnostic analysis. Programme Coordinating Unit, Global Environmental Facility Black Sea Environmental Programme publication, Istanbul.

Theocharis, A., Klein, B., Nittis, K., and Roether, W. (2002). Evolution and status of the Eastern Mediterranean Transient (1997-1999). *Journal of Marine Systems*, *33-34*, 91–116. http://doi.org/10.1016/S0924-7963(02)00054-4

Theocharis, A., Nittis, K., Kontoyiannis, H., Papageorgiou, E., and Balopoulos, E. (1999). Climatic changes in the Aegean Sea influence the eastern Mediterranean thermocline circulation (1986-1997). *Geophys. Res. Lett.*, *26*(11), 1617–1620.

Tolmazin, D. (1985). Changing Coastal oceanography of the Black Sea. I: Northwestern Shelf. *Progress in Oceanography*.

Trenberth, K. E., Large, W. G., and Olson, J. G. (1990). The Mean Annual Cycle in Global Ocean Wind Stress. *Journal of Physical Oceanography*, *20*(11), 1742–1760.

Trigo, R. M., Osborn, T. J., & Corte-Real, J. M. (2002). The North Atlantic Oscillation influence on Europe: climate impacts and associated physical mechanisms. Climate Research, 20(1), 9-17.

Tugrul, S., Basturk, O., Saydam, C., Yilmaz, A. (1992). Changes in the hydrochemistry of the Black Sea inferred from water density profiles. Nature 359:137–139.

Uz, M., Yoder, JA. (2004). High frequency and mesoscale variability in SeaWiFS chlorophyll imagery and its relation to other remotely sensed oceanographic variables. Deep-Sea Res.II 51:1001-17.

Vinogradov, M. E., Shushkina, E. A., Mikaelyan, A. S., and Nezlin, N. P. (1999). Temporal (Seasonal and Interannual) Changes of Ecosystem of the Open Waters of the Black Sea. In S. T. Besiktepe, U. Unluata, and A. S. Bologa (Eds.), Environmental Degradation of the Black Sea: Challenges and Remedies (pp. 109–129). Dordrecht: Springer Netherlands. http://doi.org/10.1007/978-94-011-4568-8_8

Volkov, D. L., Landerer, F. W. (2015). Internal and external forcing of sea level variability in the Black Sea. Climate Dynamics, 2633–2646. http://doi.org/10.1007/s00382-015-2498-0

Volpe, G., Nardelli, B. B., Cipollini, P., Santoleri, R., and Robinson, I. S. (2012). Seasonal to interannual phytoplankton response to physical processes in the Mediterranean Sea from satellite observations. Remote Sensing of Environment, 117, 223–235. http://doi.org/10.1016/j.rse.2011.09.020

Wilson, C., Coles, V. J. (2005). Global climatological relationships between satellite biological and physical observations and upper ocean properties. Journal of Geophysical Research C: Oceans, 110(10), 1–14. http://doi.org/10.1029/2004JC002724

Yunev, O. A., Carstensen, J., Moncheva, S., Khaliulin, A., Ærtebjerg, G., and Nixon, S. (2007). Nutrient and phytoplankton trends on the western Black Sea shelf in response to cultural eutrophication and climate changes, Estuar Coast Shelf Sci 74:63–76 http://doi.org/10.1016/j.ecss.2007.03.03

Yunev, O.A., Moncheva, S., Carstensen, J., (2005). Long-term variability of vertical chlorophyll a and nitrate profiles in the open Black Sea: eutrophication and climate change. Marine Ecology Progress Series 294, 95–107.

Yunev, O.A., Vedernikov, V.I., Basturk, O., Yilmaz, A., Kideys, A.E., Moncheva, S., Konovalov, S.K., (2002). Long-term variations of surface chlorophyll a and primary production in the open Black Sea. Marine ecology progress series 230, 11–28.

Zaitsev, Y.P. (1992). Recent changes in the trophic structure of the Black Sea. Fish Oceanogr 1:180–198

Zaitsev, Y.P., Mamaev,V. (1997). Marine biological diversity in the Black Sea: a study of change and decline. GEF Black Sea Environmental Programme. United Nations Publications, New York.

Zatsepin, A.G., Ginzburg, A.I., Kostianoy, A.G., Kremenetskiy, V.V., Krivosheya, V.G., Poulain, P.M., Stanichny , S.V., (2003) Observation of Black Sea mesoscale eddies and associated horizontal mixing. J. Geophys. Res., 108 (C8), pp. 1–27.

Zervakis, V., Georgopoulos, D., and Drakopoulos, P. G. (2000). The role of the North

Aegean in triggering the recent Eastern Mediterranean climatic changes. *Journal of Geophysical Research*, *105*(C11), 26103. http://doi.org/10.1029/2000JC900131

Zveryaev, I. (2015). Seasonal differences in intraseasonal and interannual variability of Mediterranean Sea surface temperature . *Journal of Geophysical Research: Oceans*, 2813–2825. http://doi.org/10.1002/2014JC010387

LIST OF ABBREVIATIONS

SST	Sea Surface Temperature
ADT	Absolute Dynamic Topography
MDT	Mean Dynamic Topography
CHL	Chlorophyll-a
CIL	Cold Intermediate Layer
AVHRR	Advanced Very High Resolution Radiometer
SEAWIFS	Sea-Viewing Wide Field-of-View Sensor
MODIS	Moderate Resolution Imaging Spectroradiometer
MERIS	MEdium Resolution Imaging Spectrometer
VIIRS	Visible Infrared Imaging Radiometer Suite
ENSO	El-Nino Southern Oscillation
NAO	North Atlantic Oscillation
EA-WR	East Atlantic West Russia index
AMO	Atlantic Multidecadal Oscillation
GHRSST	The Group for High Resolution Sea Surface Temperature
OISST	Optimally interpolated sea surface temperature
AMSR-E	The Advanced Microwave Scanning Radiometer - Earth Observing System
CCMP	Cross-Calibrated Multi-Platform
EOF	Empirical Orthogonal Functions
DINEOF	Data Interpolating Empirical Orthogonal Functions
SVD	Singular value decomposition
EMT	Eastern Mediterranean Transient
AVISO	Archiving, Validation and Interpretation of Satellite Oceanographic data
SLA	Sea level anomaly
MKE	Mean kinetic energy
GEBCO	General Bathymetric Chart of the Oceans
MMJ	Mid Mediterranean Jet

CURRICULUM VITAE

ANIL AKPINAR

Department of Oceanography, Email:akpinar.anil@gmail.com
Institute of Marine Sciences

Phone: +90-3245212406

Middle East Technical University
P.O.Box:28, 33731 Erdemli-Mersin, Turkey.

Education:

2016

Ph.D., Oceanography
Middle East Technical University,Institute of Marine Sciences
Dissertation: "Signatures of seasonal to decadal variability in the physical and biological properties of the Black Sea and Levantine as inferred by satellite remote sensing"

2010

M.Sc., Physical Oceanography
Middle East Technical University,Institute of Marine Sciences
Thesis: "Physical Characteristics of the Black Sea inferred from ARGO profiling data"

2008

B.Sc., Petroleum Engineering
Middle East Technical University

Work Experience:

12/2013-09/2016

Research Assistant in Institute of Marine Sciences, Middle East Technical University

05/2012-12/2013

Project Assistant in the EU-fp7 project: "PERSEUS (Policy-oriented Marine Environmental Research in the Southern European Seas)"-in WP3.1

09/2011-12/2011

Project Assistant, Institute of Marine Sciences, Middle East Technical University

07/2009-07/2011

Project Assistant, Institute of Marine Sciences, Middle East Technical University

07/2009-07/2012

Project Assistant, Institute of Marine Sciences, Middle East Technical University

10/2008-04/2010

Project Assistant, Institute of Marine Sciences, Middle East Technical University

Honors and Awards:

METU Best M.Sc. Thesis Award for 2009-2010, Institute of Marine Sciences, Middle East Technical University

METU Graduate Courses Performance Award for 2010-2011, Institute of Marine Sciences, Middle East Technical University

"Third Prize Best Oral Presentation" , International Conference "Marine Research Horizon 2020", 17-20 September 2013, Varna/Bulgaria

Research Interests:

- Control of physics on phytoplankton and their spatio-temporal variability.
- Climate change impacts on circulation and thermohaline structure of the ocean.
- Cold intermediate water formation dynamics and its variability.
- Mesoscale dynamics and their impact on phytoplankton.

Publications:

Akpinar, A., Fach, B.A., Oguz, T., Observing the subsurface thermal signature of the Black Sea with Argo profiling floats (submitted to Deep Sea Research I)

Akpinar, A., Arkin, S., Fach, B.A., Salihoglu, B. Inferring different phytoplankton responses to variability in the Black Sea physical environment from satellite remote sensing: seasonal to interannual time scales. (In preparation)

Akpinar, A., Fach, B.A., Recent trends in the sea surface temperature of the Black Sea. (In preparation).

Published Abstracts

Akpinar, A., Fach B.A., Oguz T. (2013) Thermohaline structure and cold intermediate layer properties of the Black Sea as inferred from Argo floats. *40th CIESM Congress Proceedings, p.132,* Marseille, France 28 October – 1 November 2013.

Kideys, A., Gücü, A.C., **Akpinar, A.**, Zenginer, A., Gazihan Akoğlu, A., Salihoğlu B., Fach, B., et al. (2014) Marine science education for primary schoolchildren - I know and protect my seas.*European Marine Science Educators Association Conference,* Gothenburg, Sweden.

Akpinar, A., Fach, B.A., Oguz, T., Salihoglu, B. (2013) Mesoscale eddies and cold water dynamics obtained from profiling floats. *"Marine Research Horizon 2020"*, Abstract ID: A11034.

Akpinar, A., Fach, B.A., Oguz, T., Salihoglu, B. (2010) Thermohaline structure of the Black Sea as inferred from Argo floats. "Geophysical Research Abstracts", Vol. 12, EGU2010-13751.

Courses / Schools

Euro-Argo, 3rd User Workshop, 17-18 June 2010, Paris/France
Euro-Argo-Black Sea: the use of Argo data in the Black Sea, 25-27 October 2010, Sofia/Bulgaria

1st "Microwave Ocean Remote Sensing" Training School of the SMOS-Mode COST Action, September 30-October 4, 2013, Barcelona/Spain

Seagoing Experience

14 days (July 2011) with *R/V-Akademik* (IO-BAS/Bulgaria) in the Central and Western Black Sea, within the scope of "Bio-Optical Characterization of the Black Sea for Remote Sensing Applications", NATO Science for Peace Project #982678.
5 days (August 2013) with *R/V Bilim-2* (IMS-METU/Turkey) in the Black Sea for deployment of Argo floats and monitoring

1 day (November 2013) with *R/V Bilim-2* (IMS-METU/Turkey) in the Eastern Mediterranean Sea (Levantine Basin) for deployment of Argo floats

34 days in total (February 2009-July 2015) with *R/V Bilim-2* (IMS-METU/Turkey) in the Eastern Mediterranean Sea (Levantine Basin) for various sea monitoring projects. Mainly responsible for CTD and ADCP measurements.

Additional Information:

Computer Skills: Linux/Unix and Windows operating systems, Matlab, IDL, Bash/Korn-Shell, GMT, Fortran, MS Office

Languages spoken: Turkish (Native), English (Fluent)